JSCSEN 73(7)683–770(2008)

Journal of the Serbian Chemical Society

Electronic version

VOLUME 73

NO 7

BELGRADE 2008

Available on line at

www.shd.org.rs/JSCS

The full search of JSCS is available through

DOAJ DIRECTORY OF OPEN ACCESS JOURNALS

www.doaj.org

Journal of the Serbian Chemical Society
JSCS@tmf.bg.ac.yu • www.shd.org.yu/JSCS

J. Serb. Chem. Soc. Vol. 73, No. 7 (2008)

CONTENTS

Published by the Serbian Chemical Society
Karnegijeva 4/III, 11120 Belgrade, Serbia
Printed by the Faculty of Technology and Metallurgy
Karnegijeva 4, P.O. Box 35-03, 11120 Belgrade, Serbia

www.shd.org.rs

Journal of the Serbian Chemical Society

JSCS@tmf.bg.ac.yu • www.shd.org.rs/JSCS

J. Serb. Chem. Soc. 73 (7) 683–690 (2008)
JSCS–3751

UDC 547.772+547.853:542.9:615.28
Original scientific paper

Characterization and biological evaluation of some novel pyrazolo[3',4':4,5]thieno[2,3-*d*]pyrimidin-8-ones synthesized *via* the Gewald reaction

DIPTI K. DODIYA, AMIT R. TRIVEDI, SAMIR H. JARSANIA, SHAILESH J. VAGHASIA and VIRESH H. SHAH*

Department of Chemistry, Saurashtra University, Rajkot-360 005, Gujarat, India

(Received 6 December 2007, revised 13 March 2008)

Abstract: The synthesis of substituted pyrazolo[3',4':4,5]thieno[2,3-*d*]pyrimidin-8-ones (**IIIa**–**j**) from 5-amino-3-methyl-1*H*-thieno[3,2-*c*]pyrazole-6-carbonitrile **(II)** is described. The key compound **II** was synthesized from (5-methyl-2,4-dihydro-3*H*-pyrazol-3-ylidene)malononitrile **I** *via* the Gewald reaction. The synthesis of the title compounds **IIIa**–**j** was accomplished by condensation of **II** with different aromatic aldehydes. The newly synthesized heterocyles were characterized by elemental analysis, IR, ^{1}H-NMR, ^{13}C-NMR and mass spectroscopic investigation. All the newly synthesized compounds were evaluated for antimicrobial activity against a variety of bacterial strains.

Keywords: pyrazolo[3',4':4,5]thieno[2,3-*d*]pyrimidin-8-ones; carbonitrile; Gewald reaction; antimicrobial activity.

INTRODUCTION

Pyrazole-containing compounds have practical applications in medicinal and agrochemical fields and the biological activities of pyrazoles[1,2] and its derivatives are well documented. The pyrazole ring is the basic moiety for a number of dyes, drugs and anaesthetics.[3,4] Substituted pyrazolopyrimidinones are found to be useful as cardiotonic,[5] herbicidal[6] and antiviral[7] agents. A literature survey revealed that substituted pyrazolopyrimidinones are potent and selective inhibitors of type 5 cyclic guanosine-3',5'-monophosphate phosphodiesterase (cGMP) PDE-5[8,9] and, as such, have utility in the treatment of male erectile dysfunction (MED) and female sexual dysfunction (FSD).[10] C-6 substituted pyrimidinone and pyrimidinedione derivatives showed selective antitumour,[11] antiviral,[12] antitubercular[13] and antifungal activity,[14] suggesting the importance of testing this family of compounds as broad-spectrum drugs.

In the search of bioactive molecules and in continuation of previous work on the development of syntheses of polyfunctionally substituted heterocyclic com-

* Corresponding author. E-mail: Shah_v_h@yahoo.com
doi: 10.2298/JSC0807683D

pounds, a novel synthetic approach for the synthesis of 6-aryl-3-methyl-1,5,6,7--tetrahydro-8*H*-pyrazolo[3',4':4,5]thieno[2,3-*d*]pyrimidin-8-ones (**IIIa**–**j**) is reported herein. All the newly synthesized compounds (**IIIa**–**j**) were evaluated for their antibacterial and antifungal activity. The biological activities of the synthesized compounds were compared with reference standard drugs.

RESULTS AND DISCUSSION

Chemistry

The synthesis of 5-amino-3-methyl-1*H*-thieno[3,2-*c*]pyrazole-6-carbonitrile (**II**) was accomplished by refluxing (5-methyl-2,4-dihydro-3*H*-pyrazol-3-ylidene)malononitrile (**I**) and sulphur in the presence of morpholine for 6 h using the Gewald reaction.[15–20] Compound **II** on reaction with different aromatic ketones in glacial acetic acid furnished the title compounds 6-aryl-3-dimethyl-1,5,6,7--tetrahydro-8*H*-pyrazolo[3',4':4,5]thieno[2,3-*d*]pyrimidin-8-ones (**IIIa**–**h**) in excellent yields (Scheme 1).

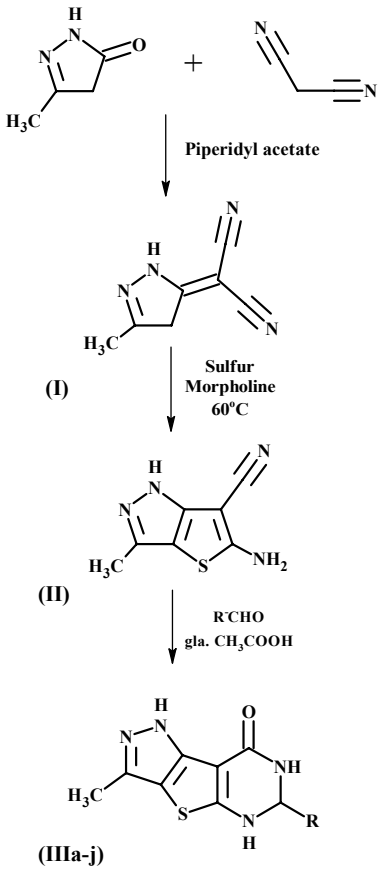

R = phenyl;
2-hydroxyphenyl;
4-hydroxyphenyl;
2-chlorophenyl;
3-chlorophenyl;
4-fluorophenyl;
2-nitrophenyl;
3-nitrophenyl;
4-nitrophenyl;
4-methoxyphenyl.

Scheme 1.

The purity of the compounds was controlled by TLC. The spectral data of all the newly synthesized compounds, given below, were in full agreement with the proposed structures.

*(5-Methyl-2,4-dihydro-3*H*-pyrazol-3-ylidene)malononitrile* ***(I)***. Yield 52 %; m.p.190–192 °C. Anal. Calcd. for $C_7H_6N_4$: C, 57.53; H, 4.14; N, 38.34. Found: C, 57.31; H, 4.02; N, 38.16. IR (KBr, cm^{-1}): 3226 (−NH), 2210 (−CN), 1658 (C=N). ^{1}H-NMR (300 MHz, $CDCl_3$, δ, ppm): 0.9 (3H, *s*, $-CH_3$), 1.9 (2H, *s*, $-CH_2$), 7.1 (1H, *s*, −NH); ^{13}C-NMR (75 MHz, DMSO-d_6, δ, ppm): 19.5, 35.1, 61.8, 113.9, 153.5, 181.3. MS (*m*/*z*): 146.

*5-Amino-3-methyl-1*H*-thieno[3,2-*c*]pyrazole-6-carbonitrile* ***(II)***. Yield 58 %; m.p. 206 °C. Anal. Calcd. for $C_7H_6N_4S$: C, 47.18; H, 3.39; N, 31.44; S, 17.99. Found: C, 46.95; H, 3.19; N, 31.23; S, 17.75. IR (KBr, cm^{-1}): 3420–3305 ($-NH_2$), 2234 (−CN), 1645 (C=N). ^{1}H-NMR (300 MHz, $CDCl_3$, δ, ppm): 2.68 (3H, *s*, $-CH_3$), 4.00 (2H, *s,* $-NH_2$). ^{13}C-NMR (75 MHz, DMSO-d_6, δ, ppm): 14.6, 105.8, 110.8, 114, 135, 136.5, 144. MS (*m*/*z*): 178.

*3-Methyl-6-phenyl-1,5,6,7-tetrahydro-8*H*-pyrazolo[3',4':4,5]thieno[2,3-*d*]pyrimidin-8-one* ***(IIIa)***. Yield 42 %; m.p. 215 °C. Anal. Calcd. for $C_{14}H_{12}N_4OS$: C, 59.14; H, 4.25; N, 19.70; O, 5.63; S, 11.28. Found: C, 59.14; H, 4.25; N, 19.57; O, 5.50; S, 11.13. IR (KBr, cm^{-1}): 3327 (−NH), 3105 (−CH, aromatic), 2970 ($-CH_3$), 1680 (C=O), 681 (C−S−C). ^{1}H-NMR (300 MHz, $CDCl_3$, δ, ppm): 2.23 (3H, *s*, $-CH_3$), 5.90 (1H, *s*, −CH), 7.24–7.72 (4H, *s*, Ar−H). ^{13}C-NMR (75 MHz, DMSO-d_6, δ, ppm): 14.6, 70.6, 106.4, 127.2, 127.4, 128.9, 136.4, 142.7, 144.9, 163.4, 166.0. MS (*m*/*z*): 284.

*6-(2-Hydroxyphenyl)-3-methyl-1,5,6,7-tetrahydro-8*H*-pyrazolo[3',4':4,5]thieno[2,3-*d*]pyrimidin-8-one* ***(IIIb)***: Yield 40 %; m.p. 208 °C. Anal. Calcd. for $C_{14}H_{12}N_4O_2S$: C, 59.14; H, 4.25; N, 19.70; O, 5.63; S, 11.28. Found: C, 58.98; H, 4.11; N, 19.56; O, 5.49; S, 11.15. IR (KBr, cm^{-1}): 3400–3100 (−OH), 3125 (−CH, aromatic), 2975 ($-CH_3$), 1682 (C=O), 680 (C−S−C). ^{1}H-NMR (300 MHz, $CDCl_3$, δ, ppm): 2.32 (3H, *s*, $-CH_3$), 6.01 (1H, *s*, −CH), 6.93–7.24 (4H, *s*, Ar−H), 5.02 (1H, *s*, −OH). ^{13}C-NMR (75 MHz, DMSO-d_6, δ, ppm): 14.7, 60.2, 106.6, 116.2, 122.3, 125.9, 128.6, 129.1, 136.6, 143.1, 145.2, 155.2, 163.2, 165.9. MS (*m*/*z*): 300.

*6-(4-Hydroxyphenyl)-3-methyl-1,5,6,7-tetrahydro-8*H*-pyrazolo[3',4':4,5]thieno[2,3-*d*]pyrimidin-8-one* ***(IIIc)***. Yield 45 %; m.p. 202 °C. Anal. Calcd. for $C_{14}H_{12}N_4O_2S$: C, 59.14; H, 4.25; N, 19.70; O, 5.63; S, 11.28. Found: C, 59.01; H, 4.13; N, 19.58; O, 5.50; S, 11.16. IR (KBr, cm^{-1}): 3450–3100 (−OH), 3110 (−C−H, aromatic), 2970 ($-CH_3$), 1685 (C=O), 685 (C−S−C). ^{1}H-NMR (300 MHz, $CDCl_3$, δ, ppm): 2.22 (3H, *s*, $-CH_3$), 5.91 (1H, *s*, −CH), 6.93–7.14 (4H, *s*, Ar−H), 5.01 (1H, *s*, −OH). ^{13}C-NMR (75 MHz, DMSO-d_6, δ, ppm): 14.6, 70.4, 106.2, 116.4, 129.1, 136.2 , 137.4, 143.1, 145.4, 157.3, 163.6, 166.7. MS (*m*/*z*): 300.

*6-(2-Chlorophenyl)-3-methyl-1,5,6,7-tetrahydro-8*H*-pyrazolo[3',4':4,5]thieno[2,3-*d*]pyrimidin-8-one (**IIId**)*: Yield 48 %; m.p. 238 °C. Anal. Calcd. for $C_{14}H_{11}ClN_4OS$: C, 52.75; H, 3.48; Cl, 11.12; N, 17.58; O, 5.02; S, 10.06. Found: C, 52.62; H, 3.37; Cl, 11.01; N, 17.42; O, 4.89; S, 9.91. IR (KBr, cm^{-1}): 3327 (–NH), 3105 (–CH, aromatic), 2970 ($–CH_3$), 1680 (C=O), 730 (C–Cl), 683 (C–S–C). ^{1}H-NMR (300 MHz, $CDCl_3$, δ, ppm): 2.36 (3H, *s*, $–CH_3$), 6.01 (1H, *s*, –CH), 7.24–7.42 (4H, *s*, Ar–H), 8.12 (1H, *s*, –NH). ^{13}C-NMR (75 MHz, DMSO-d_6, δ, ppm): 14.9, 61.3, 106.4, 126.9, 128.4, 128.7, 128.9, 133.4, 136.4, 143.2, 145.4, 163.4, 166.6. MS (*m*/*z*): 318.

*6-(3-Chlorophenyl)-3-methyl-1,5,6,7-tetrahydro-8*H*-pyrazolo[3',4':4,5]thieno[2,3-*d*]pyrimidin-8-one (**IIIe**)*. Yield 52 %; m.p. 246 °C. Anal. Calcd. for $C_{14}H_{11}ClN_4OS$: C, 52.75; H, 3.48; Cl, 11.12; N, 17.58; O, 5.02; S, 10.06. Found: C, 52.61; H, 3.35; Cl, 10.99; N, 17.42; O, 5.02; S, 10.06. IR (KBr, cm^{-1}): 3340 (−NH), 3115 (−CH, aromatic), 2975 ($−CH_3$), 1683 (C=O), 750 (C−Cl), 685 (C−S−C). ^{1}H-NMR (300 MHz, $CDCl_3$, δ, ppm): 2.39 (3H, *s*, $−CH_3$), 6.02 (1H, *s*, −CH), 7.04–7.22 (4H, *s*, Ar−H). ^{13}C-NMR (75 MHz, DMSO-d_6, δ, ppm): 14.8, 70.1, 106.3, 125.6, 127.4, 127.9, 131.0, 134.6, 136.9, 142.7, 145.2, 146.6, 163.4, 166.0. MS (*m*/*z*): 318.

*6-(4-Fluorophenyl)-3-methyl-1,5,6,7-tetrahydro-8*H*-pyrazolo[3',4':4,5]thieno[2,3-*d*]pyrimidin-8-one (**IIIf**)*. Yield 40 %; m.p. 258 °C. Anal. Calcd. for $C_{14}H_{11}FN_4OS$: C, 55.62; H, 3.67; F, 6.28; N, 18.53; O, 5.29; S, 10.61. Found: C, 55.51; H, 3.54; F, 6.13; N, 18.39; O, 5.16; S, 10.48. IR (KBr, cm^{-1}): 3335 (−NH), 3120 (−CH, aromatic), 2975 ($−CH_3$), 1685 (C=O), 710 (C−F), 689 (C−S−C). ^{1}H-NMR (300 MHz, $CDCl_3$, δ, ppm): 2.45 (3H, *s*, $−CH_3$), 5.90 (1H, *s*, −CH), 7.03–7.11 (4H, *s*, Ar–H). ^{13}C-NMR (75 MHz, DMSO-d_6, δ, ppm): 14.1, 69.6, 106.1, 115.6, 129.0, 136.1, 140.9, 141.9, 145.0, 161.3, 164.4, 166.3. MS (*m*/*z*): 302.

*3-Methyl-6-(2-nitrophenyl)-1,5,6,7-tetrahydro-8*H*-pyrazolo[3',4':4,5]thieno-[2,3-*d*]pyrimidin-8-one (**IIIg**)*. Yield 38 %; m.p. 282 °C. Anal. Calcd. for $C_{14}H_{11}N_5O_3S$: C, 51.06; H, 3.37; N, 21.27; O, 14.57; S, 9.74. Found: C, 50.93; H, 3.25; N, 21.14; O, 14.46; S, 9.60. IR (KBr, cm^{-1}): 3350 (−NH), 3112 (−CH, aromatic), 2970 ($−CH_3$), 1680 (C=O), 691 (C−S−C). ^{1}H-NMR (300 MHz, $CDCl_3$, δ, ppm): 2.35 (3H, *s*, $−CH_3$), 6.01 (1H, *s*, −CH), 7.87–7.43 (4H, *s*, Ar−H). ^{13}C-NMR (75 MHz, DMSO-d_6, δ, ppm): 14.8, 61.2, 106.1, 121.3, 128.0, 128.4, 134.9, 136.0, 137.9, 142.8, 145.4, 147.8, 163.6, 166.4. MS (*m*/*z*): 329.

*3-Methyl-6-(3-nitrophenyl)-1,5,6,7-tetrahydro-8*H*-pyrazolo[3',4':4,5]thieno-[2,3-*d*]pyrimidin-8-one (**IIIh**)*. Yield 35 %; m.p. 275 °C; Anal. Calcd. for $C_{14}H_{11}N_5O_3S$: C, 51.06; H, 3.37; N, 21.27; O, 14.57; S, 9.74. Found: C, 50.96; H, 3.24; N, 21.13; O, 14.45; S, 9.63. IR (KBr, cm^{-1}): 3350 (−NH), 3105 (−CH, aromatic), 2970 ($−CH_3$), 1682 (C=O), 687 (C−S−C). ^{1}H-NMR (300 MHz, $CDCl_3$, δ, ppm): 2.32 (3H, *s*, $−CH_3$), 6.01 (1H, *s*, −CH), 7.35–7.97 (4H, *s*, Ar−H). ^{13}C-NMR

(75 MHz, DMSO-d_6, δ, ppm): 14.6, 69.9, 106.2, 120.4, 122.7, 130.2, 133.6, 142.7, 145.2, 149.6, 163.6, 166.7. MS (*m*/*z*): 329.

*3-Methyl-6-(4-nitrophenyl)-1,5,6,7-tetrahydro-8*H-*pyrazolo[3',4':4,5]thieno-[2,3-*d*]pyrimidin-8-one (**IIIi**)*. Yield 45 %; m.p. 280 °C. Anal. Calcd. for $C_{14}H_{11}N_5O_3S$: C, 51.06; H, 3.37; N, 21.27; O, 14.57; S, 9.74. Found: C, 50.94; H, 3.26; N, 21.15; O, 14.44; S, 9.62. IR (KBr, cm^{-1}): 3340 (−NH), 3114 (−CH, aromatic), 2969 ($-CH_3$), 1682 (C=O), 687 (C−S−C). ^{1}H-NMR (300 MHz, $CDCl_3$, δ, ppm): 2.32 (3H, *s*, $-CH_3$), 5.91 (1H, *s*, −CH), 7.05–7.24 (4H, *s*, Ar−H). ^{13}C-NMR (75 MHz, DMSO-d_6, δ, ppm): 14.5, 70.7, 106.6, 121.8, 128.6, 136.6, 142.7, 144.9, 147.5, 151.9, 163.4, 166.0. MS (*m*/*z*): 329.

*3-Methyl-6-(4-methoxyphenyl)-1,5,6,7-tetrahydro-8*H-*pyrazolo[3',4':4,5]thieno[2,3-*d*]pyrimidin-8-one (**IIIj**)*. Yield 55 %; m.p. 210 °C. Anal. Calcd. for $C_{15}H_{14}N_4O_2S$: C, 57.31; H, 4.49; N, 17.82; O, 10.18; S, 10.20. Found: C, 57.19; H, 4.36; N, 17.69; O, 10.03; S, 10.08. IR (KBr, cm^{-1}): 3327 (−NH), 3105 (−CH, aromatic), 2968 ($-CH_3$), 1685 (C=O), 692 (C−S−C), 1286 (C−O−C). ^{1}H-NMR (300 MHz, $CDCl_3$, δ, ppm): 2.12 (3H, *s*, $-CH_3$), 3.98 (3H, *s*, $-OCH_3$), 5.89 (1H, *s*, −CH), 7.25–7.87 (4H, *s*, Ar−H), 8.58 (1H, *s*,–NH). ^{13}C-NMR (75 MHz, DMSO-d_6, δ, ppm): 14.7, 56.6, 70.4, 106.2, 115.2, 128.6, 136.6, 137.9, 142.6, 145.2, 159.4, 163.6, 166.6. MS (*m*/*z*): 314.

Biological screening

Microbiology. The compounds **IIIa–j** were evaluated for their antimicrobial activity against *Streptococcus pyogenes, Staphylococcus aureus, Escherichia coli, Bacillus subtillis* and antifungal activity against *Candida albicans* and *Aspergillus niger* at a concentration of 50 μg ml^{-1} in DMF using the cup-plate method.[21,22] After 24 h of incubation at 37 °C, the zones of inhibition were measured in mm. The activities were compared with those of some known antibiotics, such as ampicillin, chloramphenicol, norfloxacin and ciprofloxacin, as well as griseofulvin at the same concentration. The results are summarized in Table I.

TABLE I. Antimicrobial activity (zones of inhibition, mm) of 6-aryl-3-methyl-1,5,6,7-tetrahydropyrazolo[3',4':4,5]thieno[2,3-*d*]pyrimidin-8-ones

Compound	Antibacterial activity				Antifungal activity	
	S. pyogenes	*S. aureus*	*E. coli*	*B. subtilis*	*C. albicans*	*A. niger*
IIIa	12	12	10	9	12	11
IIIb	11	14	12	12	13	12
IIIc	12	11	13	11	12	13
IIId	11	11	12	11	11	12
IIIe	9	12	10	10	12	12
IIIf	12	12	11	11	12	11
IIIg	12	11	13	13	11	13
IIIh	10	12	12	12	12	12
IIIi	12	9	10	10	10	10
IIIj	13	14	10	10	10	10

TABLE I. Continued

Compund	Antibacterial activity				Antifungal activity	
	S. pyogenes	*S. aureus*	*E. coli*	*B. subtilis*	*C. albicans*	*A. niger*
Ampicillin	16	18	16	18	–	–
Chloramphenicol	18	16	19	16	–	–
Ciprofloxacin	23	17	20	19	–	–
Norfloxacin	22	20	22	22	–	–
Griseofluvin	–	–	–	–	20	19

EXPERIMENTAL

Melting points were determined routinely in open capillaries and are uncorrected. The formation and purity of the compounds were routinely checked by TLC using silica gel-G. The spots were located under iodine vapour or UV light. The ^{1}H-NMR and ^{13}C-NMR spectra were recorded in $CDCl_3$ on a Brucker DRX-300 at 300 MHz using TMS as the internal standard. The mass spectra were scanned on a GCMS-QP2010 instrument.

*Preparation of (5-methyl-2,4-dihydro-3*H*-pyrazol-3-ylidene)malononitrile (**I**)*

An equimolar mixture of 5-methyl-2,4-dihydro-3*H*-pyrazol-3-one and malononitrile was refluxed in the presence of piperidyl acetate (2–3 drops) for 6 h. The product obtained by pouring the reaction mixture into ice-cold water was filtered, dried and recrystallized from 95 % ethanol.

*Preparation of 5-amino-3-methyl-1*H*-thieno[3,2-*c*]pyrazole-6-carbonitrile (**II**)*

(5-Methyl-2,4-dihydro-3*H*-pyrazol-3-ylidene)malononitrile (**I**) and sulphur were refluxed in the presence of morpholine (3.0 ml) for 6 h. The product obtained by pouring the reaction mixture into ice-cold water was filtered, dried and recrystallized from 95 % ethanol.

*General procedure for synthesis of 6-aryl-3-methyl-1,5,6,7-tetrahydro-8*H*-pyrazolo[3',4':4,5]-thieno[2,3-*d*]pyrimidin-8-ones (**IIIa**–**j**)*

An equimolar mixture of 5-amino-3-methyl-1*H*-thieno[3,2-*c*]pyrazole-6-carbonitrile (**II**) and an appropriate aldehyde in glacial acetic acid (20 ml) was refluxed for 6 h. The product was isolated and recrystallized from 95 % ethanol.

Antibacterial activity

The purified compounds **IIIa**–**j** were screened for their antibacterial activity. The nutrient agar, prepared in the usual manner, was inoculated specially with 0.50 ml of 24 h old subcultures of *Streptococcus pyogenes*, *Staphylococcus aureus*, *Bacillus subtilius* and *Escherichia coli*, taken in separate conical flasks at 40–50 °C, and mixed well by gentle shaking. About 25 ml of the contents of the flask were poured and evenly spread in a Petri dish (13 mm in diameter) and allowed to settle down for 2 h. The cups (10 mm in diameter) were formed with the help of a borer in the agar medium and filled with 40 µl (40 µg ml^{-1}) solution of a sample in DMF. The plates were incubated at 37 °C for 24 h and the control was maintained with 40 µl of DMF in a similar manner. The zones of inhibition of bacterial growth were measured in mm. The antibacterial activity of the compounds **IIIa**–**j** was compared with known standard reference drugs, such as ampicillin, chloramphenicol, norfloxacin, ciprofloxacin at same concentration.

Antifungal activity

Aspergillus niger and *Candida albicans* were employed for testing the fungicidal activity using the cup plate method. The cultures were maintained on Sabouraud's agar slants. Sterilized Sabouraud's agar medium was inoculated with 0.50 ml of a 72 h old suspension of fun-

gal spores from a separate flask. About 25 ml of the inoculated medium was evenly spread in a sterilized Petri dish and allowed to settle down for 2 h. The cups (10 mm in diameter) were punched in the Petri dish and loaded with 4 μl (40 μg ml^{-1}) of solution of a sample in DMF. The plates were incubated at room temperature (30 °C) for 48 h. After completion of the incubation period, the zones of inhibition of growth by compounds **IIIa**–**j** were measured as the diameter in mm. Together with the test solution, one cup in each Petri dish was filled with solvent, which acted as the control. The antifungal activities of compounds **IIIa**–**j** were compared with the known standard drug griseofulvin.

CONCLUSIONS

To summarize, a new class of 6-aryl-3,6-dimethyl-1,5,6,7-tetrahydro-8*H*-pyrazolo[3',4':4,5]thieno[2,3-*d*]pyrimidin-8-ones (**IIIa**–**h**), were synthesized. The newly synthesized heterocycles exhibited moderate to promising antimicrobial activity against standard strains. These results make them interesting lead molecules for further synthetic and biological evaluation. It can be concluded that this class of compounds certainly hold great promise towards the pursuit of discovering novel classes of antimicrobial agents. Further studies to acquire more information concerning structure–activity relationships are in progress.

Acknowledgements. The authors are thankful to the Department of Chemistry, Saurashtra University, for providing laboratory facilities and CDRI Lucknow for providing the ^{1}H-NMR, ^{13}C-NMR and mass spectral facilities.

И З В О Д

КАРАКТЕРИЗАЦИЈА И БИОЛОШКО ТЕСТИРАЊЕ НОВИХ ПИРАЗОЛО[3',4':4,5]ТИЈЕНО[2,3-*d*] ПИРИМИДИН-8-ОНА ДОБИЈЕНИХ ПРИМЕНОМ GEWALD-ОВЕ РЕАКЦИЈЕ

DIPTI K. DODIYA, AMIT R. TRIVEDI, SHAILESH J. VAGHASIA и VIRESH H. SHAH

Department of Chemistry, Saurashtra University, Rajkot-360 005, Gujarat, India

Описана је синтеза супституисаних пиразоло[3',4':4,5]тијено[2,3-*d*]пиримидин-8-она (**IIIa**–**j**) из 5-амино-3-метил-1*H*-тијено[3,2-*c*]пиразол-6-карбонитрила (**II**). Кључно једињење **II** синтетизовано је из (5-метил-2,4-дихидро-3*H*-пиразол-3-илиден)малононитрила (**I**) применом Gewald-ове реакције. Синтеза једињења **IIIa**–**j** извршена је кондензацијом једињења **II** са различитим ароматичним алдехидима. Ново-добијена хетероциклична једињења окарактерисана су помоћу елементалне анализе и IR, ^{1}H-NMR, ^{13}C-NMR и MS спектралних података. Сва једињења тестирана су на антимикробну активност према различитим бактеријским сојевима.

(Примљено 6. децембра 2007, ревидирано 13. марта 2008)

REFERENCES

1. W. E. Kirkpatrick, T. Okabe, I. W. Hillyard, R. K. Robins, A. T. Dren, T. Novinson, *J. Med Chem*. **20** (1977) 386
2. A. A. Elagamy, F. M. A. El-Taweel, F. A. Amer, H. H. Zoorob, *Arch. Pharm.* **246** (1987) 320
3. (a) A. N. Kost, I. I. Grandberg, in *Advances in Heterocyclic Chemistry*, A. R. Katritzky Ed., Academic Press, New York, 1996, p. 347; (b) H. B. Nihset, *J. Chem. Soc*. **12** (1938) 1568
4. G. W. Raiziss, L. W. Clemence, M. Friefelder, *J. Am. Chem. Soc*. **63** (1941) 2739

5. Warner-Lambert Co., Jpn. Kokai Tokkyo Koho Jp., 61, 236, 778, 1986
6. S. D. Lindell, B. A. Moloney, B. D. Hewitt, C. G. Earnhaw, P. J. Philip, J. E. Dancer, *Bioorg. Med. Chem. Lett*. **9** (1999) 1985
7. Y. S. Sanghvi, S. B. Larson, D. F. Smee, G. R. Revankar, R. K. Robins, *Nucleosides, Nucleotides* **10** (1991) 1417
8. M. K Bunnage, J. P. Mathias, S. D. A. Street, A. Wood, PCT Int. Appl. WO, 14, 333, 487, 1999
9. A. S. Bell, N. K. Terrett, Eur. Pat. EP 526, 004, 1993
10. P. C. Doherty, Jr., V. A. Place, W. L. Smith, PCT Int. Appl. 9, 921, 558, 1999
11. (a) G. M. Szczech, P. Furman, G. R. Painter, D. W. Barry, K. Borroto-Esoda, T. B. Grizzle, M. R. Blum, J. P. Sommadossi, R. Endoh, T. Niwa, M. Yamamoto, C. Moxham, *Antimicrob. Agents Chemother.* **44** (2000) 123; (b) F. J. Giles, E. J. Feldman, G. J. Roboz, R. A. Larson, S. W. Mamus, J. E. Cortes, S. Verstovsek, S. Federl, M. Talpaz, M. Beran, M. Albitar, S. M. O'Brien, H. M. Kantarjian, *Leuk. Res.* **27** (2003) 1091; (c) F. J. Giles, *Expert Rev. Anticancer Ther.* **2** (2002) 261; (d) J. Toyohara, A. Hayashi, M. Sato, A. Gogami, H. Tanaka, K. Haraguchi, Y. Yoshimura, H. Kumamoto, Y. Yonekura, Y. Fujibayashi, *Nucl. Med. Biol.* **30** (2003) 687; (e) T. J. Mangner, R. W. Klecker, L. Anderson, A. F. Shields, *Nucl. Med. Biol.* **30** (2003) 215; (f) J. Toyohara, Y. Fujibayashi, *Nucl. Med. Biol.* **30** (2003) 681; (g) F. Dieterle, S. Müller-Hagedon, H. M. Liebich, G. Gauglitz, *Artif. Intell. Med.* **28 (**2003) 265
12. (a) D. C. Rowley, M. S. T. Hansen, D. Rhodes, C. A. Striffer, H. Ni, J. A. McCammon, F. D. Bushman, W. Fenical, *Bioorg. Med. Chem.* **10** (2002) 3619; (b) A. Arnaud, L. Fontana, A. J. Angulo, Á. Gil, J. M. López-Pedrosa, *Clin. Nutr.* **22** (2003) 391; (c) J. E. Gallant, *J. Clin. Virol.* **25** (2002) 317
13. (a) P. Molina, E. Aller, A. Lorenzo, P. Lopez-Cremades, I. Rioja, A. Ubeda, M. C. Terencio, M. J. Alcaraz, *J. Med. Chem.* **44** (2001) 1011; (b) A. Kumar, S. P. Sinha, M. S. Chauhan, *Bioorg. Med. Chem. Lett.* **12** (2002) 667
14. (a) J. B. Bher, T. Gourlain, A. Helimi, G. Guillerm, *Bioorg. Med. Chem. Lett.* **13 (**2003) 1713; (b) H. P. De Koning, M. I. Al-Salabi, A. M. Cohen, G. H. Coombs, J. M. Wastling, *Int. J. Parasitol.* **33** (2003) 821
15. K. Gewald, *Chem. Heterocycl. Compd*. *Engl.Transl.* **12** (1976) 1077
16. E. C. Taglor, G. Berger, *J. Org. Chem.* **32** (1967) 2376
17. V. P. Arya, S. J. Shenoy, *Indian J. Chem.* **10** (1972) 815
18. A. Rosoasky, K. K. N. Chen, M. Lin. *J. Med. Chem*. **16** (1973) 191
19. L. G. Sharanina, S. N. Barana, *Chem. Heterocycl. Compd. Engl. Transl.* **10** (1974) 171
20. S. A. Swelam, M. E. A. Abdel Salam, O. L. Zaki, *Indian J. Heterocycl. Chem*. **8** (1999) 257
21. A. L. Barry, in *The Antimicrobic Susceptibility Test: Principles and Practices*, A. L. Barry Ed., Lea and Febiger, Philadelphia, PA, 1976, p. 180
22. *Manual of Clinical microbiology*, 6th Ed., P. R. Murray, E. J. Baron, M. A. Pfaller, F. C. Tenover, H. R. Yolken, Eds., ASM Press, Washington DC, 1995, p. 15.

www.shd.org.rs

Journal of the Serbian Chemical Society

JSCS@tmf.bg.ac.yu • www.shd.org.rs/JSCS

J. Serb. Chem. Soc. 73 (7) 691–701 (2008)
JSCS–3752

UDC 547.1–304+542.91:543.612
Original scientific paper

Analysis of amphetamines illegally produced in Serbia§

MARINA NEVEŠĆANIN[1], SONJA BANOVIĆ STEVIĆ[1]*, SLOBODAN PETROVIĆ[2#] and VLATKA VAJS[3#]

[1]*Institute of Security, Kraljice Ane bb, 11 000 Belgrade,* [2]*Faculty of Technology and Metallurgy, University of Belgrade, Karnegijeva 4, 11120 Belgrade and* [3]*Faculty of Chemistry, University of Belgrade, Studentski Trg 16, 11001 Belgrade, Serbia*

(Received 25 March 2008)

Abstract: Forensic practice in the Republic of Serbia faced the illegal production of amphetamine for the first time in 2003. This paper presents the results of the chemical characterization of 32 batches of amphetamine samples from three separate cases, for the purpose of identification of the active components and additives. Through the profiling of impurities of all samples, using gas chromatography/mass spectrometry (GC/MS), 30 compounds associated with amphetamine were identified. The results of the analysis of powder tartrate, sulfate and phosphate salts of amphetamine, as well as variously formulated tablets are presented in this study. The analyses showed that the amphetamines were synthesized by the Leuckart method in all cases.

Keywords: amphetamine; impurity profiling; Leuckart synthesis.

INTRODUCTION

Abuse of amphetamine type stimulants (ATS) is on the rise worldwide. According to UNODC data, the number of ATS users is larger than the number of heroin and cocaine users combined. The situation is similar on the illegal market of the Republic of Serbia: ATS abuse is increasing; ecstasy tablets containing the active agent MDMA are the most common, amphetamines are less common, while abuse of methamphetamine is negligible. According to 2003 data, Europe is considered the largest consumer and producer of amphetamine. Reports submitted to Interpol by East European member countries mention the production of amphetamine tablets intended for the illicit market in the Middle Eastern countries. Three illegal amphetamine laboratories in parallel producing tablets were discovered on the territory of the Republic of Serbia in 2003. According to UN

§ A part of this work was presented at the 17th Meeting of the International Association of Forensic Sciences, Hong Kong, 2006.

* Corresponding author. E-mail: sonjabs@ib.bitsyu.net

Serbian Chemical Society member.

doi: 10.2298/JSC0807691N

data, one of them was among the largest discovered to date in Europe, with an estimated production of several tons of amphetamine salts. All the discovered tablets had the characteristic "captagon" logo on them, and were never again found on the illegal market of the Republic of Serbia.

Amphetamine ((±)-2-amino-1-phenylpropane), one of the oldest synthetic stimulants, was first synthesized in 1887. The synthesis of amphetamine by the Leuckart method[1] is most commonly performed illegally and is accompanied by varying levels of impurities in the final product, depending on the quality of the starting materials, route of synthesis, reaction conditions, extent of purification of the final product and, above all, on the skills of the clandestine chemist.[2–8]

"Captagon" is a trademark of a drug containing the active substance fenethylline hydrochloride, a theophylline derivative of amphetamine having effects similar to those of amphetamine. It is used in medicine as a medicament for hyperactivity disorders in children, but is also subject to abuse.[9] The primary market for fenethylline has traditionally been countries located on the Arabian Peninsula, namely Saudi Arabia, Kuwait and Qatar, where fenethylline is one of the most popular drugs among the younger population.[10] Tablets with the "Captagon" logo have also been seized in Turkey, where illegal production was also discovered.[11] In Jordan, a transient country for illicit Captagon tablets, geographically located between the European countries, where they are produced, and the Arabian Peninsula consuming countries, multiple capture of such tablets have been accomplished. Alabdalla in his study determined the chemical composition of those seized tablets.[12] The common point of all the published analyses of "Captagon" tablets is the absence of fenethylline and the presence of amphetamine in combination with caffeine, quinine and several other substances.[10–12]

In this study, the powder substances and tablets seized in police raids on illegal laboratories were analyzed and compared. The results of routine chemical characterization based on the identification of components through FTIR and GC/MS, as well as the results of the determination of organic impurities, in order to determine the route of synthesis, through GC/MS[13,14] are quoted. This is one of the first studies of this type conducted in our laboratory; therefore, identification was made through comparison with bibliographical data[15–20] and NIST database spectra, without any reference standards.

EXPERIMENTAL

Materials and reagents

In this study, 32 types of amphetamine samples from three different criminal cases of illegal production on the territory of the Republic of Serbia were analyzed. From case I, 3 kinds of powder samples (I-10–I-12, from seizures of 6.74, 2.36 and 48 kg, respectively) and 20 types of tablets (total weight of 33.06 kg) of various colors and forms were analyzed (I-1–I-9 and I-13–I-23). From case II, 7 white-colored powder samples (4 kg in 7 separate packets, II-1––II-7), as well as tablets (total weight of 12 kg, II-8) were analyzed. From case III, tablets (III-1)

with the same appearance and content, seized in the tablet production plant, were analyzed. The average weight of a tablet from all three seized batches was 170 mg, while average dimensions were 8 mm in diameter and 3.5 mm in thickness. They were of different colors (brown, cocoa, beige, yellow, pink, pastel pink, ivory, gray and white), and were marked with the "Captagon" logo on one side, and scored on the other, as shown in Fig. 1.

Fig. 1. Photograph of a tablet produced in Serbia.

The D,L-amphetamine reference standard ($C_9H_{13}N\times HCl$) was obtained from the UN (Lipomed, Switzerland). All the reagents used in the study (chloroform, toluene, octadecane, KBr, tris, water) were of analytical grade purity.

Instrumentation

Infrared spectra (450–4000 cm^{-1}) of the compounds were obtained using the KBr disc technique or thin films on KBr plates; Thermo Nicolet 5700 and Spectrum One (Perkin–Elmer) instruments were used for the measurements.

Gas chromatography/mass spectrometry was performed using a ThermoFinnigan TraceGC gas chromatograph interfaced with an ion trap PolarisQ mass spectrometer. One microliter of each extract was injected in the splitless mode using a CombiPal autosampler. The column was an Rtx-5MS capillary column (crossbond 5 % diphenyl–95 % dimethylpolysiloxane); 30 m (*L*)×0.32 mm (i.d.) with a 0.25 μm film thickness. The oven temperature was programmed as follows: initial temperature 90 °C, delay for 1.0 min, ramp to 300 °C at a rate of 8.0 °C min^{-1}, held for a further 10 min). The injection port and transfer line temperatures were set to 250 and 275 °C, respectively. The ion source temperature was set at 230 °C, while the flow rate of He carrier gas was fixed at 1.0 ml min^{-1}. The mass spectrometer was tuned to electron impact ionization (EI); the mass spectra were recorded in intervals from *m*/*z* 30 to 300.

Sample preparation

Standard extraction procedure. Preparation of the sample for conventional chemical characterization was made according to the traditional fractional extraction method, depending on the solubility specific to a particular class of compounds, followed by successive measurement of the extracts or residues by FTIR and/or GC/MS. Traditional wet-chemistry anion tests were used to determine sulfate, phosphate and tartrate.[13]

Extraction of impurities. Amphetamine powder samples (200±5 mg of each sample) and thoroughly crushed whole pills (average mass 170±5 mg) were dissolved in Tris buffer (4.0 ml, 0.10 M, pH 8.10) and the mixture was shaken for 10 min. Toluene (200 μl) containing octadecane as internal standard (10 μg ml^{-1}) was added and the test tube shaken for a further 10 min and then centrifuged at 3000 rpm for 3.0 min. An aliquot of the organic layer was analyzed by GC/MS.

RESULTS AND DISCUSSION

Powder substances from case I were identified by infrared spectrometry as amphetamine tartrate (I-10), amphetamine sulfate (I-11) and mixture of amphetamine sulfate and lactose (I-12), while all 7 powder substances from case II (II-1––II-7) were amphetamine phosphate salts. The infrared spectrum of the amphetamine tartrate salt (detected for the first time in Serbia) is shown in Fig. 2.

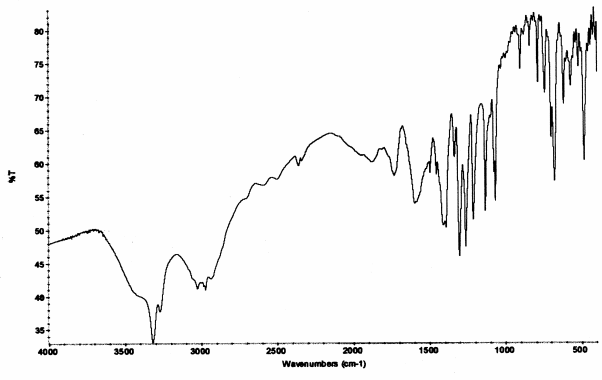

Fig. 2. Infrared spectrum of amphetamine tartrate.

The physical characteristics and logo of the tablets were almost identical in all three cases. Amphetamine (in concentrations ranging from 4.0 to 25 %) was identified in all the analyzed tablets. The chemical characterization of the illegal amphetamine tablets produced in Serbia is shown in Table I; wherein the composition of selected tablets of heterogeneous contents are shown from case I, while II-8 and III-1 refer to cases II and III, where there was no difference in their content and appearance.

TABLE I. Substances detected in nine tablets as representative of the total seized batch

Sample	Color	Amphetamine			Adulterant				Diluents		
		Sulfate	Tartrate	Phosphate	Caffeine	Quinine	Amino-pyrine	Ranitidine	Lactose	Microcr. cellulose	Others[a]
I-4	Pink	√[b]			√		√		√	√	√
I-5	White	√							√	√	√
I-14	Pastel pink	√	√			√			√	√	√
I-20	Gray	√				√	√		√	√	
I-21	Beige	√			√	√		√	√	√	√
I-22	Ivory	√	√		√	√	√		√	√	√
I-23	Yellow	√	√		√	√			√	√	
II-8	Pink			√	√	√			√		√
III-1	Pink			√	√	√			√		√

[a]Povidone and/or starch/stearic acid/glucose; [b]detected

White tablets (5 kinds), which were all from case I but found at different locations in the tablet producing plant, contained solely amphetamine sulfate in higher concentrations, whereas the colored tablets (17 kinds) contained a mixture of amphetamine salts, caffeine and quinine, and, in some cases, aminopyrine and ranitidine. Lactose, microcrystal cellulose, povidone and/or starch/stearic acid/glucose were used as excipients.

It is interesting that within a single clandestine laboratory various salts and huge variations in the diluents, adulterants and excipients were found.

A complete analysis of the impurities present was performed by GC/MS. The compounds were identified based on comparison with reference spectra (Wiley and NIST database) or comparing the ion chromatograms with the spectra from the available literature.

The chromatograms of the accompanying impurities in three types of amphetamine salt samples are shown in Fig. 3.

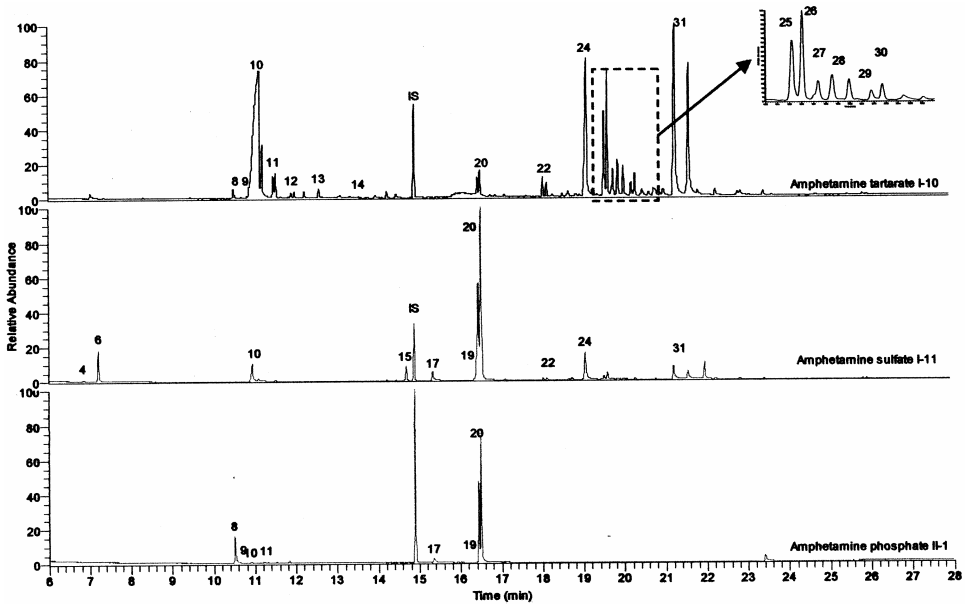

Fig. 3. Chromatograms between 6 and 28 min of impurities in tartrate, sulfate and phosphate amphetamine salts with expansion of the data between 19.30 and 20.70 min, and the identity of the main peaks.

A list of the main impurities and their characteristic mass ions found as a result of GC/MS analysis is given in Table II. The identification numbers associated with the compounds is connected with the annotated peaks in Figs. 3 and 4.

Some of the listed compounds were not visible in the chromatograms (Figs. 3 and 4) because they were either not present or present in only trace amounts in the selected samples. Impurity origins quoted in Table II are not exclusive.

All the samples analyzed in this study contained benzyl methyl ketone (BMK, R_t = 5.3 min), identified using extracted ion chromatograms, although its peak was irresolvable from the much larger amphetamine peak. The main product, amphetamine (R_t = 5.3 min) is not visible within the time range presented in Figs. 3 and 4.

Compounds which eluted at 10.51 and 10.84 min in an abundance ratio of about 5:1 were identified as 4-methyl-5-phenylpyrimidine (8) and 4-benzylpyrimidine (9). These are impurities connected entirely with the Leuckart method of

amphetamine synthesis.[8] The peak eluting at 11.13 min retention time is *N*-formylamphetamine (10), which can, when remaining in large quantities as a consequence of incomplete hydrolysis, mask the presence of pyrimidine derivatives under the given chromatographic conditions.

TABLE II. Compounds detected in samples through gas chromatograph/mass spectrometry

Compound	*m/z*	R_t	Origin
Amphetamine	44, 91, 120	5.35	Major product
Benzyl methyl ketone (P2P)	43, 91, 134	5.35	Precursor
Methamphetamine	58, 91, 92, 65	6.08	By-product
N-Ethylamphetamine	72, 44, 91	6.84	By-product
N,*N*-Dimethylamphetamine	72, 91, 65	7.01	By-product
Isopropylamphetamine	86, 44, 91, 120	7.22	By-product
Ephedrine/pseudoephedrine	58, 77, 105	9.04	Adulterant/ /contaminant
4-Methyl-5-phenylpyrimidine	170, 169, 102, 115	10.51	By-product
4-Benzylpyrimidine	169, 170, 115, 91	10.84	By-product
N-Formylamphetamine	118, 72, 91, 44	11.13	Intermediate
Unidentified-11	198, 197, 115, 116	11.54	Unknown
N-Formylmethamphetamine	86, 58, 118	11.91	Intermediate
Unidentified-13	100, 72, 44	12.58	Unknown
1,3-Diphenyl-2-propanone	91,65, 119, 210	13.53	Impurity BMK (P2P)
N-(*β*-Phenylisopropyl)benzaldimine	132, 105, 91	14.68	By-product
Octadecane	57	14.90	IS
1,3-Diphenylisopylamine	120, 91, 103	15.34	By-product
Caffeine	194	15.84	Adulterant
α-Methyldiphenethylamine	148, 105, 91	16.40	By-product
Bis(*β*-phenylisopropyl)amine[a]	162, 91, 119, 44	16.42, 16.50	By-product
Aminopyrine	231, 97, 56	17.06	Adulterant
N,*N*-Bis(*β*-phenylisopropyl)methylamine[a]	176, 91, 58, 119	18.03, 18.13	By-product
N-benzoylamphetamine	105, 148, 77, 118	18.62	By-product
Unidentified-24	44, 91, 162, 65	19.10	Unknown
Pyridine P1[b]	273	19.51	By-product
Pyridine P2[b]	272, 273	19.60	By-product
Pyridine P3[b]	258, 259	19.73	By-product
Pyridine P4[b]	258	19.85	By-product
Pyridine P5[b]	258	19.99	By-product
Pyridine P6[b]	272	20.27	By-product
N,*N*-Bis(*β*-phenylisopropyl)formamide[a]	190, 91, 119, 162	21.20, 21.56	By-product
Unidentified-32	91, 132, 133, 222	26.24	Unknown
Quinine	136	26.69	Adulterant

[a]Stereoisomers; [b]temporarily identified compound

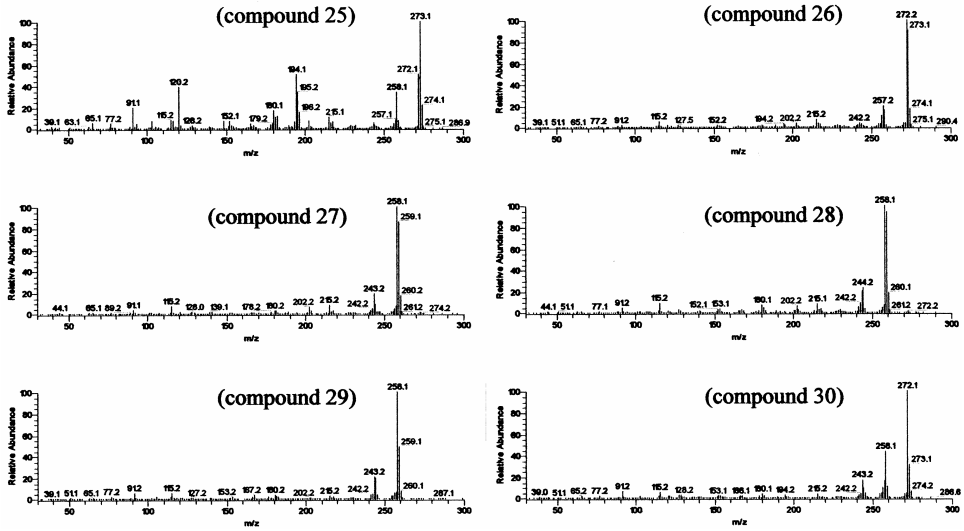

Fig. 4. Profiling of selected tablets with the identity of the major peaks.

Three pairs of peaks eluting at 16.42/16.50, 18.03/18.13, and 21.20/21.56 min show the elution characteristics of non-resolved stereoisomers and the mass spectra of bis(*β*-phenylisopropyl)amine (20), *N,N*-bis(*β*-phenylisopropyl)methylamine (22) and *N,N*-bis(*β*-phenylisopropyl)formamide (31).

As by-products in the analyzed samples, methamphetamine (R_t = 6.13 min), *N*-formyl methamphetamine (R_t = 11.91 min), *N*-ethylamphetamine (R_t = 6.84 min), *N,N*-dimethylamphetamine (R_t = 7.01 min) and isopropylamphetamine (R_t = 7.22 min) were also found.

The origin of 1,3-diphenyl-2-propanone (R_t = 13.53 min) is the impurity of the starting material BMK (P2P) and it is supposed that 1,3-diphenyl-isopropylamine (R_t = 15.34 min) was formed in the course of amphetamine synthesis as the aminated derivative of the above mentioned ketone.

For the following group of compounds, the identification approach had a temporary character: in the time interval between 19 and 21 min (Fig. 3), a group of compounds elute showing poor mass spectra with fragmentation with base peaks at *m*/*z* 258, 259 or 272, 273 (Fig. 5). The high abundance of such ions could indicate the presence of very stable molecules which do not readily undergo the fragmentation process. The most likely structure of these molecules is composed of the so-called pyridines, well known from the literature on the preparation of amphetamine by the Leuckart synthesis as "high-boiling pyridines".[3,16–18]

Through extraction of ion *m*/*z* 105, a chromatogram was obtained with the peaks of *α*-methyldiphenethylamine (R_t = 16.40 min) and *N*-benzoylamphetamine (R_t = 18.62 min).[18,19]

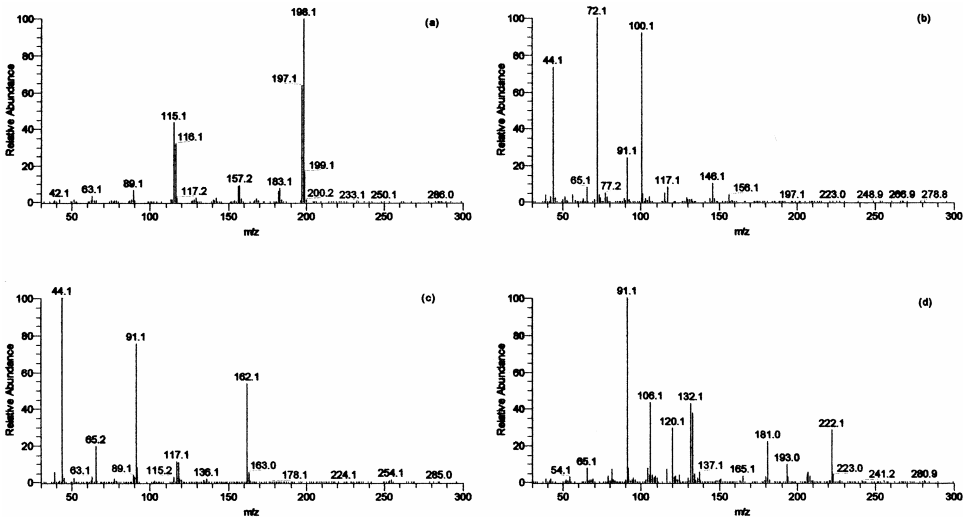

Fig. 5. Mass spectra of the pyridine derivatives with M_r = 259 and 273 g mol^{-1}.

The occurrence of Schiff bases in illicit amphetamine preparations has already been published by Theeuwen and Verweij.[20] These authors stated that imines could be found in every amphetamine synthesis in which P2P was employed as a precursor. Due to their instability in strongly acid environment, after the second step of the Leuckart synthesis, detection of imines in relatively small quantities is to be expected. *N*-(*β*-Phenylisopropyl)benzalimine was also identified in the tablets, although only in traces, at 14.68 min.

Neither a comprehensive bibliographical search, nor spectral analysis, resulted in the final identification of compounds marked with the numbers 11, 13, 24 and 32, the mass spectra of which are shown in Fig. 6. Unidentified compound 11, detected in all the samples, has the fragmentation of 5-benzyl-2,3-dimethylpyrazine or 2-benzyl-5,6-dimethylpyrazine; as for compound 13, it is assumed to be *N,N*-diethylamphetamine. The unidentified compound 24 is also noteworthy; in all the analyzed samples it eluted at 19.09 min, with a fragmentation very similar to that of compound 20, but with different relative ion ratios.

Although the amphetamine sulfate and tartrate originated from the same illegal production, a difference in their impurity levels was evident. It was revealed that although compound 20 was the dominant impurity in amphetamine sulfate, it was only found in traces when compared to compound 10 and its methylized (22) and formylized (31) derivatives in the tartrate salt.

The amphetamine phosphate samples from case II were poorer and only compound 20 was detected as the main impurity, with traces of compound 8. The absence of compound 10 was easily noticeable, which corresponds to earlier findings (internal unpublished results) connected with the establishment of proofs in the production plant itself, which indicated a thorough approach to the synthesis,

where control of the hydrolysis stage of *N*-formylamphetamine to amphetamine by TLC was performed in the plant. The conclusion that the synthetic route was Leuckart reaction was made because of the presence of compound 8.

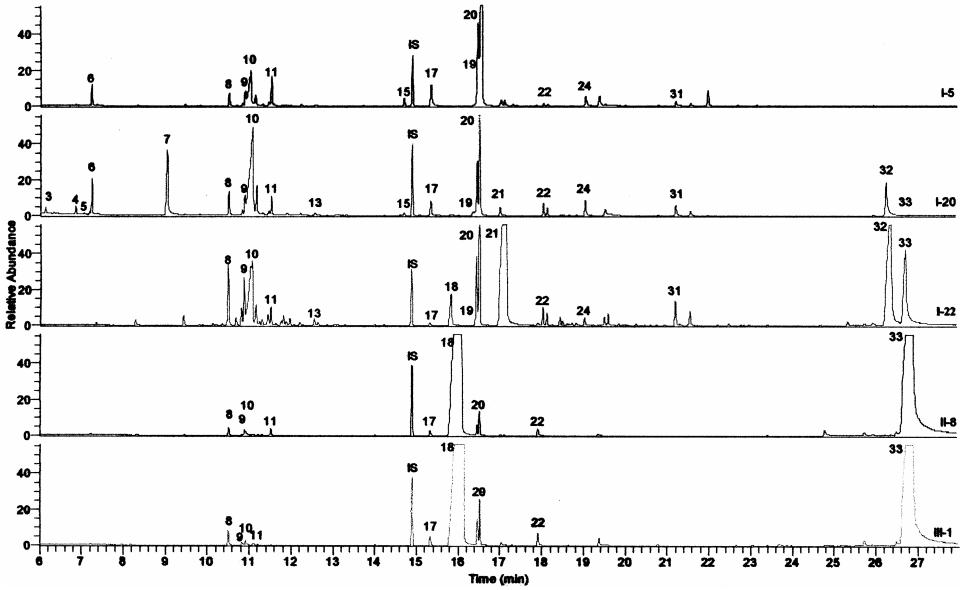

Fig. 6. Mass spectra of unidentified compounds: (a) compound 11; (b) compound 13; (c) compound 24; (d) compound 32.

Among the impurities detected in the analyzed tablets are all the impurities also contained in the powder substances (compounds 3, 4, 5, 6, 8, 9, 10, 11, 12, 13, 15, 17, 19, 20, 22, 24 and 31 listed in Table II and shown in Figs. 3 and 4). The impurity profiling chromatograms of selected tablets from case I, II and III, the chemical characterization of which were given in Tables I and II, are shown in Fig. 4.

The analyzed white tablets (5 types) found at different locations in the tablet--making plant (case I) had a relatively similar characteristic impurity profile, as they contained solely amphetamine sulfate. The main impurity was compound 20. The content of impurities, *i.e.*, their relative main impurity concentration ratio, varied more in the colored tablets (15 types), which could be explained by the presence of a mixture of amphetamine salts. However, this evidence is not conclusive, as the origin of the production batches could not be determined. The main impurities in these cases were compounds 10, 20 and 8.

In some tablets, ephedrine/pseudoephedrine was identified (R_t = 9.04 min), for which it is supposed that it was present as a contaminant from the tablet-making process, or a deliberately added adulterant.

In tablets containing aminopyrine (Fig. 4, chromatograms I-20 and I-22) the peak at retention time 26.24 min belongs to the unidentified compound 32, the mass spectrum of which is shown in Fig. 6d.

Impurity profiling of tablets from cases II and III (Fig. 4, chromatograms II-8 and III-1) shows their essential similarity in the presence of compound 20, as the main impurity, and compounds 8, 9 and 10, as well as a significant dissimilarity from the profile of all the tablets from case I.

CONCLUSION

It was established that the amphetamines produced in clandestine labs in Serbia were in the form of sulfates, tartrates and phosphates. The amphetamine tartrate form is reported for the first time in the Republic of Serbia. From the results of the analysis of the tablets, it should be emphasized that they contained a mix of amphetamine salts and a great variety of additives. The complex mixtures of additives used included caffeine, quinine, aminopyrine, ranitidine, lactose, glucose, starch, microcrystal cellulose, povidone and/or stearic acid. Although engraved with the usual logo previously encountered in captagon, the tablets did not contain fenethylline. The presence of the synergically acting amphetamine, caffeine and quinine, as well as the characteristic logo, suggest that all the seized quantities were intended for the illegal market as surrogate for captagon. The impurity profiles of all the analyzed samples show that the synthetic route for amphetamine was the Leuckart reaction.

И З В О Д

АНАЛИЗА АМФЕТАМИНА ИЛЕГАЛНО ПРОИЗВЕДЕНОГ У СРБИЈИ

МАРИНА НЕВЕШЋАНИН[1], СОЊА БАНОВИЋ СТЕВИЋ[1], СЛОБОДАН ПЕТРОВИЋ[2] и ВЛАТКА ВАЈС[3]

[1]Институт безбедности, Краљице Ане бб, 11000 Београд, [2]Технолошко–металуршки факултет Универзитета у Београду, Карнегијева 4, 11120 Београд и [3]Хемијски факултет Универзитета у Београду, Студентски трг 16, Београд

Форензичка пракса у Републици Србији се први пут срела са илегалном производњом амфетамина 2003. године. У овом раду представљени су резултати хемијске карактеризације 32 врсте узорака амфетамина који потичу из три одвојена случаја у циљу идентификације активних компоненти и адитива. Профилисањем нечистоћа свих узорака помоћу гасно–масене спектрометрије идентификовано је 30 једињења повезаних са амфетамином. Дати су резултати анализа прашкастих тартаратних, сулфатних и фосфатних соли амфетамина као и различито формулисаних таблета. Анализе нечистоћа су показале да је у свим случајевима синтеза амфетамина вршена Leuckart-овом реакцијом.

(Примљено 25. марта 2008)

REFERENCES

1. M. L. Moore, *The Leuckart reaction, Organic reaction*, Vol. V, John Wiley, New York, 1949
2. *Drug characterization/Impurity profiling*, UN, Vienna, 2000, ST/NAR/32
3. A. M. Van der Ark, A. M. A. Verweij, A. Sinnema, *J. Forensic Sci.* **23** (1978) 693

4. T. C. Kram, *J. Forensic Sci.* **24** (1979) 596
5. A. Sinnema, A. M. A. Verweij, *Bull. Narc.* **33** (1981) 37
6. M. Lambrechts, K. E. Rasmussen, *Bull. Narc.* **36** (1984) 47
7. M. Lambrechts, T. Klemetsrud, K. E. Rasmussen, H. J. Storesund, *J. Chromatogr. A* **284** (1984) 499
8. A. M. A. Verweij, *Forensic Sci. Rev.* **1** (1989) 1
9. *Martindale: the complete drug reference*, S. C. Sweetman, Ed.,The Pharmaceutical Press, London, 2002, p. 1509
10. *Fenethylline and the Middle East. A Brief Summary*, Drug Enforcement Administration, USA, 2003, DEA-03046
11. E. Seven, T. Bora, M. Çavuş, D. N. Inceoğlu, E. Ö. Azak, in *Proceedings of the 3rd EAFS Meeting*, Istanbul, Turkey, (2003)
12. M.A. Alabdalla, *Forensic Sci. Int.* **152** (2005) 185
13. *Recommended methods for testing amphetamine and methamphetamine*, UN, New York, 1987, ST/NAR/9
14. K. Andersson, K. Jalava, E. Lock, Y. Finnon, S. Stevenson, L. Aalberg, H. Huizer, E. Kaa, A. Lopes, A. Poortman-van der Meer, M. D. Cole, J. Dahlén, E. Sippola, *Forensic Sci. Int.* **169** (2007) 64
15. V. Ottaviano, C. Furnari, F. Rosati, *Ann. 1st Super Sanità* **38** (2002) 331
16. L. Aalberg, K. Andersson, C. Bertler, H. Borén, M. D. Cole, J. Dahlén, Y. Finnon, H. Huizer, K. Jalava, E. Kaa, E. Lock, A. Lopes, A. Poortman-van der Meer, E. Sippola, *Forensic Sci. Int.* **149** (2005) 219
17. E. Lock, L. Aalberg, K. Andersson, J. Dahlén, M. D. Cole, Y. Finnon, H. Huizer, K. Jalava, E. Kaa, A. Lopes, A. Poortman-van der Meer, E. Sippola, *Forensic Sci. Int*. **169** (2007) 77
18. K. Andersson, E. Lock, K. Jalava, H. Huizer, S. Jonson, E. Kaa, A. Lopes, A. Poortman-van der Meer, E. Sippola, L. Dujourdy, J. Dahlén, *Forensic Sci. Int.* **169** (2007) 86
19. Y. Qi, I. Evans, A. McCluskey, *Forensic Sci. Int*. **169** (2007) 173
20. A. B. E. Theeuwen, A. M. A. Verweij, *Forensic Sci. Int.* **15** (1980) 237.

www.shd.org.rs

Journal of the Serbian Chemical Society

JSCS@tmf.bg.ac.yu • www.shd.org.rs/JSCS

J. Serb. Chem. Soc. 73 (7) 703–711 (2008)
JSCS–3753

UDC **Satureja horvatii*:665.52/.54:615.28–188
Original scientific paper

Chemical composition and antimicrobial activity of the essential oil from *Satureja horvatii* Šilić (Lamiaceae)

BRANISLAVA LAKUŠIĆ[1]*, MIHAILO RISTIĆ[2], VIOLETA SLAVKOVSKA[1], JELENA ANTIĆ STANKOVIĆ[3] and MARINA MILENKOVIĆ[3]

[1]*Institute of Botany, Faculty of Pharmacy, University of Belgrade, Vojvode Stepe 450, 11000 Belgrade,* [2]*Institute for Medicinal Plant Research "Josif Pančić", Tadeuša Košćuškog 1, 11000 Belgrade and* [3]*Institute of Microbiology, Faculty of Pharmacy, University of Belgrade, Vojvode Stepe 450, 11000 Belgrade, Serbia*

(Received 16 October 2007, revised 18 January 2008)

Abstract: The present paper describes the chemical composition and antimicrobial activity of the essential oil of the endemic species *Satureja horvatii* Šilić, collected in Montenegro. The essential oil was obtained from the aerial parts of the plant by hydrodistillation and analyzed by GC–MS. From the 34 compounds representing 100 % of the oil, the major compound was the phenolic monoterpene thymol (63.37 %). The oil contained smaller amounts of γ-terpinene (7.49 %), carvacrol methyl ether (4.92 %), carvacrol (4.67 %), *p*-cymene (4.52%), α-terpinene (1.81 %), borneol (1.58 %), α-thujene (1.56 %), β-caryophyllene (1.55 %) and β-myrcene (1.44 %). The antimicrobial activity of the essential oil of *S. horvatii* was evaluated using the agar diffusion and broth microdilution methods. The essential oil exhibited antimicrobial activity to varying degrees against all the tested strains. The maximum activity of *S. horvatii* oil was observed against Gram-positive bacteria (*Micrococcus luteus, Staphylococcus epidermidis, Staphylococcus aureus* and *Enterococcus faecalis*) and against the yeast (*Candida albicans*). The oil exhibited moderate activity against the Gram-negative bacteria *Escherichia coli* and *Klebsiella pneumoniae* and weak activity against *Pseudomonas aeruginosa*. This study confirms that the essential oil of *S. horvatii* possesses antimicrobial activities *in vitro* against medically important pathogens.

Keywords: *Satureja horvatii*; endemic species; essential oil; GC–MS; antimicrobial activity.

INTRODUCTION

The genus *Satureja* L. includes about 200 species of herbs and shrubs, often aromatic, with a centre of distribution in the Mediterranean Basin. In the area of the central and western Balkans, nine species of this genus have been registered.[1]

* Corresponding author. E-mail: blakusic@pharmacy.bg.ac.yu
doi: 10.2298/JSC0807703L

Most of them are the well-known species *S. montana* L., *S. hortensis* L., *S. kitaibelii* Wierzb. Ex Heuff. and *S. cuneifolia* L., and all are used in traditional medicine on the Balkan Peninsula.

Satureja horvatii Šilić is an endemic relict species of the Orjen–Lovćen mountain massive (Montenegro), with a high content of the essential oil of up to 4 %.[2,3] To the best of our knowledge, there are published reports only about the chemical composition of its essential oil.

In parallel with the rapid development of a wide range of antibacterial agents since the 1940s, bacteria have proved extremely adept at developing resistance to each new employed agent. The rapidly increasing incidence of bacterial resistance to antimicrobial agents has become a serious problem worldwide. Resistance mechanisms have been identified and described for all the known antibiotics currently available for clinical use.[4] The antimicrobial activity of plant oils and extracts has been recognised for many years. With the increasing tendency for the use of volatile oils in the pharmaceutical industries, a systematic examination of essential oils for antimicrobial activity has become important.

The essential oils isolated from various *Satureja* species have been shown to have biological and pharmacological activities, such as antibacterial, fungicidal and antiviral,[5–7] anti-oxidant,[8] antispasmodic and antidiarrhoeal.[9]

This paper reports a phytochemical analysis and the *in vitro* antimicrobial activity of the essential oil of the endemic species *S. horvatii*.

EXPERIMENTAL

Plant material

The plant material of *S. horvatii* was collected on Mount Orjen (Montenegro), in Orjenske lokve locality (1580 m a. s. l.), in July 2006. The sample was gathered before the flowering period. A voucher specimen is kept at the Institute of Botany Herbarium, Faculty of Pharmacy, University of Belgrade.

Isolation of the essential oil

The aerial parts of the plant were dried at room temperature and hydrodistilled (100 g) for 3 h, using a Clevenger-type apparatus. The oil yield was 4.2 %.

Gas chromatography–mass spectrometry

*Gas chromatography***.** A Hewlett Packard, HP-5890 gas chromatograph, equipped with a split-splitless injector, a fused silica capillary column HP-5 (25 m×0.32 mm; 0.5 μm film thickness), and FID, was employed. Oil solutions in ethanol (≈ 1 %) were injected in the split mode (1:30). The injector and detector (FID) temperatures were 250 and 300 °C, respectively, while the column temperature was linearly programmed from 40 to 240 °C (4.0 °C min^{-1}).

Gas chromatography–mass spectrometry. The analyses were performed on a Hewlett Packard, HP G1800C gas chromatograph equipped with split-splitless injector and a HP-5MS capillary column (30 m×0.25 mm; 0,25 μm film thickness). The chromatographic conditions were as metioned in preceding paragraph. Injector was heated at 250 °C, detector (MSD) was heated at 280 °C, while the column temperature was linearly programmed from 40 to 240 °C (4.0 °C min^{-1}). The EIMS spectra (70 eV) were obtained in the scan mode in m/z range 40–400.

Component identification and quantification

Identification of individual constituents was made by comparison of their retention times with those of analytical standards of the available terpenoids and by a computer search, matching the mass spectral data with those held in the Wiley 275 library of mass spectra. Confirmation was performed using AMDIS software. For quantification purposes, relative area percentages obtained by FID were used.

Antimicrobial activity

Antibacterial and antifungal activities of the essential oil of *S. horvatii* were evaluated by the agar diffusion method[10] using a panel which included laboratory control strains obtained from the American Type Culture Collection (Rockville, MD, USA): Gram-positive bacteria *Staphylococcus aureus* (ATCC 25923), *Staphylococcus epidermidis* (ATCC 12228), *Micrococcus luteus* (ATCC 10240), *Enterococcus faecalis* (ATCC 29212), *Bacillus subtilis* (ATCC 6633BB), *Bacillus cereus* (ATCC 11778), Gram-negative *Escherichia coli* (ATCC 25922), *Pseudomonas aeruginosa* (ATCC 27853) and *Klebsiella pneumoniae* (NCIMB 9111) bacteria and one strain of yeast *Candida albicans* (ATCC 10259).

The active cultures for the experiments were prepared by transferring a loopful of cells from stock cultures to flasks containing Müller–Hinton broth (MHB, Torlak, Belgrade) for the bacteria and Sabouraud dextrose broth (Torlak, Belgrade) for the yeast. The cultures were incubated without agitation for 24 h at 37 and 25 °C for the bacteria and yeast, respectively. The cultures were diluted with fresh Müller–Hinton broth and Sabouraud dextrose broth to achieve optical densities corresponding to 2.0×10^6 colony forming units (CFU/ml) for the bacteria and 2×10^5 CFU/ml for *C. albicans*. A suspension of the tested microorganisms (100 μl) was distributed on the solid media, *i.e.*, Müller–Hinton agar or Sabouraud dextrose agar. One drop (15 μl) of a 4 % and one of a 2 % solution of the essential oil in absolute ethanol were poured onto the prepared agar. Ampicillin (10 μg), amikacin (30 μg), bacitracin (10 μg) and nystatin (100 units) discs were used to control the sensitivity of the tested microorganisms.

These plates were then incubated at 37 °C for 24 h for the bacteria and at 30 °C for 48 h for the *C. albicans*. The results of agar diffusion assays were evaluated by measuring zone of inhibition (in mm) after incubation. All the experiments were performed in triplicate and the average value and standard deviation (SD) were calculated for the diameters of the inhibition zone.

*Determination of the minimal inhibitory concentration (*MIC*)*

The broth microdilution method was used to determine the minimal inhibitory concentration (*MIC*) according to the National Committee for Clinical Laboratory Standards.[11] The *MIC* is defined as the lowest concentration of the essential oil at which the microorganism does not demonstrate visible growth. All tests were performed in Müller–Hinton broth supplemented with Tween 80 detergent (final concentration of 0.5 % v/v), with the exception of the yeast when Sabouraud dextrose broth supplemented with Tween 80 was used. A serial doubling dilution of the oil was prepared in a 96-well microtiter plate over the concentration range 0.02–80.00 μl ml^{-1}, including one growth control and one sterility control (MHB + Tween 80 + + test oil). Overnight broth cultures of each strain were prepared and the final concentration in each well was adjusted to 2.0×10^6 CFU/ml for the bacteria and 2.0×10^5 CFU/ml for the yeast, and these were confirmed by viable counts. The plates were incubated under normal atmospheric conditions at 37 °C for 24 h for the bacteria and at 26 °C for 48 h for the yeast. The bacterial growth was indicated by the presence of a white "pellet" on the well bottom.[12] All determinations were performed in duplicate.

RESULTS AND DISCUSSION

Chemical composition of the essential oil

The chemical composition of the essential oil of *S. horvatii* is presented in Table I. The identified compounds (thirty-four components) amounted to 100 % of the oil. The dominant constituents were monoterpene compounds in an amount of 97.24 % (hydrocarbons: 19.79 %; oxygenated monoterpenes: 77.45 %), while the quantity of sesquiterpene compounds was 2.76 % (hydrocarbons: 2.53 %; oxygenated sesquiterpenes: 0.23 %).

TABLE I. Chemical composition of *S. horvatii* essential oil determined by GC and GC–MS

No.	Constituents	$I^{a,13}$	Area, %
1	*α*-Thujene	924	1.56
2	*α*-Pinene	932	0.72
3	Camphene	946	0.47
4	Sabinene	969	0.06
5	*β*-Pinene	974	0.25
6	1-Octen-3-ol	974	0.25
7	*β*-Myrcene	988	1.44
8	*α*-Phellandrene	1002	0.26
9	Δ^3-Carene	1008	0.06
10	*α*-Terpinene	1114	1.81
11	*p*-Cymene	1020	4.52
12	*β* –Phellandrene	1025	0.60
13	*cis*- *β*-Ocimene	1032	0.15
14	*trans*-*β*-Ocimene	1044	0.05
15	*γ*-Terpinene	1054	7.49
16	*cis*-Sabinene hydrate	1065	0.71
17	*α*-Terpinolene	1086	0.09
18	Linalool	1095	0.38
19	Borneol	1165	1.58
20	Terpinen-4-ol	1174	0.47
21	*α*-Terpineol	1186	0.91
22	Carvacrol methyl ether	1241	4.92
23	Thymol	1289	63.73
24	Carvacrol	1298	4.67
25	Thymol acetate	1349	0.08
26	*β*-Caryophyllene	1417	1.55
27	Aromadendrene	1439	0.10
28	*α*-Humulene	1452	0.06
29	*γ*-Muurolene	1478	0.07
30	Germacrene D	1484	0.23

[a]Kovats index

TABLE I. Continued

No.	Constituents	$I^{a,13}$	Area, %
31	Bicyclogermacrene	1500	0.45
32	δ-Cadinene	1522	0.08
33	Spathulenol	1577	0.12
34	Caryophyllene oxide	1582	0.11
Monoterpene compounds			97.24
	Monoterpene hydrocarbons	–	19.79
	Oxygenated monoterpene	–	77.45
Sesquiterpene compounds		–	2.76
Sesquiterpene hydrocarbons		–	2.53
Oxygenated sesquiterpenes		–	0.23
Total			100

[a]Kovats index

The oil of *S. horvatii* is characterized by a high content of the phenolic monoterpene thymol (63.73 %). Other important compounds were the monoterpene hydrocarbons γ-terpinene (7.49 %), *p*-cymene (4.52 %), and the oxygenated compounds carvacrol methyl ether (4.92 %), carvacrol (4.67 %) and borneol (1.58 %). The essential oil also contained smaller percentages of α-thujene (1.56 %), β-caryophyllene (1.55 %) and β-myrcene (1.44 %).

Other *Satureja* species, such as *S. montana* and *S. subspicata* have lower content of essential oil (0.3–1.8 %), the main constituent of which is carvacrol (16.8––45.7 %), an isomer of thymol. Thymol in these species was registered in concentrations of less than 5 %.[14–16]

The chemical composition of the essential oils of *Satureja* spp. shows a large interspecies and intraspecies variability, which depends upon genetic factors, environmental factors, and stage of the plant development.[17,18]

Antimicrobial activity

Numerous studies have demonstrated that the essential oils of *Satureja* species are among the most potent essential oils with regard to antimicrobial properties.[15,19–21] This was confirmed and extended in the present study. According to the results, the essential oil had great *in vitro* antimicrobial activities against all nine bacteria and the yeast species tested (Tables II and III). These results are comparable to previously published activities for *Satureja* species.[16]

The data obtained from the agar diffusion method indicated that the inhibitory effect increased with increasing oil concentration from 2 to 4 %. The strongest inhibition zones (26–32 mm) were detected for the Gram-positive bacteria. Among them *M. luteus* was found to be the most sensitive. The oil also exhibited high antimicrobial activity against important human pathogens, such as *S. aureus* and *E. faecalis*. The Gram-negative strains displayed variable degrees of suscep-

tibility. Maximum activity was observed against *E. coli* and *K. pneumoniae* (22––28 mm), while *P. aeruginosa* exhibited weak inhibition zones (10–14 mm).

TABLE II. Antimicrobial activity of *S. horvatii* essential oil expressed by the diameter of the inhibition zone (mm)

Microorganism	Essential oil		Ampicillin	Amikacin	Bacitracin	Nystatin
	2.0 %	4.0 %	10 μg/disc	30 μg/disc	10 μg/disc	100 units/disc
S. aureus ATCC 25923	24.3±1.0	26.5±0.9	35.0±7.0	26.5±2.1	n.t.[a]	n.t.
S. epidermidis ATCC 12228	23.0±0	26.5±1.0	12.0	n.t.	n.t.	n.t.
M. luteus ATCC 10240	30.5±3.0	32.0±2.0	33.0	n.t.	16.7±1.2	n.t.
E. faecali ATCC 29212	26.0±1.0	27.5±2.4	16.0	n.t.	n.t.	n.t.
B. subtilis ATCC6633bb	23.2±1.3	30.0±0	15.0	n.t.	n.t.	n.t.
B. cereus ATCC 11778	19.0±1.2	26.0±0.8	12.0±3.4	n.t.	n.t.	n.t.
E. coli ATCC 25922	24.8±0.9	26.6±0.5	20.5±0.7	20.0	n.t.	n.t.
K. pneumoniae NCIMB 9111	22.2±2.3	24.0±0	17.0±4.2	n.t.	n.t.	n.t.
P. aeruginosa ATCC 27853	10.0±3.7	14.5±0.5	10.0	27.5±3.5	n.t.	n.t.
C. albicans ATCC 10259	23.5±1.0	26.0±2.5	n.t.	n.t.	n.t.	20.0±0.87

[a]Not tested

The *in vitro* antimicrobial activity of *S. horvatii* essential oil was evaluated by the broth microdilution method and expressed as the minimum inhibitory concentration. In liquid medium, the essential oil was active against all the test strains. The inhibitory properties of the oil were observed within a range of concentrations from 0.10 to 16.00 μl ml^{-1}. The oil exhibited the highest inhibitory effect against the Gram-positive bacteria *S. epidermidis*, *M. luteus* and *S. aureus*. The oil was effective against Gram-negative *E. coli* and *K. pneumoniae* (2.50 and 4.00 μl ml^{-1}, respectively), while *P. aeruginosa* seemed to be more resistant to the investigated oil (16.00 μl ml^{-1}).

In the present study, it was confirmed that Gram-positive bacteria are more sensitive to the investigated oil than Gram-negative bacteria (Tables II and III). The relative tolerance of Gram-negative bacteria to essential oils has been ascribed to the presence of a hydrophilic outer layer, which can block the penetration of hydrophobic components through the target cell membrane.[22] The essential oils rich in phenolic compounds are widely reported to exhibit high levels of antimicrobial activity.[20,23,24] The major component of *S. horvatii* was the phe-

nolic monoterpene thymol. Since the active antimicrobial compounds of essential oils are phenolics and terpenes, it seems reasonable that their mode of action might be similar to that of other phenolic compounds. Most of the studies on the mechanism of phenolic compounds focused on their effects on cellular membranes, altering its function, causing swelling and increasing its permeability. Increases in cytoplasmic membrane permeability appear to be a consequence of the loss of the cellular pH gradient, decreased ATP levels, and loss of the proton motive force, which lead to cell death.

TABLE III. Antimicrobial activity of *S. horvatii* essential oil expressed as *MIC* (μl/ml)

Microorganism	Essential oil	Ampicillin	Amikacin	Bacitracin	Nystatin
S. aureus (ATCC 25923)	0.20	0.50	n.t.[a]	n.t.	n.t.
S. epidermidis (ATCC 12228)	0.10	1.0	n.t.	n.t.	n.t.
M. luteusi (ATCC 10240)	0.10	0.50	n.t.	n.t.	n.t.
E. faecali (ATCC 29212)	0.40	0.50	n.t.	n.t.	n.t.
B. subtilis (ATCC6633bb)	2.00	1.00	n.t.	n.t.	n.t.
B. cereus (ATCC 11778)	2.50	1.00	n.t.	n.t.	n.t.
E. coli (ATCC 25922)	2.50	2.00	0.50	n.t.	n.t.
K. pneumoniae (NCIMB 9111)	4.00	2.00	n.t.	n.t.	n.t.
P. aeruginosa (ATCC 27853)	16.00	n.t.	1.00	n.t.	n.t.
C. albicans (ATCC 10259)	0.40	n.t.	n.t.	n.t.	0.50

[a]Not tested

A number of reports indicate that essential oils containing carvacrol, eugenol or thymol have the highest antimicrobial properties.[25] However, the antimicrobial activities of *Satureja* species do not arise only from the thymol and carvacrol content since the oil of *S. cuneifolia*, which is relatively rich in β-cubebene, limonene, α-pinene, spathulenol and β-caryophyllene also displayed relatively good activity.[15] Some studies reported that whole essential oils have a greater antibacterial activity than the major components mixed,[26,27] which suggests that the minor components are critical to the activity and could also affect the antimicrobial properties.

CONCLUSIONS

The essential oil of *S. horvatii* exhibited antimicrobial activity to varying degrees against all the tested strains. The maximum activity was observed against Gram-positive bacteria (*M. luteus*, *S. epidermidis*, *S. aureus* and *E. faecalis*) and against the yeast (*Candida albicans*). The oil exhibited moderate activity against the Gram-negative bacteria *E. coli* and *K. pneumoniae* and weak activity against *P. aeruginosa.* This study confirms that the essential oil of *S. horvatii* possesses antimicrobial activities *in vitro* against medically important pathogens.

Acknowledgements. The authors are grateful to the Ministry of Science of the Republic of Serbia (Project No.143012) for financial support.

ИЗВОД

ХЕМИЈСКИ САСТАВ И АНТИМИКРОБНА АКТИВНОСТ ЕТАРСКОГ УЉА ВРСТЕ *Satureja horvatii* Šilić (Lamiaceae)

БРАНИСЛАВА ЛАКУШИЋ[1], МИХАИЛО РИСТИЋ[2], ВИОЛЕТА СЛАВКОВСКА[1], ЈЕЛЕНА АНТИЋ СТАНКОВИЋ[3] И МАРИНА МИЛЕНКОВИЋ[3]

[1]Институт за ботанику, Фармацеутски факултет, Универзитет у Београду, Војводе Степе 450, 11000 Београд, [2]Институт за проучавање лековитог биља "Јосиф Панчић", Тадеуша Кошћушког 1, Београд и [3]Институт за микробиологију, Фармацеутски факултет, Универзитет у Београду, Војводе Степе 450, 11000 Београд

У раду је дат хемијски састав и антимикробна активност етарског уља, ендемичне врсте *Satureja horvatii* Šilić, сакупљане у Црној Гори. Етарско уље је дестилацијом воденом паром изоловано из надземног дела биљке и анализирано методом GC–MS. 34 компоненте чине 100 % уља, а главна компонента је тимол (63,37 %). Уље је садржало и мањи проценат γ-терпинена (7,49 %), карвакрол-метил-етра (4,92 %), карвакрола (4,67 %), *p*-цимена (4,52 %), α-терпинена (1,81 %), борнеола (1,58 %), α-тујена (1,56 %), β-кариофилена (1,55 %) и β-мирцена (1,44 %). Антимикробна активност етарског уља *S. horvatii* је испитивана коришћењем агар дифузионе и бујон микродилуционе методе. Етарско уље је показало различит степен антимикробне активности на тестиране организме. Уље *S. horvatii* је испољило максималну активност на грам-позитивне бактерије *Micrococcus luteus, Staphylococcus epidermidis, Staphylococcus aureus* и *Enterococcus faecalis* и на гљивицу *Candida albicans*. Уље је показало умерену активност на грам-негативне бактерије *Escherichia coli* и *Klebsiella pneumoniae* и слабу на *Pseudomonas aeruginosa*. Истраживањем је утврђено да етарско уље ендемичне врсте *S. horvatii* поседује антимикробну активност у *in vitro* условима на значајне медицинске патогене.

(Примљено 16. октобра 2007, ревидирано 18. јануара 2008)

REFERENCES

1. Č. Šilić, *Monografija rodova Satureja* L., *Calamintha* Miller, *Micromeria* Bentham, *Acinos* Miller *i Clinopodium* L. *u flori Jugoslavije,* Zemaljski Muzej BiH, Sarajevo, 1979, p. 72 (in Serbian)
2. S. Pavlović, P. Živanović, R. Jančić, S. Vujčić, G. A. Kuznjecova, A. L Ševarda, *Proceedings of Matica srpska for natural sciences* **66** (1984) 5 (in Serbian)
3. S. Pavlović, P. Živanović, R. Jančić, B. Todorovic, A. L. Ševarda, G. A. Kuznjecova, *Biosystematics* **12** (1987) 19 (in Serbian)
4. A. C. Fluit, M. E. Jones, F. J. Schmitz, J. Acar, R. Gupta, J. Verhoef, *Clin. Infect. Dis*. **30** (2000) 454
5. L. Panizzi, G. Flamini, P. L. Ciani, I. Morelli, *J. Ethnopharmacol*. **39** (1993) 167
6. N. Bezić, M. Skočibušić, V. Dunkić, *Acta Bot. Croat*. **58** (1999) 99
7. K. Yamasaki, N. M. Kawahata, M. H. Otake, N. Ueba, *Biol. Pharm. Bull*. **21 (**1998) 829
8. A. Radonić, M. Miloš, *Free Radical Res*. **37** (2003) 673
9. V. Hajhashemi, H. Sadrael, A. R. Ghannadi, M. Mohseni, *J. Ethnopharmacol*. **71** (2000) 187
10. P. Hili, C. S. Evans, R. G. Veness, *Lett. Appl. Microbiol.* **24** (1997) 269
11. *Performance standards for anti-microbial susceptibility testing: eleventh informational supplement*, Document M100-S11, NCCLS 2001 – National Committee for Clinical Laboratory Standards, Wayne, PA, (2001)
12. F. Candan, M. Unlu, B. Tepe, D. Daferera, M. Polissiou, A. Sökmen, A. Akpulat, *J. Ethnopharmacol*. **87** (2003) 215

13. R. P. Adams, *Identification of Essential Oil Components by Gas Chromatography/Mass Spectrometry*, 4th Ed., Allured Publishing Corporation, Carol Stream, IL, 2007
14. D. Kuštrak, J. Kuftinec, N. Blažević, M. Maffei, *J. Essent. Oil Res*. **8** (1996) 7
15. M. Skočibušić, N. Bezić, *Phytotherapy Res.* **18** (2004) 967
16. M. Skočibušić, N. Bezić, V. Dunkić, *Food Chem.* **96** (2006) 20
17. V. Slavkovska, R. Jančić, S. Bojović, S. Milosavljević, D. Đoković, *Phytochemistry* **57** (2001) 71
18. M. Skočibušić, N. Bezić, V. Dunkić, *Eur. Food Res. Technol*. **218** (2004) 367
19. M. Ciani, L. Menghini, F. Mariani, R. Pagiotti, A. Menghini, F. Faticheti, *Biotechnol. Lett*. **22** (2000) 1007
20. H. D. Dorman, S. G. Deans, *J. Appl. Microbiol.* **88** (2000) 308
21. M. Gulluce, M. Sokmen, D. Daferera, G. Agar, H. Ozkan, N. Kartal, *J. Agric. Food Chem.* **51** (2003) 3958
22. C. M. Mann, S. D. Cox, J. L. Markham, *Lett. Appl. Microbiol.* **30** (2000) 294
23. H. Baydar, O. Sagdic, G. Özkan, T. Karadogan, *Food Control* **15** (2004) 169
24. R. W. Lambert, P. N. Skandamis, P. Coote, G. Nychas, *J. Appl. Microbiol.* **91** (2001) 453
25. B. J. Juven, J. Kanner, F. Schved, H. Weisslowicz, *J. Appl. Bacteriol.* **76** (1994) 626
26. A. O. Gill, P. Delaquis, P. Russo, R. A. Holley, *Int. J. Food Microbiolog*. **73** (2002) 83
27. A. Mourey, N. Canillac, *Food Control* **13** (2002) 289

www.shd.org.yu

J. Serb. Chem. Soc. 73 (7) 713–726 (2008)
JSCS–3754

Journal of the Serbian Chemical Society

JSCS@tmf.bg.ac.yu • www.shd.org.yu/JSCS
UDC 546.472+547.979.733:543.422.25
Original scientific paper

Studies on Zn(II) monohydroxyphenyl mesoporphyrinic complexes. Synthesis and characterization

RICA BOSCENCU[1], RADU SOCOTEANU[2]*, ANABELA S. OLIVEIRA[3] and LUIS FILIPE VIEIRA FERREIRA[3]

[1]*"Carol Davila" University of Medicine and Pharmacy, Faculty of Pharmacy, Inorganic Chemistry Department, Traian Vuia 6, Bucharest,* [2]*Romanian Academy, Institute of Physical Chemistry "I. G. Murgulescu", Splaiul Independentei 202, 77208 Bucharest, Romania and* [3]*Centro de Química-Física Molecular, Complexo Interdisciplinar, Instituto Superior Técnico, Universidade Técnica de Lisboa, Av. Rovisco Pais 1049-001, Lisbon, Portugal*

(Received 27 July, revised 29 October 2007)

Abstract: A series of four Zn(II) complexes with asymmetrical porphyrinic ligands were synthesized: [5-(4-hydroxyphenyl)-10,15,20-triphenyl-21*H*,23*H*-porphinato]Zn(II) (Zn(II)TPPOH$_P$), [5-(3-hydroxyphenyl)-10,15,20-triphenyl-21*H*,23*H*-porphinato]Zn(II) (Zn(II)TPPOH$_M$), [5-(2-hydroxyphenyl)-10,15,20-triphenyl-21*H*,23*H*-Zn(II)-porphinato]Zn(II) (Zn(II)TPPOH$_O$) and the well-known (5,10,15,20-tetraphenyl-21*H*,23*H*-porphinato]Zn(II) (Zn(II)TPP) as reference, in a 1:1 mole ratio. In all cases, the free-base porphyrin served as a tetradentate ligand through the four pyrrole nitrogen atoms. The complexes were characterized by elemental analysis, FTIR and UV–Vis spectroscopy, which fully confirmed the structure of the complexes. UV–Vis showed that the spectral absorption of the four complexes was blue-shifted by at least 50 nm compared to that of the free ligands. Also important structural data were obtained from several different NMR experiments (including ^{1}H-NMR, ^{13}C-NMR, DEPT, COSY, HMBC and HMQC). Influences of external substituents on the porphyrin ring were observed.

Keywords: asymmetric porphyrins; Zn(II) porphyrin complexes; sensitizers for photodynamic therapy; molecular absorption coefficients; NMR spectroscopy.

INTRODUCTION

Tetrapyrrolic macrocycles (*i.e.*, porphyrins) play highly diverse and fundamental roles in biological systems.[1,2] They readily combine with metals, coordinating with them in the central cavity.[1,2] One of the more recent and promising applications of metalloporphyrins in medicine is their employment in the detection and cure from tumors, for which they are being intensively investigated as second and third generation photosensitizers for cancer photodynamic therapy (PDT), as efficient sensitizing agents in the photodegradation of malignant tis-

* Corresponding author. E-mail: psradu@yahoo.com
doi: 10.2298/JSC0807713B

sues.[3–9] PDT is a new, non-surgical, technique for cancer treatment. After administration of a photosensitizer, which is selectively retained by tumor cells, subsequent irradiation with light in the red region of the visible spectrum (within the so-called phototherapeutic window, where light can penetrate living tissues) in the presence of oxygen specifically inactivates neoplastic cells.[3–13]

In spite of some promising studies with other classes of compounds,[14–20] the only PDT photosensitizers already approved for human treatment have a porphyrin-like heterocyclic ring structure, although they absorb only weakly at about 620 nm and are a complex and non-separable mixture of monomers, dimers, and higher oligomers.[21,22]

The increasing need for higher efficiency against tumors continues to determine a great number of synthetic studies directed to the synthesis of single pure porphyrinic compounds with well-established structures and which efficiently absorb light at longer wavelengths[22,23] (in the red region of the absorption spectra, 630–680 nm, in the so-called phototherapeutical window, where the light deeply penetrates body tissues[3–12]), have relevant singlet oxygen quantum yields,[24,25] photostability[26,27] and low toxicity.[28]

In order to achieve the most appropriate locations at the level of the various cellular constituents, photosensitizers further need to possess the most adequate structural characteristics.[29] By modifying the charge density and its distribution at the periphery of the porphyrinic macrocycle, in the meso-position (an H has to be substituted by one −OH functional group), it is possible to control the route of these compounds to the target cells.[26,29–31]

In the present study, a series of new mesoporphyrinic complexes, monohydroxyphenyl Zn(II)-substituted porphyrin complexes, [5-(*x*-hydroxyphenyl)-10,15,20--triphenyl-21*H*,23*H*-porphinato]Zn(II) (*x* = 2, 3 and 4) (Scheme 1), were synthesized and characterized for use in PDT, with a prevalence to the latter mentioned objective.

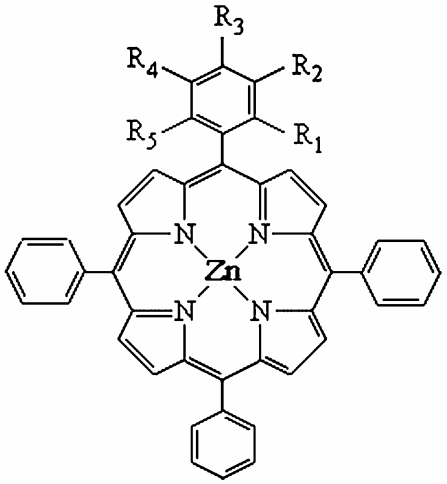

Scheme 1. Structure of the mono-hydroxy-substituted Zn(II)-porphyrin complexes. For Zn(II)TPP as the reference: $R_{1\text{-}5}$ = H; for Zn(II)TPPOH$_O$: R_1 = OH and $R_{2\text{-}5}$ = H; for Zn(II)TPPOH$_M$: $R_{1,3\text{-}5}$ =H and R_2 = OH; for Zn(II)TPPOH$_P$: $R_{1,2,4,5}$ = H and R_3 = OH.

EXPERIMENTAL

Materials and methods

Commercially available chemicals and solvents were used as received from Aldrich, Merck and Sigma.

The elemental analysis of C, H and N was performed with an automatic Carlo Erba L-1108 analyzer. The metallic ion was determined gravimetrically and volumetrically.

The IR spectra were recorded with a FTIR 400D Nicolet Impact spectrometer. The samples, previously dried at 150 °C for 24 h, were measured as KBr pellets of spectroscopic purity. The spectra were measured in the 4000–500 cm^{-1} spectral range.

The NMR spectra were recorded with a 400 MHz Bruker NMR Spectrometer. ^{1}H-NMR, ^{13}C-NMR, DEPT 90, HMQC, HMBC and COSY spectra were measured.

The molecular absorption spectra were recorded with a Specord M400 Carl Zeiss Jena UV–Vis spectrometer, assisted by an internal computer, within the spectral range of 210–900 nm. All spectra were recorded in a mono-beam system, in order to eliminate the specific absorption of the solvent and the absorption differences caused by the optical pathway. For measurement of UV–Vis absorption both polar (chloroform) and non-polar (benzene) solvents were used.

Synthesis of the Zn(II) complexes

The methods presented in the literature[32,33] for the synthesis of metalloporphyrins, usually result in very low yields, mainly because of the high temperatures and low pH of the environment used during the synthesis. For this reason, the synthesis of the complexes in the present work was instead conducted at moderate temperatures and in the presence of a basic catalyst, 2,6-dimethylpyridine, which determined the removal of a proton from the inner nitrogen atoms inside the porphyrinic macrocycle, thereby enabling the production of the complex. These new experimental conditions considerably reduced the duration of synthesis and increased the yield of the reaction to around 90 %.

Solutions (≈ 10^{-4} M) of each of the four porphyrinic ligands (TPP, $TPPOH_O$, $TPPOH_M$ and $TPPOH_P$)[34] in chloroform were gently heated under stirring until the ligand crystals were completely dissolved. Then, several drops of 2,6-dimethylpyridine were added, together with the appropriate amount of a methanolic solution of $ZnCl_2$ to give a 1:1 stoichiometric ratio. The reaction mixture was refluxed under continuous stirring for 1 h at 55 °C. The presence of the complex in the reaction mixture was monitored during the course of the reaction by thin layer chromatography. After cooling, the reaction mixture was purified by passing it through an alumina chromatographic column. The excess metallic salt was retained by the alumina, while chloroform containing the complex (the deep violet-colored complex was the second band passing through the chromatographic column) was collected. The solutions of the complexes in chloroform were concentrated by simple distillation. The obtained violet crystals were dried at ≈ 100 °C for 12 h.

RESULTS AND DISCUSSION

Elemental analysis

The results of the elemental analysis of the four ligands combinations with Zn(II) are given in Table I.

The experimental values obtained for the percentage elemental analysis of carbon, hydrogen, nitrogen and zinc are in accordance with the theoretical values calculated on the basis of a 1:1 Zn (II):porphyrinic ligand stoichiometry, thus confirming this stoichiometry for all the four synthesized metalloporphyrinic complexes.

TABLE I. Results of elemental analysis

Complex	Content, %							
	C		H		N		Zn	
	Calcd.	Found	Calcd.	Found	Calcd.	Found	Calcd.	Found
Zn(II)TPP	77.86	77.25	4.16	4.50	8.25	8.35	9.64	9.29
Zn(II)TPPOH$_O$	76.06	75.90	4.06	4.12	8.06	8.32	9.42	9.15
Zn(II)TPPOH$_M$	76.06	75.70	4.06	4.19	8.06	8.12	9.42	9.19
Zn(II)TPPOH$_P$	76.06	75.89	4.06	4.21	8.06	8.15	9.42	9.23

IR Spectra

The most relevant results extracted from the IR spectra of the synthesized Zn(II) complexes, together with those for the corresponding free complexes are given in Table II.[34]

The IR spectra of the four Zn-free complexes, *i.e.*, TPP, TPPOH$_O$, TPPOH$_M$, TPPOH$_P$, were previously analyzed.[34] In agreement with the structure of the free complexes, the presence of the characteristic bands of ν_{O-H} (obviously not present for TPP) and ν_{N-H} in the spectral range 3410–3528 cm^{-1} and 3314–3448 cm^{-1} could be identified.[34]

TABLE II. Characteristic IR vibrations of the free-base porphyrins and of the mono-hydroxy-substituted Zn(II) complexes

Characteristic vibration	$\bar{\nu}$ / cm^{-1}							
	TPP[34]	Zn(II)TPP	TPPOH$_O$[34]	Zn(II)-TPPOH$_O$	TPPOH$_M$[34]	Zn(II)-TPPOH$_M$	TPPOH$_P$[34]	Zn(II)-TPPOH$_P$
ν_{O-H}	–	–	3528	3533	3521	3494	3527	3525
ν_{O-H} associated	–	–	3424	3429	3424	3429	3410	3412
ν_{N-H}	3448	–	3448	–	3440	–	3430	–
ν_{N-H} associated	3316	–	3316	–	3316	–	3314	–
$\nu_{C=NH}$	1557	–	1558	–	1558	–	1557	–
ν_{C-O}	–	–	1176	1176	1178	1177	1170	1171

As reported before,[34] two bands corresponding to ν_{N-H} were present: the first one, well individualized in the region 3430–3448 cm^{-1}, can be attributed to ν_{N-H} stretching vibrations; the second one, less intense, in the 3314–3316 cm^{-1} range corresponds to the stretching vibration $\nu_{N-H associated}$. A band attributed to $\nu_{C=NH}$ was also present at 1557–1558 cm^{-1}.

Comparing the IR spectra corresponding to the newly synthesized complex *versus* those for the corresponding free ligand (as can be seen in Table II), the disappearance of three bands from the spectrum of the zinc containing complexes was evidenced. The absence of these bands for Zn(II)TPP and Zn(II)TPPOH$_X$ is very clear evidence for the removal of one proton from the =NH groups (nitrogen atoms in the positions 21 and 23 at the inner part of the porphyrinic ring (Scheme 1),

which confirms coordination of the metallic ion to the nitrogen atoms of the porphyrinic macrocycle.

The presence of the −OH functional group in $TPPOH_O$, $TPPOH_M$, $TPPOH_P$[34] and in the corresponding complex combinations with Zn(II) ions was fully confirmed by the IR spectra, in which two bands in the spectral ranges of 3494––3533 cm^{-1} and 3412–3429 cm^{-1} (3521–3528 cm^{-1} and 3410–3424 cm^{-1} for the $TPPOH_X$ free base) corresponding to ν_{O-H} and $\nu_{O-H associated}$ vibrations were identified. For all non-symmetrically substituted compounds (both the free bases[34] and the Zn(II) complexes), a medium intensity band in the 1170–1178 cm^{-1} (1171–1177 cm^{-1} for the metal-containing complexes) spectral range was identified, which was attributed to the ν_{C-O}. The presence of this band in all three Zn(II) complexes further confirms that the −OH functional group was not lost upon metal complexation with the asymmetric porphyrinic macrocycle. Accordingly, neither ν_{O-H} nor ν_{C-O} bands were present for TPP[34] and Zn(II)TPP.

All infrared spectral features described above for the free bases and the Zn(II) complexes fully support and confirm that Zn(II) inclusion onto $TPPOH_O$, $TPPOH_M$, $TPPOH_P$ was fully successful without the destruction of the monohydroxy substitution of the phenyl group of the porphyrinic ligand. The same results were observed before for Cu(II) inclusion on the same ligands.[35] As already stressed, this type of substitution was previously identified as being extremely important for the appropriate location of these types of compounds in biological media.[26,29–31]

NMR experiments

To clearly illustrate the relation between structure and NMR spectra, the *β*-pyrrole *meso*-positions (according to the Fischer rule) in terms of the arrangement of hydroxyl substituents are presented in Scheme 2, in which the ortho-, meta- and para-positions are indicated by b', c' and d', respectively.

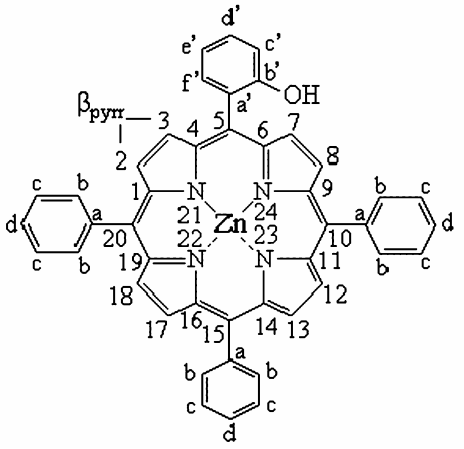

Scheme 2. Complete atomic numbering of the $TPPOH_O$ structure for NMR assignment.

The chemical shifts and multiplicities of the ^{1}H-NMR signals for the Zn(II) complexes and other important complementary data provided by the ^{13}C-NMR spectra are presented in Table III.

TABLE III. Chemical shifts and multiplicities of the ^{1}H-NMR and ^{13}C-NMR signals for the Zn(II) complexes

Complex	^{1}H-NMR	^{13}C-NMR
Zn(II)TPP	7.79–7.71 (12H, *m*, *m*-Ph, *p*-Ph) 8.22 (8H, *dd*, *o*-Ph); 8.94 (8H, *s*, β_{pyrr})	121.1 ($C_{5,10,15,20}$); 126.5; 127.4 ($C_{\beta_{pyrr}}$) 132.0; 134.4; 142.8
Zn(II)TPPOH$_O$	7.34 (1H, *t*, c'-Ph); 7.53–7.51 (1H, *m*, e'-Ph); 7.79–7.68 (1H, *m*, d'-Ph); 7.79–7.68 (9H, *m*, c,d-Ph); 7.98 (1H, *d*, f'-Ph); 8.21 (6H, *d*, b-Ph); 8.95–8.89 (8H, *m*, β_{pyrr})	119.3 (C_5); 121.2 ($C_{10,15,20}$); 115.2 ($C_{c'}$); 126.5 (C_c); 127.5 (C_d); 128.8 ($C_{d'}$); 130.0 ($C_{a'}$); 130.8 (C_8); 131.1 ($C_{e'}$); 132.0 ($C_{2,3,\ 8,12,13,17,18}$ β_{pyrr}); 132.7 (C_7); 134.9 (C_b); 142.7 (C_a); 142.8 ($C_{f'}$); 155.5 ($C_{b'}$)
Zn(II)TPPOH$_M$	6.99 (1H, *t*, e'-Ph); 7.43 (1H, *t*, f'-Ph); 7.56 (1H, *m*, d'-Ph); 7.73 (1H, *s*, b'-Ph); 7.75 (9H, *m*, c,d-Ph); 8.19 (6H, *t*, b-Ph); 8.92 (6H, *m*, $H_{2,3,\ 8,12,13,17,18}$ β_{pyrr}); 8.97 (1H, *t*, H_7 β_{pyrr}); 9.02 (1H, *d*, H_3 β_{pyrr})	114.6 ($C_{e'}$); 120.2 ($C_{f'}$); 121.0 (C_5); 121.9 ($C_{10,15,20}$); 126.5 (C_c); 127.4 (C_d); 127.6 ($C_{b'}$); 129.6 ($C_{d'}$); 131.9 ($C_{2,8,12,13,17,18}$ β_{pyrr}); 132.3 (C_7); 134.4 (C_b); 142.8 (C_a); 144.3 ($C_{a'}$); 150.6 ($C_{c'\text{-}OH}$)
Zn(II)TPPOH$_P$	6.99 (1H, *t*, c'-Ph); 7.43 (1H, *t*, b'-Ph); 7.56 (1H, *m*, e'-Ph); 7.73 (1H, *s*, f'-Ph); 7.75 (9H, *m*, c,d-Ph); 8,19 (6H, *t*, b-Ph); 8,92 (6H, *m*, $H_{2,8,12,13,17,18}$ β_{pyrr}); 8.97 (1H, *t*, H_7 β_{pyrr}); 8.97 (1H, *t*, H_7 β_{pyrr}); 9.02 (1H, *d*, H_3 β_{pyrr})	113.5 ($C_{c',e'}$); 120.4 (C_5); 121.0 ($C_{10,15,20}$); 126.5 (C_c); 127.4 (C_d); 131.9 ($C_{2,8,12,13,17,18}$ β_{pyrr}); 132.0 ($C_{3,7}$ β_{pyrr}); 134.4 (C_b); 135.2 ($C_{a'}$); 135.5 ($C_{b',f'}$); 142.7 (C_a); 155.3 ($C_{d'\text{-}OH}$)

The high frequency region of the ^{1}H-NMR spectra ($\delta \approx 9$ ppm) shows the chemical shifts for the pyrrole hydrogen atoms (β_{pyrr}). The observed differences in the signals are due to the vicinity of the substituted phenyl.

Several other experiments, *i.e.*, DEPT 90, HMQC, HMBC and COSY, were also performed. Due to the higher capacity of 2D spectra (which present on same image cross-peaks of ^{1}H-NMR and ^{13}C-NMR for HMQC and HMBC, and proton coupling for COSY), it was possible to identify several carbon atoms and also to elucidate the differences between the influence of the hydroxyl substituent on its surroundings in dependence on whether it was positioned in the *o*-, *m*- or *p*-position, as shown in Figs. 1 to 3.

The HMQC data for Zn(II)TPPOH$_O$ (Fig. 1a, inset) shows the bonding between the pyrrolic protons and the corresponding carbon atoms. The cross-peak revealed the connection between C_7, C_8 and the rest of $C_{\beta_{pyrr}}$ on one side and the H_{pyrr} on the other.

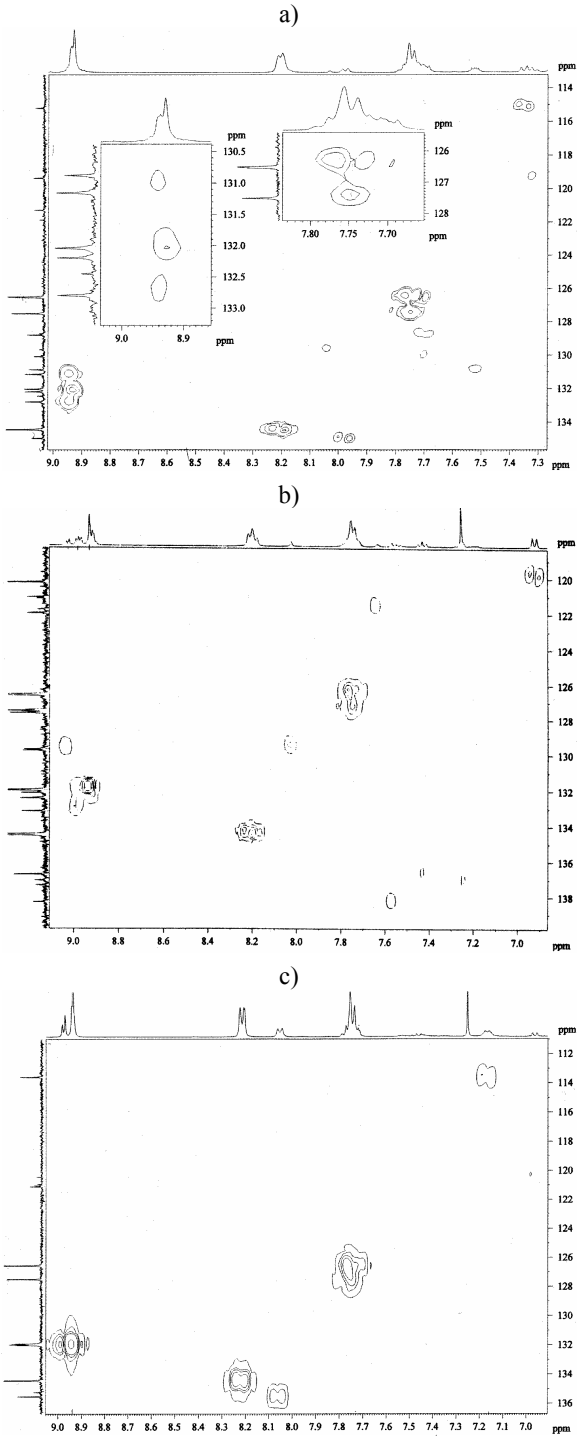

Fig. 1. HMQC spectra for (a) Zn(II)TPPOH$_O$, (b) Zn(II)TPPOH$_M$ and (c) Zn(II)TPPOH$_P$.

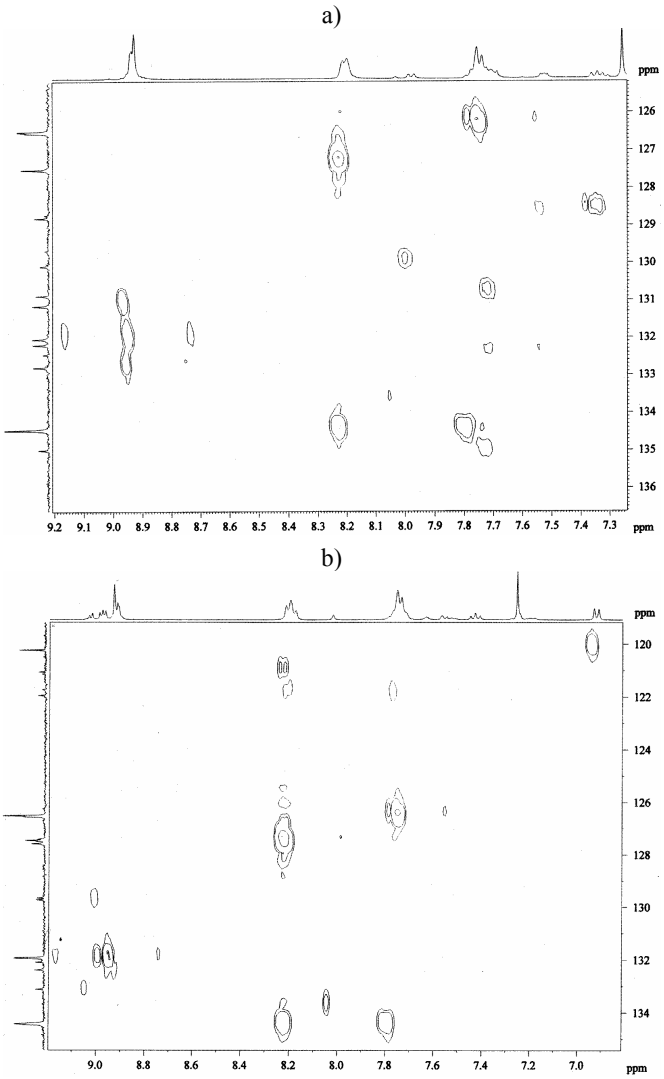

Fig. 2. HMBC spectra for (a) Zn(II)TPPOH$_O$ and (b) Zn(II)TPPOH$_M$.

These kind of data permitted the establishment of the correct interpretation of the C signals and, more important, of the influence of the −OH group on the environment (especially the atoms in the β-pyrrolic positions 2, 3, 7 and 8). The C signal is influenced by the presence of the −OH group, at 132.7, 132.3 and 132.0 ppm for Zn(II)TPPOH$_O$, Zn(II)TPPOH$_M$ and Zn(II)TPPOH$_P$, respectively. Due to the symmetry of the compound, this C type is identical with the C_{3pyrr}. This situation was also confirmed by HMBC (Fig. 2). The presence of the −OH group in the ortho-, meta- and para-positions was also confirmed by the differences in the H–H coupling.

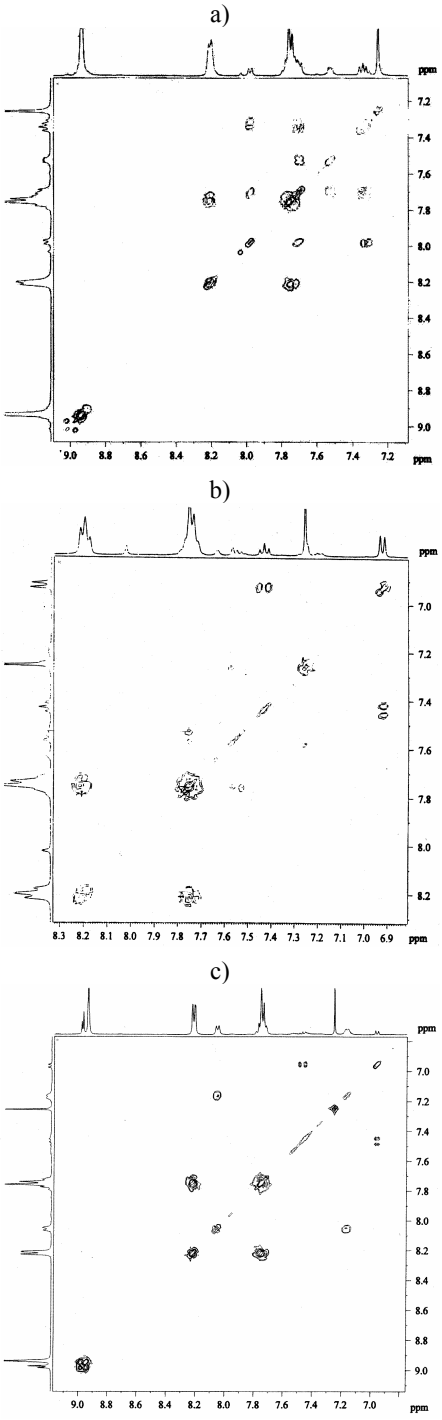

Fig. 3. COSY spectra for:
(a) Zn(II)TPPOH$_O$,
(b) Zn(II)TPPOH$_M$ and
(c) Zn(II)TPPOH$_P$.

Molecular electronic spectra

The molecular electronic absorption spectra are usually used for quantitative determinations of compounds, but in the case of porphyrinic compounds, they were shown to be real "fingerprints".[1,2,12,36–38] Despite the great number of atoms in their structures (typically 40–80 atoms) and of the complex structures adopted by the free base porphyrins and their metal containing complexes, the spectral analysis of their UV–Vis molecular electronic absorption spectra is still an efficient method for the identification of porphyrin. This is explained by the fact that the peripheral substitutions do not significantly disturb the inner π electron ring of the porphyrinic macrocycle, which is responsible for the active electronic transitions in the above-mentioned spectral range.[1,27,39–42]

The molecular electronic absorption spectra of the newly synthesized Zn(II) complexes were measured at room temperature in benzene and chloroform solutions at 20–30 °C, in order to gain evidence for their structures and to determine their molar absorption coefficients at various wavelengths. A series of subsequent dilutions (≈ 10^{-4}–10^{-6} M) were performed in order to obtain absorbance values in the range 0–1.0 and thereby to ensure the maximum accuracy of the determinations. The time required for the complete dissolution of the compounds ranged from several seconds, in the case of chloroform, to several days, for some of the compounds in benzene.

The maxima of the absorption bands and the corresponding molar absorption coefficients of the Zn(II) complexes synthesized in this work are given in Table IV. The four Zn(II) complexes all displayed Soret bands, peaking at 422–424 nm, accompanied by two Q bands peaking in the 548–554 nm and 588–594 nm spectral range.

TABLE IV. UV–Vis spectral characteristics of the mono-hydroxy-substituted Zn(II) complexes

Complex	λ / nm | $\varepsilon \times 10^{-2}$ / m^2 mol^{-1}					
	Solvent					
	Chloroform			Benzene		
	Soret	Q (1,0)	Q (0,0)	Soret	Q (1,0)	Q (0,0)
Zn(II)TPP	422 | 265	552 | 14	594 | 3.9	422 | 253	548 | 14	588 | 2.2
Zn(II)TPPOH$_O$	424 | 252	554 | 12	594 | 3.6	424 | 269	550 | 14	590 | 2.7
Zn(II)TPPOH$_M$	424 | 300	552 | 13	594 | 3.9	424 | 288	550 | 13	588 | 2.4
Zn(II)TPPOH$_P$	424 | 333	554 | 15	594 | 5.1	424 | 277	550 | 15	590 | 3.3

The spectra of the newly synthesized compounds are quite similar to those of symmetrically tetra-substituted compounds, both in shape and in the ratio between the absorption band intensities.

The molar absorption coefficients did not undergo significant changes (see Table IV). The values for the reference compounds were in good agreement with those presented in the literature.[43]

The two Q bands for Zn(II) metalloporphyrins underwent a hypsochromic shift and a partial overlap, as already reported in the literature for other metallo-

porphyrins of the same type[1,12,40] and was also observed for the inclusion of Cu(II) in the same ligands.[35] When using chloroform as the solvent, an absorption band could be observed with a maximum at λ = 552–554 nm, as well as another band at λ = 594 nm, which partially overlaps the first one. In the case of the solutions in benzene, the above-mentioned overlap was slightly more evident, but two absorption bands could still be distinctly identified, displaying absorption maxima, respectively, at λ = 548–550 nm and at λ = 588–590 nm. Similar results were observed for Cu(II) complexes with the same ligands.[35] These results are strikingly different from those of the corresponding free bases,[34] for which four Q bands could clearly be identified. The decrease in the number of Q bands was reported previously for several other metalloporphyrins[1,12,40] and is the consequence of metal inclusion in the free base ligand.[1]

Metal inclusion in the macrocycle increases the symmetry of the latter and conduces its coordination geometry to a higher symmetry class (D_{4h}) than that of the free base porphyrins (D_{2h}). This latter fact yields a simplified Q band spectra which usually collapses from four to only two bands.[1] Therefore, these UV–Vis results present a further strong proof of Zn(II) inclusion on the TPP and $TPPOH_X$ ligands.

As can be seen from Table IV, the spectra of the three Zn(II) non-symmetrical complexes are quite similar to that of Zn(II)TPP, a symmetrically tetra-substituted compound, both in shape and in the ratio between the absorption band intensities. The molar absorption coefficients did not undergo significant changes, apart from the fact that they are mostly slightly higher for the non-symmetrical substituted porphyrinic complexes. Only ε_{Soret}(Zn(II)TPP) = 253×10^2 m^2 mol^{-1} as compared with $\varepsilon_{Soret}(Zn(II)TPPOH_O) = 269\times10^2$ m^2 mol^{-1}, $\varepsilon_{Soret}(Zn(II)TPPOH_M) = 288\times10^2$ m^2 mol^{-1} and $\varepsilon_{Soret}(Zn(II)TPPOH_P) = 277\times10^2$ m^2 mol^{-1} was measured in benzene. The same tendency was observed in chloroform and it was mostly observed both for the Soret and Q bands (see Table IV).

The influence of the solvent on the molar absorption coefficients could be easily observed for the Q bands: the absorption coefficients (ε) were always higher in the case of chloroform. These spectral differences among the spectra of the three mono-hydroxy-substituted Zn(II) porphyrin complexes are explained by the influence of the non-symmetrical substituent *vs.* the inner π-electron ring of the macrocycle (Scheme 1). When the −OH group assumes various positions in the phenyl nucleus (ortho-, meta- or para-), its influence is limited to the π electron of the phenyl. The angles of 70–80° between the phenyl and the tetrapyrrolic macrocycle would practically prevent conjugation. The disturbance of the inner π-electron ring of the macrocycle, which is responsible for the UV–Vis absorption spectra of the porphyrin compounds, is implicitly irrelevant. Regarding the potential inductive effect, it is practically terminated at a distance of 3–5 atoms due to the presence of the oxygen atom towards the electron ring.

The spectra recorded in the above-mentioned solvents (both polar and non-polar) did not provide evidence for the existence of self-association processes in the

investigated concentration range ($c = 10^{-4}$–10^{-6} M). The absence of an isosbestic point in the plot of the absorption spectra of these compounds with increasing concentrations, from 10^{-6} to 10^{-4} M, is strong proof for this.

The spectral absorptions of the Zn(II) complexes can be further compared with those of the free bases (with their Soret band always peaking at 420 nm and their typical four Q bands absorbing at 514–516 nm, 548–550 nm, 590–592 nm and 648–652 nm) for the same solvent, benzene.[34] From the comparison, it can be observed that in practice the Zn(II) complexation did not shift the global absorption features of these compounds into the red region of the spectra. Thus, comparing the data of the Zn(II) complexes with the data previously published for the free bases, the absorption of the latter ones extends up to 670 nm, while those of the metal containing complex had already attained zero by 600–630 nm. A similar result was observed for Cu(II) complexation with the same ligands.[34]

CONCLUSIONS

In this paper, the synthesis of four Zn(II) complexes, one with TPP and the other three with non-symmetrically −OH substituted mesoporphyrinic ligands is presented. A new synthetic method, conducted at moderate temperatures and low pH, was successfully employed, which enabled a reduction of the synthesis time and markedly increased yields of the reaction, to about 90 %. The compounds were synthesized foreseeing their use as PDT sensitizers that could appropriately locate in cellular components. For the latter three Zn(II) complexes, for which the charge density and its distribution at the periphery of porphyrinic macrocycle was modified by the inclusion of an OH group, it is possible to anticipate that their route and localization at the cellular level could be controlled, while keeping most of their relevant photochemical properties intact.

Elemental analysis of the synthesized complexes confirmed Zn(II) inclusion in TPP, as well as in the three non-symmetrically −OH substituted porphyrinic ligands, having a 1:1 stoichiometry for all the four complexes.

The spectral properties of the four Zn(II) complexes were investigated by FTIR, NMR and UV–Vis spectroscopy. FTIR spectra fully confirmed the structure of the herein prepared compounds: Zn(II) coordination to the symmetric and to the non-symmetric ligands was further confirmed; the ionic metal coordination to the porphyrinic ligand does not affect the asymmetric substitution of the ligand. NMR techniques together revealed the complete structure and the influences of the unsymmetrical substituents on the porphyrinic ring. From UV–Vis absorption, it could be observed that although the non-symmetric substitution did not significantly change the absorption properties of the ligands, the Zn(II) complexation unfortunately did not result in the desired improvement of the absorption properties of these porphyrinic compounds towards the red region of the spectra, whereby their absorption would have been shifted into the phototherapeutical window. This result is fully explained by the collapse and overlap of the

four Q bands into only two Q bands, resulting from an increase in the symmetry of the coordination geometry which is experienced by the compounds upon Zn(II) complexation.

И З В О Д

ПРОУЧАВАЊЕ Zn(II) МОНОХИДРОКСИФЕНИЛ-МЕЗОПОРФИРИНСКИХ КОМПЛЕКСА. СИНТЕЗА И КАРАКТЕРИЗАЦИЈА

RICA BOSCENCU[1], RADU SOCOTEANU[2], ANABELA S. OLIVEIRA[3] и LUIS FILIPE VIEIRA FERREIRA[3]

[1]Carol Davila" University of Medicine and Pharmacy, Faculty of Pharmacy, Inorganic Chemistry Department, Traian Vuia 6, Bucharest, [2]Romanian Academy, Institute of Physical Chemistry "I. G. Murgulescu", Splaiul Independentei 202, 77208 Bucharest, Romania and [3]Centro de Química-Física Molecular, Complexo Interdisciplinar, Instituto Superior Técnico, Universidade Técnica de Lisboa, Av. Rovisco Pais 1049-001, Lisbon, Portugal

Синтетисана је серија од четири Zn(II) комплекса са асиметричним порфиринским прстеновима: [5-(4-хидроксифенил)-10,15,20-трифенил-21*H*,23*H*-порфинато]Zn(II) (Zn(II)TPPOH$_P$), [5-(3-хидроксифенил)-10,15,20-трифенил-21*H*,23*H*-порфинато]Zn(II) (Zn(II)TPPOH$_M$), [5-(2-хидроксифенил)-10,15,20-трифенил-21*H*,23*H*-порфинато]Zn(II) (Zn(II)TPPOH$_O$) и добро познати (5,10,15,20-тетрафенил-21*H*,23*H*-порфинато]Zn(II) (Zn(II)TPP), који је коришћен као референтна супстанца, у 1:1 молском односу. У свим случајевима слободна база порфирин деловала је као тетрадентат преко четири атома азота пирола. Комплекси су окарактерисани елементалном анализом, FTIR и UV–Vis спектроскопијом, чиме су утврђене структуре комплекса. UV–Vis спектри су показали да је спектрална апсорпција четири комплекса померена ка плавом подручју најмање за 50 nm у односу на слободне лиганде. Важни структурни подаци су добијени и из неколико различитих NMR експеримената (^{1}H-NMR, ^{13}C-NMR, DEPT, COSY, HMBC and HMQC). Уочен је и утицај спољних супституената на порфиринском прстену.

(Примљено 27. јула, ревидирано 29. октобра 2007)

REFERENCES

1. L. R. Milgrom, *What Porphyrins are and What they do*, *The Colours of Life. An Introduction to the Chemistry of Porphyrins and Related Compounds*, Oxford University Press, Oxford, 1977, p. 1
2. L. R. Milgrom, F. O'Neill, in *The Chemistry of Natural Products*, R. H. Thomson, Ed., Blackie Academic & Professional, London, 1993, pp. 329–376
3. L. I. Grossweiner, *The Science of Phototherapy*, *Photodynamic Therapy*, CRC Press, London, 1994, p. 139
4. J. S. McCaughan Jr., *Drugs & Aging* **15** (1999) 49
5. J. D. Spikes, G. Jori, *Lasers Med. Sci.* **2** (1987) 3
6. D. Kessel, T. H. Chou, *Adv. Exp. Med. Biol.* **160** (1983) 115
7. G. Jori, E. Reddi, L. Tomio, F. Calzavara, *Adv. Exp. Med. Biol.* **160** (1983) 193
8. T. J. Dougherty, J. E. Kaufman, A. Goldfarb, K. R. Weishaupt, D. Boyle, A. Mittleman, *Cancer Res.* **38** (1978) 2628
9. T. J. Dougherty, C. J. Gomer, B. W. Henderson, G. Jori, D. Kessel, M. Korbelik, J. Moan, Q. Peng, *J. Natl. Cancer Inst.* **90** (1998) 889
10. T. J. Dougherty, *Photochem. Photobiol.* **58** (1993) 895
11. L. C. Penning, T. M. Dubbelman, *Anticancer Drugs* **5** (1994) 139
12. R. Bonnett, *Chemical Aspects of Photodynamic Therapy*, Gordon and Breach Science Publishers, Amsterdam, 2000

13. C. Schweiter, R. Schmidt, *Chem. Rev.* **103** (2003) 1685
14. M. Wainwright, *Chem. Soc. Rev.* **25** (1996) 351
15. R. W. Redmond, M. B. Srichai, J. M. Bilitz, D. D. Schlomer, M. Kreig, *Photochem. Photobiol.* **60** (1994) 348
16. M. Krieg, J. M. Bilitz, M. B. Srichai, R. W. Redmond, *Biochim. Biophys. Acta* **1199** (1994) 149
17. P. F. Santos, L. V. Reis, I. Duarte, J. P. Serrano, P. Almeida, A. S. Oliveira, L. F. Vieira Ferreira, *Helv. Chim. Acta* **88** (2005) 1135
18. P. F. Santos, L. V. Reis, P. Almeida, A. S. Oliveira, L. F. Vieira Ferreira, *Photochem. Photobiol.* **163** (2004) 267
19. P. F. Santos, L. V. Reis, P. Almeida, A. S. Oliveira, L. F. Vieira Ferreira, *J. Photochem. Photobiol.* **160** (2003) 159
20. E. Arunkumar, P. K. Sudeep, P. V. Kamat, B. C. Noll, B. D. Smith, *New J. Chem.* **31** (2007) 677
21. R. R. Allison, G. W. Downie, R. Cuenca, X. H. Hu, C. J. H. Childs, C. H. Sibata, *Photodiagn. Photodyn. Ther.* **1** (2004) 27
22. M. Kreimer-Birnbaum, *Semin. Hematol.* **26** (1989) 157
23. J. G. Moser, *Photodynamic Tumor Therapy. 2nd & 3rd Generation Photosensitizers: Quantitative Data on 2nd and 3rd Generation Photosensitizers*, Harwood Academic Publishers, Amsterdam, 1998
24. F. Postino, M. Mora, M. A. DeMadariaga, S. Nonell, M. L. Sagrista, *Int. J. Pharm*. **278** (2004) 239
25. I. Scalise, E. N. Durantini, *J. Photochem. Photobiol., A* **162** (2004) 105
26. R. B. Boyle, D. Dolphin, *Photochem. Photobiol.* **64** (1996) 469
27. I. J. MacDonald, T. J. Dougherty, *J. Porphyrins Phthalocyanines* **5** (2001) 105
28. E. S. Nyman, P. H. Hynninen, *J. Photochem. Photobiol. B* **73** (2004) 1
29. F. Ricchelli, G. Jori, S. Gobbo, M. Tronchin, *Biochim. Biophys. Acta* **1065** (1991) 42
30. J. Osterloh, M. G. H. Vicente, *J. Porphyrins Phthalocyanines* **6** (2002) 305
31. L. Milgrom, S. MacRobert, *Chem. Br.* **34** (1998) 45
32. J. W. Buchler, in *Porphyrins and Metaloporphyrins*, K. M. Smith, Ed., Elsevier, Amsterdam, 1975, p. 157
33. R. F. Pasternack, E. J. Gibbs, A. Gaudemer, *J. Am. Chem. Soc.* **107** (1985) 8179
34. R. Boscencu, D. Licsandru, R. Socoteanu, A. S. Oliveira, L. F. Vieira Ferreira, *Rev. Chim.* **58** (2007) 498
35. R. Boscencu, R. Socoteanu, A. S. Oliveira, L. F. Vieira Ferreira, V. Nacea, G. Patrinoiu, *Pol. J. Chem*. **82** (2008) 509
36. M. Goutermann, *J. Mol. Spectrosc.* **6** (1961) 138
37. M. Goutermann, G. H. Wagniere, *J. Mol. Spectrosc.* **11** (1963) 108
38. M. Goutermann, in *The Porphyrins*, D. Dolphin, Ed., Academic Press, New York, 1978, p. 1
39. D. J. Quimby, F. R. Longo, *J. Am. Chem. Soc.* **97** (1975) 5111
40. A. Harriman, *J. Chem. Soc. Faraday Trans*. **77** (1981) 369
41. R. Boscencu, V. Nacea, D. Licsandru, D. Negoiu, *Rev. Chim.* **53** (2002) 619
42. R. Boscencu, D. Licsandru, D. Negoiu, V. Nacea, *Rev. Chim.* **54** (2003) 256
43. L. C. Telmo Figueiredo, R. A. W. Johnstone, A. M. P. Sant Ana Sörensen, D. Burget, P. Jacques, *Photochem. Photobiol.* **69** (1999) 517.

Journal of the Serbian Chemical Society
JSCS@tmf.bg.ac.yu • www.shd.org.yu/JSCS
J. Serb. Chem. Soc. 73 (7) 727–734 (2008)
JSCS–3755
UDC 547–304.6+546.742'982'922:543.42
Original scientific paper

Ni(II), Pd(II) and Pt(II) complexes with ligand containing thiosemicarbazone and semicarbazone moiety: synthesis, characterization and biological investigation

SULEKH CHANDRA* and MONIKA TYAGI

Department of Chemistry, Zakir Husain College, J. L. N. Marg, New Delhi – 110 002, India

(Received 28 November 2007, revised 2 April 2008)

Abstract: The synthesis of nickel(II), palladium(II) and platinum(II) complexes with thiosemicarbazone and semicarbazone of *p*-tolualdehyde are reported. All the new compounds were characterized by elemental analysis, molar conductance measurements, magnetic susceptibility measurements, mass, ^{1}H-NMR, IR and electronic spectral studies. Based on the molar conductance measurements in DMSO, the complexes may be formulated as $[Ni(L)_2Cl_2]$ and $[M(L)_2]Cl_2$ (where M = Pd(II) and Pt(II)) due to their non-electrolytic and 1:2 electrolytic nature, respectively. The spectral data are consistent with an octahedral geometry around Ni(II) and a square planar geometry for Pd(II) and Pt(II), in which the ligands act as bidentate chelating agents, coordinated through the nitrogen and sulphur/oxygen atoms. The ligands and their metal complexes were screened *in vitro* against fungal species *Alternaria alternata*, *Aspergillus niger* and *Fusarium odum*, using the food poison technique.

Keywords: thiosemicarbazone; semicarbazone; transition metal complexes; spectral studies; biological screening.

INTRODUCTION

Thiosemicarbazones have aroused considerable interest in the field of chemistry and biology due to their antibacterial, antifungal, antimalarial, antineoplastic and antiviral activities.[1–5] The biological activities of thiosemicarbazones are considered to be related to their ability to form chelates with metals. The biological activities of metal complexes differ from those of either the free ligands or metal ions and increased or decreased activities in relation to the non-complexed thiosemicarbazones have been reported for several transition metal complexes.[6] After the discovery of the chemotherapeutically active platinum complexes of thiosemicarbazide derivatives,[7] most of the thiosemicarbazone compounds showing biological activities were synthesized. Among the metal complexes of

* Corresponding author. E-mail: schandra_00@yahoo.com
doi: 10.2298/JSC0807727C

thiosemicarbazones, the palladium(II) chelates have been especially studied regarding their antitumour potentials.[8,9] Moreover, palladium(II) complexes with nitrogen-containing ligands are the subject of intensive biological evaluation in the search for less toxic and more selective anticancer therapies.[10,11] In addition to these, Ni(II) and Pt(II) complexes of thiosemicarbazones have been reported as compounds that present biological activity.[12,13a]

In view of the above discussion, in the present paper the synthesis, spectral and antifungal studies of the bidentate ligands (Fig. 1) with the Ni(II), Pd(II) and Pt(II) metal ions are reported.

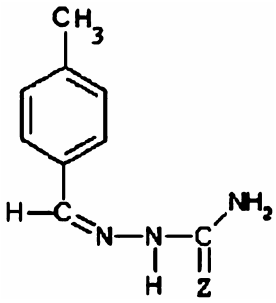

Z =S, for L^1
Z =O, for L^2

Fig. 1. Structure of the ligands.

EXPERIMENTAL

All the employed chemicals were of analytical grade and procured from Sigma–Aldrich and Fluka. The metal salts were purchased from Merck and were used as received. All the employed solvents were of standard spectroscopic grade.

Synthesis of the ligands

Ligand L^1. A hot ethanolic solution (20 ml) of thiosemicarbazide (1.82 g, 0.020 mol) and an ethanolic solution (20 ml) of *p*-tolualdehyde (2.18g, 0.020 mol) were mixed slowly with constant stirring. This mixture was refluxed at 70–80 °C for 3 h. On cooling, a white coloured compound precipitated out, which was filtered, washed with cold EtOH and dried under vacuum over P_4O_{10}. Yield 62 %; m.p. 225 °C. Anal. Calcd. (%) for $C_9H_{11}N_3S$ (193): C, 55.95; H, 5.69; N, 21.76. Found: C, 56.01; H, 5.73; N, 22.81.

Ligand L^2. An aqueous solution (20 m.) of semicarbazide hydrochloride (2.22 g, 0.020 mol) and an ethanolic solution (20 ml) of *p*-tolualdehyde (2.18 g, 0.020 mol) were mixed in the presence of sodium acetate (2.72 g, 0.020 mol). The reaction mixture was stirred vigorously for 1 h. On cooling, a white coloured compound precipitated out, which was filtered, washed with cold EtOH and dried under vacuum over P_4O_{10}. Yield 65 %; m.p. 205 °C. Anal. Calcd. (%) for $C_9H_{11}N_3O$ (177): C, 61.02; H, 6.21; N, 23.72. Found C, 61.11; H, 6.18; N, 23.66.

Synthesis of complexes

A hot ethanolic solution (20 ml) of the required metal salts (0.010 mol) was mixed with a hot ethanolic solution (20 ml) of the required ligand (0.010 mol). This reaction mixture was continuously stirred and refluxed for 4 h at 75 °C. On cooling, a coloured complex separated out, which was filtered, washed with cold ethanol and dried under vacuum over P_4O_{10}.

Physical measurements

Elemental analysis was performed on a Carlo-Erba EA 1106 elemental analyzer and the nitrogen content of the complexes was determined using the Kjeldahl method.[13b] The molar conductivity was measured on a Elico CM82T conductivity bridge. The magnetic moment was measured at room temperature on a Gouy balance using $CuSO_4 \cdot 5H_2O$ as the callibrant. Electronic impact mass spectra were recorded on a JEOL JMS-DX-303 mass spectrometer. The ^{1}H-NMR spectra of the ligands were recorded at room temperature on a Brucker Advance DPX-300 spectrometer using DMSO-d_6 as the solvent. The IR spectra were recorded as KBr pellets on a FTIR spectrum BX-II spectrometer. The electronic spectra were recorded in DMSO on a Shimadzu UV mini-1240 spectrophotometer.

Antifungal screening

The *in vitro* biological screening effects of the investigated compounds were tested against the fungal species *Alternaria alternata*, *Aspergillus niger* and *Fusarium odum* by the food poison method[14] using a potato dextrose agar medium. The stock solutions of compounds were prepared by dissolving the compounds in DMSO. Chlorothalonil was used as a commercial fungicide and DMSO served as the control. Appropriate quantities of the compounds in DMSO were added to obtain a concentration of 250 and 500 ppm of the compound in the medium. The medium was poured into a set of two Petri plates under aseptic conditions in a laminar flow hood. After solidification of the medium in the plates, a mycelial disc of 0.5 cm in diameter, cut from the periphery of a 7-day old culture, was aseptically inoculated upside down in the centre of the Petri plates. These treated Petri plates were incubated at 26±1 °C until fungal growth in the control Petri plates was almost complete.

The mycelial growth of the fungi (mm) in each Petri plates was measured diametrically and the growth inhibition (I, %) was calculated using the formula:

$$I = \frac{d_C - d_T}{d_C} \times 100$$

where d_C and d_T are the diameters of the fungus colony in the control and test plates, respectively.

RESULTS AND DISCUSSION

Based on the elemental analyses, the complexes were assigned the compositions shown in Table I. The molar conductance data of the Ni(II) complexes in DMSO lay in the range 8.0–11 Ω^{-1} cm^2 mol^{-1}, indicating their non-electrolytic nature. However, the Pd(II) and Pt(II) complexes are 1:2 electrolytes with conductance values of 208–217 Ω^{-1} cm^2 mol^{-1}. Thus, these complexes may be formulated as $[Ni(L)_2Cl_2]$ and $[M(L)_2]Cl_2$ (where L = L^1 and L^2, M = Pd(II) and Pt(II)).

The electron-impact mass spectra of the ligands L^1 and L^2 are shown in Figs. 2 and 3, respectively.

The ^{1}H-NMR spectra (Table II) of the free ligands show three singlets at δ 3.41–3.45, 11.90–11.95 and 8.02–8.08 ppm due to the $-NH_2$ proton, −NH proton and azomethine proton (−CH=N−), respectively.

The IR spectra (KBr, cm^{-1}) of the free ligands display two sharp bands at *ca.* 3420 and 3350 cm^{-1}, assignable to the asymmetric and symmetric NH_2 group,

respectively; 1606, 1597 ν(C=N), 765 ν(C=S), 1680 ν(C=O), 440–452 ν(M−N), 304–312 ν(M−S) and 408–418 ν(M−O). The important IR bands are given in Table II.

TABLE I. Molar conductance and elemental analysis data of the complexes

Complex	Molar conductance Ω^{-1} cm^2 mol^{-1}	Colour	M.p. °C	Yield %	Elemental analysis Found (Calcd.), %			
					M	C	H	N
$[Ni(L^1)_2Cl_2]$	8	Green	250	68	11.39	41.53	4.20	16.31
$NiC_{18}H_{22}N_6S_2Cl_2$					(11.43)	(41.86)	(4.26)	(16.28)
$[Ni(L^2)_2Cl_2]$	11	Green	262	65	12.28	44.56	4.49	17.40
$NiC_{18}H_{22}N_6O_2Cl_2$					(12.19)	(44.62)	(4.55)	(17.36)
$[Pd(L^1)_2]Cl_2$	212	Brown	270	60	18.78	38.30	3.88	14.88
$PdC_{18}H_{22}N_6S_2Cl_2$					(18.82)	(38.36)	(3.91)	(14.92)
$[Pd(L^2)_2]Cl_2$	208	Grey	257	62	20.02	40.62	4.09	15.89
$PdC_{18}H_{22}N_6O_2Cl_2$					(19.96)	(40.68)	(4.14)	(15.81)
$[Pt(L^1)_2]Cl_2$	214	Yellow	280	60	29.88	33.20	3.42	12.82
$PtC_{18}H_{22}N_6S_2Cl_2$					(29.91)	(33.13)	(3.37)	(12.88)
$[Pt(L^2)_2]Cl_2$	217	Yellow	272	63	31.52	34.79	3.62	13.59
$PtC_{18}H_{22}N_6O_2Cl_2$					(31.45)	(34.84)	(3.55)	(13.55)

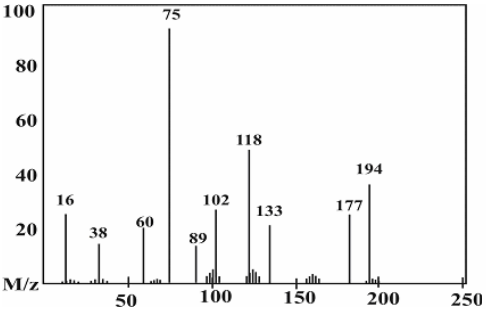

Fig. 2. Electron-impact mass spectrum of ligand L^1.

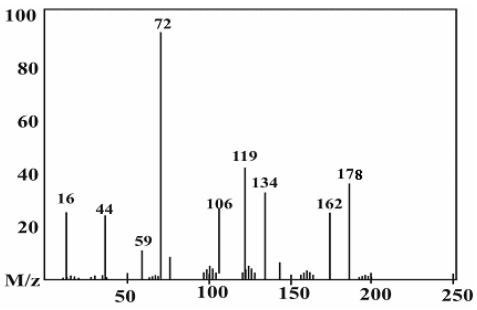

Fig. 3. Electron-impact mass spectrum of ligand L^2.

TABLE II. ^{1}H-NMR and IR spectral data of the ligands and their complexes

Compound	^{1}H-NMR (δ, ppm)			IR (cm^{-1})					
	–NH_2	–NH	HC=N	ν(C=N)	ν(C=S)	ν(C=O)	ν(M–S)	ν(M–O)	ν(M–N)
L^1	3.42	11.92	8.06	1606	765	–	–	–	–
L^2	3.45	11.90	8.02	1597	–	1680	–	–	–
$[Ni(L^1)_2Cl_2]$	3.43	11.93	8.20	1620	752	–	308	411	452
$[Ni(L^2)_2Cl_2]$	3.41	11.95	8.28	1609	–	1665	305	408	445
$[Pd(L^1)_2]Cl_2$	3.44	11.90	8.32	1625	740	–	312	410	448
$[Pd(L^2)_2]Cl_2$	3.42	11.94	8.26	1612	–	1652	310	413	440
$[Pt(L^1)_2]Cl_2$	3.43	11.90	8.18	1622	745	–	304	415	443
$[Pt(L^2)_2]Cl_2$	3.44	11.91	8.30	1615	–	1662	307	418	450

The magnetic moment of Ni(II) complexes lies in the range 2.95–2.98 μ_B, corresponding to two unpaired electrons. These values are in tune with a high spin configuration and show the presence of an octahedral environment around the Ni(II) ion. However, all the Pd(II) and Pt(II) complexes (Table III) show diamagnetic behaviour.

TABLE III. Magnetic moments and electronic spectral data of the complexes

Complexes	μ_{eff} / μ_B	λ_{max} / nm	Assignments
$[Ni(L^1)_2Cl_2]$	2.95	982	$^3A_{2g}$ (F) → $^3T_{2g}$(F) (ν_1)
		697	$^3A_{2g}$ (F) → $^3T_{1g}$(F) (ν_2)
		395	$^3A_{2g}$ (F) → $^3T_{1g}$(P) (ν_3)
$[Ni(L^2)_2Cl_2]$	2.98	973	$^3A_{2g}$ (F) → $^3T_{2g}$(F) (ν_1)
		702	$^3A_{2g}$ (F) → $^3T_{1g}$(F) (ν_2)
		405	$^3A_{2g}$ (F) → $^3T_{1g}$(P) (ν_3)
$[Pd(L^1)_2]Cl_2$	Diamagnetic	480	$^1A_{1g}$→ $^1A_{2g}$(ν_1)
		452	$^1A_{1g}$→ $^1B_{1g}$(ν_2)
		390	$^1A_{1g}$→ ^1E_g(ν_3)
$[Pd(L^2)_2]Cl_2$	Diamagnetic	472	$^1A_{1g}$→ $^1A_{2g}$(ν_1)
		443	$^1A_{1g}$→ $^1B_{1g}$(ν_2)
		397	$^1A_{1g}$→ ^1E_g(ν_3)
$[Pt(L^1)_2]Cl_2$	Diamagnetic	530	$^1A_{1g}$→ $^1A_{2g}$(ν_1)
		416	$^1A_{1g}$→ $^1B_{1g}$(ν_2)
		362	$^1A_{1g}$→ ^1E_g(ν_3)
$[Pt(L^2)_2]Cl_2$	Diamagnetic	520	$^1A_{1g}$→ $^1A_{2g}$(ν_1)
		410	$^1A_{1g}$→ $^1B_{1g}$(ν_2)
		345	$^1A_{1g}$→ ^1E_g(ν_3)

The electronic spectra of the Ni(II) complexes display three absorption bands in the ranges of 973–982 nm, 697–702 nm and 395–405 nm. These bands may be assigned to three spin-allowed transitions: $^3A_{2g}$ (F) → $^3T_{2g}$ (F) (ν_1), $^3A_{2g}$ (F) → → $^3T_{1g}$ (F) (ν_2) and $^3A_{2g}$ (F) → $^3T_{1g}$ (P) (ν_3), respectively. The positions of these bands indicate that the complexes have an octahedral environment.[15–18]

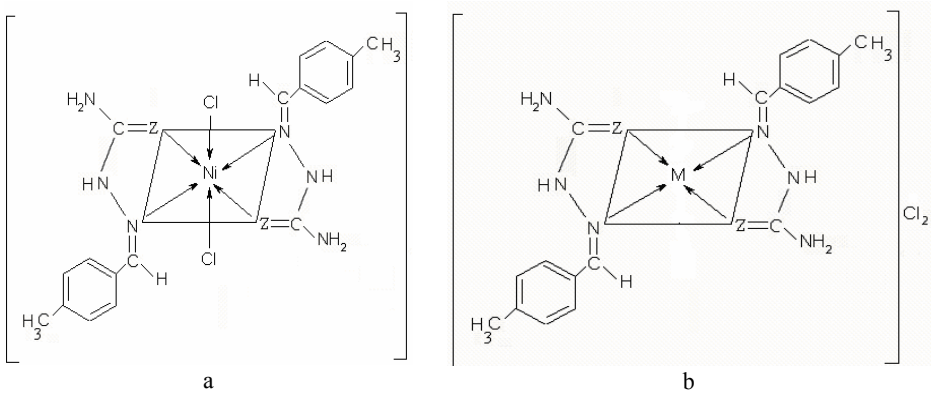

Fig. 4. Suggested structure of the complexes (M = Pd(II) and Pt(II); Z = S/O).

The electronic spectra of the Pd(II) and Pt(II) complexes show three d–d spin-allowed transitions. These correspond to the transitions from the three lower lying d levels to the empty $d_{x^2-y^2}$ orbital. The ground state is $^1A_{1g}$. The three d–d transitions were observed in the regions 472–530, 410–452 and 345–397 nm. These bands are attributed to $^1A_{1g} \rightarrow {}^1A_{2g}$ (ν_1), $^1A_{1g} \rightarrow {}^1B_{1g}$ (ν_2) and $^1A_{1g} \rightarrow {}^1E_g$ (ν_3) transitions, respectively. The electronic spectra of these complexes indicate square planar geometry around the Pd(II) and Pt(II) ion.[19,20]

Based on the above spectral studies, the structures shown in Fig. 4 may be suggested for the complexes.

The results of fungicidal screening (Fig. 5) show that the metal complexes have a higher antimicrobial activity than the free ligands. The increased activity of the metal chelates can be explained based on the chelation theory.[21] On chelation, the polarity of the metal ion is reduced largely due to the overlap of the ligand orbital and the partial sharing of the positive charge of the metal ion with the donor groups. Furthermore, it increases the delocalization of the π-electrons over the whole chelating ring and enhances the penetration of the complexes into lipid membranes and blocking of the metal binding sites in the enzymes of microorganisms. There are other factors which also increase the activity, such as solubility, conductivity and bond length between the metal and the ligand.

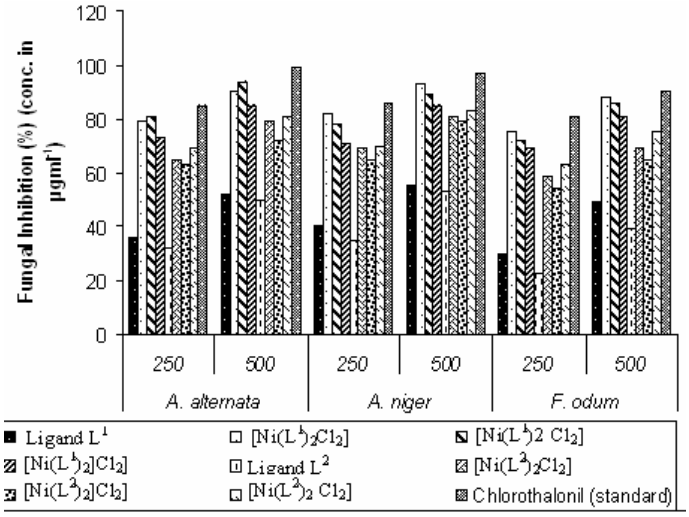

Fig. 5. Biological activity of the compounds.

CONCLUSIONS

The present study revealed octahedral geometry around the Ni(II) and square planar geometry around the Pd(II) and Pt(II) complexes, in which the ligands act as bidentate chelating agents coordinating through the nitrogen and sulphur/ /oxygen atoms.

The determined antimicrobial activities indicate that the metal chelates show a greater inhibitory effect than the parent ligands. It is also proposed that concentration plays a vital role in increasing the degree of inhibition; as the concentration increases, the activity increases. It is also interesting to note that the sulphur bonded ligands and their complexes are more active than the oxygen bonded ligands and their complexes.

Acknowledgement. The authors are thankful to the DRDO, New Delhi for financial support.

И З В О Д

Ni(II), Pd(II) И Pt(II) КОМПЛЕКСИ СА ЛИГАНДИМА КОЈИ САДРЖЕ ТИОСЕМИКАРБАЗОНСКУ И КАРБАЗОНСКУ ГРУПУ: СИНТЕЗА, КАРАКТЕРИЗАЦИЈА И БИОЛОШКА ИСТРАЖИВАЊА

SULEKH CHANDRA и MONIKA TYAGI

Department of Chemistry, Zakir Husain College, J. L. N. Marg, New Delhi – 110 002, India

Приказана је синтеза никал(II), паладијум(II) и платина(II) комплекса са тиосемикарбазоном и семикарбазоном *p*-толуалдехида. Нова једињења су окарактерисана елементалном анализом, мерењем молске проводљивости и магнетне сусцептибилности, као и ^{1}H-NMR, IR и електронском спектроскопијом. На основу молске проводљивости у DMSO, могуће формуле комплекса су $[Ni(L)_2Cl_2]$ и $[M(L)_2]Cl_2$ (M = Pd(II) and Pt(II)) због њихове неелектролитске и 1:2 електролитске природе, респективно. Спектрални подаци су у складу са октаедарском геометријом око Ni (II) и квадратно-планарном геометријом око Pd(II) and Pt(II), у којима су лиганди бидентатни хелатни агенси, везани преко азотовог и сумпоровог/кисеониковог атома. Биолошка активност лиганада и њихових металних комплекса испитивана је *in vitro* према гљивичним врстама *Alternaria alternata*, *Aspergillus niger* и *Fusarium odum* помоћу технике тровања храном.

(Примљено 28. новембра 2007, ревидирано 2. априла 2008)

REFERENCES

1. D. X. West, S. B. Padhye , P. S. Sonawane, *Struct. Bond.* **1** (1991) 76
2. A. K. EI-Sawaf, D. X. West, F. A. EI-Saied, R. M. EI-Bahnasaway, *Synth. React. Inorg. Met. Org. Chem.* **27** (1997) 1127
3. D. X. West, A. E. Liberta, S. B. Padhye, R. C. Chikate, P. B. V. Sonawane, A. S. Kumbhar, R. G. Yerande, *Coord. Chem. Rev.* **123** (1993) 49
4. D. R. Smith, *Coord. Chem. Rev.* **164** (1997) 575
5. M. M. B. Pessoa, G. F. S. Andrade, V. R. P. Monteiro, M. L. A. Temperini, *Polyhedron* **20** (2001) 3133
6. A. E. Liberta , D. X. West, *BioMetals* **5** (1992) 121
7. P. Mantegazza, R. Tommasini, *Farmaco* **6** (1951) 264
8. H. B. Tosi, *Inorg. Chim. Acta* 125 (1986) 173
9. I. H. Hall, C. B. Lackey, T. D. Kistler, R. W. Durhan Jr., E. M. Jouad, M. A. Khan, X. D. Thanh, S. Djebbar-Sid, O. Benali Baitich, G. M. Bouet, *Pharmazie* **55** (2000) 937
10. M. A. Jakupec, M. Galanski, B. K. Keppler, *Rev. Physiol. Biochem. Pharmacol*. **146** (2003) 53

11. L. Giovagnini, L. Ronconi, D. Aldinucci, D. Lorenzon, S. Sitran, D. Fregona, *J. Med. Chem.* **48** (2005) 1588
12. S. Chandra, S. Raizada, M. Tyagi, A. Gautam, *Bioinorg. Chem. Appl.* **2007** (2007) 51483
13. a) D. Kovala-Demertzi, A. Domopoulou, M. A. Demertzis, G. Valle, A. Papageorgio, *J. Inorg. Biochem.* **68** (1997) 147; b) *Vogel's Text Book Practical Organic Chemistry*, B. S. Furniss, A. J. Hannaford, P. W. G. Smith, A. R. Tatchell, Eds., Longman, London, 1989
14. R. K. Agarwal, L. Singh, D. K. Sharma, *Bioinorg. Chem. Appl.* **2006** (2006) 59509
15. S. Chandra, U. Kumar, *J. Saudi Chem. Soc.* **7** (2003) 337
16. S. Chandra, A. Kumar, *J. Indian Chem. Soc.* **84** (2007) 55
17. S. Chandra, U. Kumar, *Spectrochim. Acta* **61A** (2005) 219
18. S. Chandra, A. Kumar, *Spectrochim. Acta* **66A** (2007) 1347
19. D. X. West, M. M.Salberg, G. A. Bain, A. E. Liberta, J. Valdes-Martinez , S. Hernandez--Orteza, *Transition Met. Chem.* **21** (1996) 206
20. B. B. Mahapatra, D. Panda, *Transition Met. Chem.* **41** (1979) 809
21. S. K. Sengupta, O. P. Pandey, B.K. Srivastava, V. K. Sharma, *Trans. Met. Chem.* **23** (1998) 349.

Journal of the Serbian Chemical Society
JSCS@tmf.bg.ac.yu • www.shd.org.yu/JSCS
J. Serb. Chem. Soc. 73 (7) 735–744 (2008)
JSCS–3756
UDC 547.466.24+547.831:544.35:531.3
Original scientific paper

Effect of excess free energy of solvents on the oxidation of methionine by quinolinium fluorochromate. A kinetic study

D. S. BHUVANESHWARI[1] and K. P. ELANGO[2]*

[1]*Department of Chemistry, PSNA College of Engineering and Technology, Dindigul – 624 622, Tamilnadu and* [2]*Department of Chemistry, Gandhigram Rural University, Gandhigram – 624 302, Tamilnadu, India*

(Received 18 October 2007, revised 5 May 2008)

Abstract: The oxidation of methionine by quinolinium fluorochromate (QFC) was studied in the presence of chloroacetic acid, in water/organic solvent mixtures of varying excess molar free energy function. The reaction is first order with respect to both QFC and acid. The reaction rates were determined at different temperatures and the activation parameters computed. The rate data was correlated with different solvent parameters using linear multiple regression analysis. From the results, information on the solvent–reactants and the solvent–transition state interactions was obtained.

Keywords: solvent effect; kinetics; methionine.

INTRODUCTION

Studies of the kinetics of the oxidation of organic compounds in non-aqueous and aqua–organic solvent mixtures[1–6] revealed the important role of non-specific and specific solvent effects on the reactivity. It is of great interest to study the kinetics of oxidation of methionine in binary solvent mixtures, which are more complex than pure solvents, due to the varying degrees of solute–solvent interactions. In a pure solvent, the composition of the microsphere of solvation of a solute, the so-called cybotatic region, is the same as in the bulk solvent but in binary mixtures, the composition in this microsphere can be different. The solute can interact to a different degree with the components of the mixture and this difference in the interactions is reflected in the composition of the microsphere of solvation. The effect of varying the composition of a mixture from the bulk solvent to the solvation sphere is called preferential solvation.[7]

It was shown that the reactivity is influenced by the preferential solvation of the reactants and/or transition state through non-specific and specific solvent–solvent–solute interactions. Furthermore, it was established that the technique of

* Corresponding author. E-mail: drkpelango@rediffmail.com
doi: 10.2298/JSC0807735B

correlation analysis might be used well to separate and quantify such solvent–solvent–solute interactions on reactivity. Extensive studies on the mechanism of oxidation of methionine (Met) by several oxidants have been reported. This sulphur containing essential amino acid is reported to behave differently, in comparison to other amino acids, towards many oxidants.[8–12] This may well be due to the presence of an electron-rich sulphur centre, which is easily oxidisable.

Quinolinium fluorochromate (QFC) was reported to be a mild, stable and selective oxidant.[13] A perusal of the literature showed that there seems to be a very few reports using QFC. Blandamer and Burgess[14] classified aqueous mixtures based on their thermodynamic properties, particularly their molar excess functions, X^E. Thus, in this article, the kinetics and mechanism of the oxidation of methionine by QFC in water/1,4-dioxane (apolar, aprotic, hydrogen bond acceptor solvent), water/DMF (polar, aprotic, hydrogen bond acceptor solvent), water/acetonitrile, water/acetone (both dipolar aprotic non-hydrogen bond donor solvent), and water/*t*-BuOH (protic, hydrogen bond donor solvent) mixtures of varying mole fractions, with the view of comprehending the utility of studies of solvent variation in the understanding of the mechanism of this biologically important amino acid, as it may reveal the mechanism of amino acid metabolism. Furthermore, solvent mixtures are very useful for studying solvent effects upon reactions, since the properties of various mixed solvents can be adjusted continuously by changing the composition of the mixture.

EXPERIMENTAL

Materials

All the employed chemicals and solvents were of analytical grade. Methionine (SRL, India) was used as supplied. Quinolinium fluorochromate (QFC) was prepared by a reported method[13] and its purity was checked by the iodometric method. Doubly distilled water was used for all purposes.

Kinetic measurements

The reactions were performed under pseudo-first order conditions by keeping the substrate in excess over QFC. The progress of the reactions was monitored by estimating the unreacted oxidant iodometrically at 25±0.2 °C. The rate constants were determined by the least squares method, from the linear plots of log titre *versus* time. Duplicate runs showed that the rate constants were reproducible to within ±3 %. The stoichiometry and product analysis were performed as reported earlier.[11,12]

Data analysis

Correlation analyses were performed using Microcal Origin (version 6.0) computer software. The goodness of the fit is discussed using the correlation coefficients and standard deviations.

RESULTS AND DISCUSSION

The kinetics of oxidation of methionine by QFC was studied in water at 25±0.2 °C in the presence of chloroacetic acid. The effect of added organic co-sol-

vent, *viz*. DMF, 1,4-dioxane, acetone, *t*-BuOH and MeCN on the kinetics of oxidation was also investigated at varying mole fractions of the co-solvents. The stoichiometry of the reaction between methionine and QFC was found to be 1:1, corresponding to the following equation:

$$Me–S–R + O_2CrFOQuH \rightarrow Me–S(O)–R + OCrFOQuH$$

The product analysis was carried out under kinetic conditions. The oxidation of methionine resulted in the formation of the corresponding sulphoxide, which was confirmed using GC–MS (*m*/*z* 166) and its fragmentation at *m*/*z* 102, as well from the IR spectra (S=O stretching frequency at 1066 cm^{-1}):

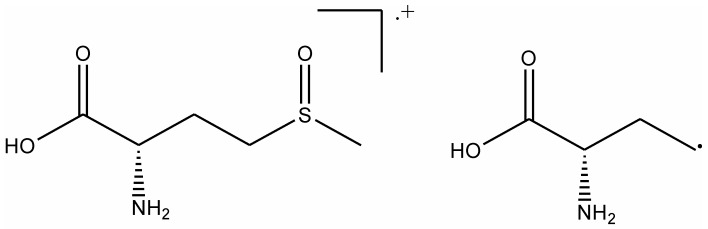

m/z 166 m/z 102

The reactions were of first order with respect to QFC. Furthermore, the values of k_{obs} were independent of the initial concentration of QFC (Table I). The reaction was catalyzed by hydrogen ions and the order with respect to H^+ was one. The reaction rate increased linearly with increasing concentration of Met. The order of the reaction with respect to Met was also one. Furthermore, the plot $1/k_{obs}$ *versus* $1/c$(Met) was linear (r = 0.982, slope = 4.519±0.48) with a positive intercept on the rate ordinate, which indicates that the reaction follows a Michalies–Menten type mechanism. Therefore, the rate law can be represented as:

$$-dc(QFC)/dt = k\, c(Met)\, c(QFC)\, c(H^+)$$

The oxidation of Met in a nitrogen atmosphere failed to induce the polymerization of acrylonitrile. Furthermore, the rate of oxidation decreased with the addition of Mn(II), indicating the involvement of a two-electron reduction of Cr(VI) to Cr(IV). Therefore, a one-electron oxidation, giving rise to free radicals, is unlikely. The rate of oxidation of Met was determined at different temperatures and the activation parameters were calculated at 35 °C: $\Delta H^{\#}$ = 19.8 kJ mol^{-1}, $\Delta S^{\#}$ = = –211 J K^{-1} mol^{-1} and $\Delta G^{\#}$ = 84.7 kJ mol^{-1}. These activation parameters are comparable with those for the oxidation of Met by other halochromates.[11,12,15]

The influence of solvent on the rate of the reaction was studied in water–organic solvent mixtures at different mole fractions of organic co-solvent, *viz*. 1,4-dioxane, DMF, acetonitrile, acetone and *t*-BuOH. The results in Table II indicate that the rate constants (k_2) are remarkably sensitive to the nature and the composition of the mixed solvent.

Solvent variations may effect the kinetics and the energy of the electron transfer processes in a complex manner, particularly in mixed solvent media as the physico–chemical properties of mixed solvent media are often quite different form those of the pure solvents or of their ideal mixtures.[16] The dependence of the kinetic parameters for reactions on the composition of mixed aqueous solvents often affords complicated patterns. In aqueous solutions, at least, it has become clear that an important aspect of the activation process is the reorganization of the solvent surrounding the reacting solute(s). Not surprisingly, such reorganizations will be profoundly affected by the addition of a co-solvent to these aqueous solutions. Indeed, it is now clearly recognized that the action of the non-aqueous component of a mixture is more than that of a simple diluent of water or a modifier of its dielectric properties.[14]

TABLE I. Pseudo-first order rate constants for the oxidation of Met by QFC in water at 25±0.2 °C

c(Met) / 10^{-2} mol dm^{-3}	c(QFC) / 10^{-3} mol dm^{-3}	c(Acid) / mol dm^{-3}	k_{obs} / 10^{-4} s^{-1}
2.0	1.00	0.30	4.28
2.0	1.25	0.30	4.31
2.0	1.50	0.30	4.28
2.0	1.75	0.30	4.29
2.0	2.00	0.30	4.12
1.0	1.00	0.30	2.20
1.5	1.00	0.30	2.85
2.0	1.00	0.30	4.28
2.5	1.00	0.30	5.29
3.0	1.00	0.30	6.12
2.0	1.00	0.30	2.85[a]
2.0	1.00	0.10	1.57
2.0	1.00	0.20	2.94
2.0	1.00	0.30	4.28
2.0	1.00	0.40	6.24
2.0	1.00	0.50	7.23

[a]Contained 5×10^{-4} M Mn(II)

TABLE II. Effect of added organic co-solvents on the rate constant (k_{obs} / 10^{-4} s^{-1}) of the oxidation of methionine by QFC at 25 °C

Mole fraction of organic co-solvent	DMF	1,4-Dioxane	Acetone	*t*-BuOH	MeCN
0	4.28	4.28	4.28	4.28	4.28
0.10	1.01	3.86	4.23	4.25	3.63
0.20	0.50	3.48	4.24	4.25	3.50
0.30	0.36	3.42	4.34	4.36	3.85
0.40	0.27	3.51	4.45	4.52	3.91
0.50	0.23	3.84	4.51	4.64	4.11
0.60	0.18	4.38	4.60	4.73	4.28
0.70	0.15	5.32	4.67	4.84	4.36

The binary aqueous mixtures chosen for the present study represent various classes of solvent mixtures according to Blandamar and Burgess.[14] Aqueous mixtures have been classified based on their thermodynamic properties, particularly their molar excess functions, X^E. Water/1,4-dioxane, water/acetone and water/*t*-BuOH mixtures are examples of the typical aqueous (TA) class, for which the excess Gibbs function, G^E, is positive. Water/MeCN is classified as a typical non-aqueous positive (TNAP) mixture (G^E is positive). Water/DMF falls into the typical non-aqueous negative (TNAN) category, for which G^E is negative.

The properties of TA mixtures are particularly sensitive to the mole fraction of the non-aqueous co-solvent, x_2. At low mole fractions, TA solvents exerts a water structure-forming action, the solvent co-spheres around each solute molecule overlap and mutually enhance water–water interactions. As more co-solvent is added, the mole fraction exceeds a critical mole fraction, x_2*, where there is insufficient water to maintain a three-dimensional hydrogen-bonded network of water molecules. In the TNAP mixtures, the co-solvent exerts a depolymerising effect on water and in this sense is a structure breaker. In TNAN mixtures, inter-component association occurs which leads to a breakdown of the water–water interactions. Further, an extra-thermodynamic analysis indicates that, at least qualitatively, if G^E is positive, the solute should be more soluble in the mixture than predicted from its solubility in the individual pure solvents.[14]

A plot of log k_{obs} *versus* the mole fraction of organic co-solvent, x_2, is depicted in Fig. 1, from which it is evident that in these aqueous organic solvent mixtures, the rate initially decreased with increasing mole fraction of the organic co-solvent up to ≈ 0.3. With further increase in the amount of co-solvent, in the case of the TAP and TNAP mixtures, the rate of oxidation markedly increased with increasing x_2, while in the TNAN mixtures, the rate decreased very slightly. In other words, when a TAP/TNAP co-solvent was added the rate increased as G^E increased and when a TNAN co-solvent was added, it decreased as G^E decreased. This may be because the transition state was stabilized by the addition of a TAP/TNAP co-solvent; consequently, the rate increased with increasing mole fraction of co-solvent. However, in the water/DMF mixture, the transition state was not stabilized largely, as it is less soluble in the mixtures, as predicted by the negative value of G^E, hence the rate of the reaction decreased. This decrease in the rate, however, was very small. This may be due to the stabilization of the transition state through other specific/non-specific solute–solvent–solvent interactions.

The influence of relative permittivity, ε_r, on the rate can be described by the equation of Laidler and Eyring:[17]

$$\frac{\mathrm{d}\ln k}{\mathrm{d}(1/\varepsilon_r)} = e^2 Z^2 \left(\frac{1}{r} - \frac{1}{r^*}\right) / 2kT \qquad (1)$$

where k is the rate, Z the net charge, r the effective radius and r^* the radius of the activated species. A plot of log k_{obs} *versus* $1/\varepsilon_r$ was nonlinear in all the studied aqua–organic solvent mixtures. A representative plot is shown in Fig. 2, from which it is evident that in the TNAN mixture, the rate of the reaction decreased curvi-linearily with decreasing relative permittivity of the medium. However, in the case of TAP and TNAP mixture, with decreasing relative permittivity, the rate of the reaction initially decreased and after a certain point, it increases.

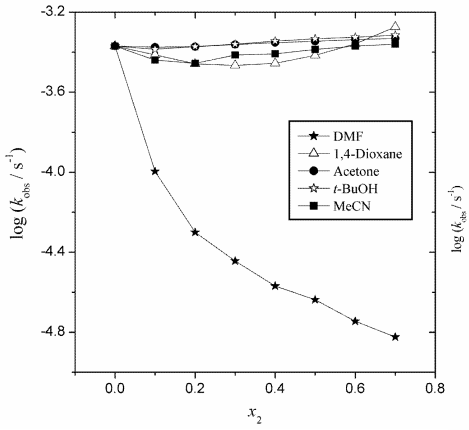

Fig. 1. Plot of log k_{obs} *vs*. mole fraction of the co-solvent, x_2, for the oxidation of methionine by QFC.

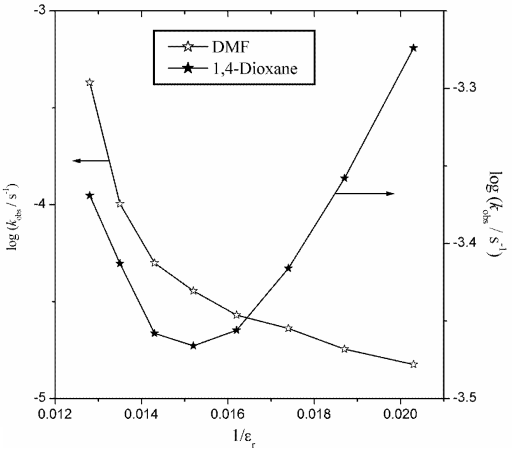

Fig. 2. Plot of log k_{obs} *vs.* $1/\varepsilon_r$ for the studied aqua/organic mixtures.

The solvent effect was also analyzed using the Reichardt solvent parameter $E_T(30)$, which is defined as the solvent micropolarity.[18] Plots of log k_{obs} *versus* $E_T(30)$ for all the water/organic co-solvent mixtures were also nonlinear. This observation, together with the dependence of the rate on the relative permittivity of the medium is parallel to the previously discussed variation of the rate with G^E. These results indicate that the correlations between log k_{obs} and the macroscopic solvent parameters, such as relative permittivity and micropolarity, are poor, *i.e.*, no single solvent parameters can completely explain the effect of the solvent on the reactivity.

The simplicity of idealized electrostatic models for the description of solvation of ions and dipolar molecules, considering solvents as non-structured continua, has led to the use of physical constants, such as relative permittivity, ε_r, refractive index, n, and functions thereof, as macroscopic solvent parameters for the evaluation of medium effects. However, solute–solvent interactions occur on a molecular microscopic level within a structured discontinuum consisting of individual solvent molecules, capable of mutual solvent–solvent interactions. For this reason and because they neglect specific solute–solvent interactions, the electrostatic approach to medium effects often failed in the correlation of the ob-

served solvent effects with physical solvent parameters. In reality, satisfactory quantitative descriptions of medium effects have taken into account all non-specific and specific solvent–solvent–solute interactions. The separation of the solvent polarity into the non-specific and specific solvent–solvent–solute interaction mechanism is purely formal, but, if this separation can be reasonably realised, the resultant parameters may be used to interpret solvent effects through such multiple correlations, thus providing information about the type and magnitude of the interactions with the solvent.[18]

This kind of dual dependency of the reactivity on the solvent composition is illustrated by the Kamlet–Taft solvatochromic comparison method.[19] This method may be used to unravel, quantify, correlate and rationalize multiple interacting solvent effects on reactivity. Thus, the rate data were correlated with solvatochromic parameters in the form of the following linear solvation energy relationship (LSER):

$$\log k = A_0 + s\pi^* + a\alpha + b\beta \quad (2)$$

where π^* is an index of the solvent dipolarity/polarizability, which measures the ability of the solvent to stabilize a charge or a dipole by virtue of its dielectric effect, α is the solvent hydrogen bond donor (HBD) acidity, which describes the ability of the solvent to donate a proton, β is the solvent hydrogen bond acceptor (HBA) basicity, which provides a measure of the ability of the solvent to accept a proton (donate an electron pair), in a solute to solvent hydrogen bond, and A_0 is the regression value of the solute property in the reference solvent cyclohexane. The regression coefficients, s, a and b, measure the relative susceptibilities of the solvent dependent solute property $\log k_{obs}$ to the indicated solvent parameter. These solvatochromic parameters for the aqueous organic mixtures used in the present study were obtained from the literature.[20] The rate of oxidation in the solvent mixture studied show good correlations with solvent *via* the above LSER. The correlation results obtained are given below.

In water/DMF mixtures:

$$\log k_{obs} = -2.806\pm1.92 - (0.414\pm0.55)\pi^* + (0.888\pm0.45)\alpha - (2.468\pm1.72)\beta$$
$$(N = 8;\ R = 0.999;\ R^2 = 0.998;\ Sd = 0.02;\ P_\alpha = 24\ \%;\ P_\beta = 65\ \%;\ P_{\pi^*} = 11\ \%)$$

In water/1,4-dioxane mixtures:

$$\log k_{obs} = -0.874\pm0.83 - (1.330\pm0.89)\pi^* + (0.122\pm0.72)\alpha - (1.889\pm0.85)\beta$$
$$(N = 8;\ R = 0.974;\ R^2 = 0.953;\ Sd = 0.04;\ P_\alpha = 4.0\ \%;\ P_\beta = 57\ \%;\ P_{\pi^*} = 39\ \%)$$

In water/acetone mixtures:

$$\log k_{obs} = -2.041\pm0.78 - (0.782\pm0.25)\pi^* + (0.007\pm0.21)\alpha - (0.911\pm0.58)\beta$$
$$(N = 8;\ R = 0.945;\ R^2 = 0.894;\ Sd = 0.01;\ P_\alpha = 0\ \%;\ P_\beta = 54\ \%;\ P_{\pi^*} = 46\ \%)$$

In water/*t*-BuOH mixtures:

$$\log k_{obs} = -3.165\pm0.01 - (0.121\pm0.05)\pi^* - (0.023\pm0.04)\alpha - (0.096\pm0.03)\beta$$
$$(N = 8;\ R = 0.997;\ R^2 = 0.994;\ Sd = 0.002;\ P_\alpha = 10\ \%;\ P_\beta = 40\ \%;\ P_{\pi^*} = 50\ \%)$$

In water/MeCN mixtures:

$$\log k_{obs} = -2.645\pm0.20 - (0.028\pm0.22)\pi^* - (0.252\pm0.25)\alpha - (0.847\pm0.26)\beta$$
$$(N = 8;\ R = 0.940;\ R^2 = 0.882;\ Sd = 0.02;\ P_\alpha = 22\ \%;\ P_\beta = 76\ \%;\ P_{\pi^*} = 2.0\ \%)$$

Such good correlations, with an explained variance of 94–99 % in the aqua––organic solvent mixtures, indicate the existence of non-specific and specific solvent–solute interactions. From the values of the regression coefficients, the contribution of each parameter (P_x), on a percentage basis, to the reactivity were calculated.[21] The following conclusions were drawn from the systematic correlation studies:

i) In all the investigated solvent mixtures, except MeCN, the contribution of both specific and non-specific solute–solvent interactions play dominant roles, as indicated by the percentage contributions of the α, β and π^* terms. In case of MeCN, the contribution of the specific property is dominant.

ii) The contribution of the solvent HBA term is dominant in all the mixtures, except *t*-BuOH, as indicated by the percentage contributions of this term, P_β compared to P_α and P_{π^*}. This may be because all the co-solvents are typical HBA solvents. Hence, increasing the mole fraction of these solvents in the mixture increases the solute–solvent interactions through the HBA property.

iii) The sign of the coefficient of the α term is positive in the water/DMF, water/1,4-dioxane and water/acetone mixtures, suggesting that the transition state–solvent interactions, through specific HBD property, dominate over the reactant–solvent interactions.

iv) In water/*t*-BuOH and water/MeCN mixtures, the sign of the coefficient of the α term is negative, indicating the reactants are solvated through HBD property to a larger extent than the transition state.

v) The sign of the coefficient of the β and π^* terms in all the investigated mixtures is negative, indicating the reactants are solvated to a larger extent than the transition state through the HBA and dipolarity/polarizability properties.

Therefore, it is concluded that both specific (microscopic) and non-specific (macroscopic) solute–solvent–solvent interactions play a dominant role in governing the reactivity of the substrate under investigation.

Mechanism

Under the experimental conditions employed in the present study, methionine is oxidized to the corresponding sulphoxide stage only. Based on the above kinetic observations, *i.e.*, the first order dependence on *c*(Met), *c*(QFC) and *c*(Acid), the following mechanism is proposed for the oxidation of methionine by QFC. The linear increase in the rate with acidity suggests the involvement of proto-

nated QFC in the rate-determining step. In the first step, QFC becomes protonated. The protonated QFC attacks the substrate to form a complex, in a pre-equilibrium step, which subsequently decomposes to give the products in a slow step. The proposed scheme envisages an oxygen atom transfer from the oxidant, which is in agreement with earlier observations involving the oxidation of sulphur-containing compounds with halochromates. The electrophilic attack on the sulphide sulphur can be viewed as an S_N2 reaction. An S_N2-like transition state (more hydrophobic) is supported by the observed solvent effects:

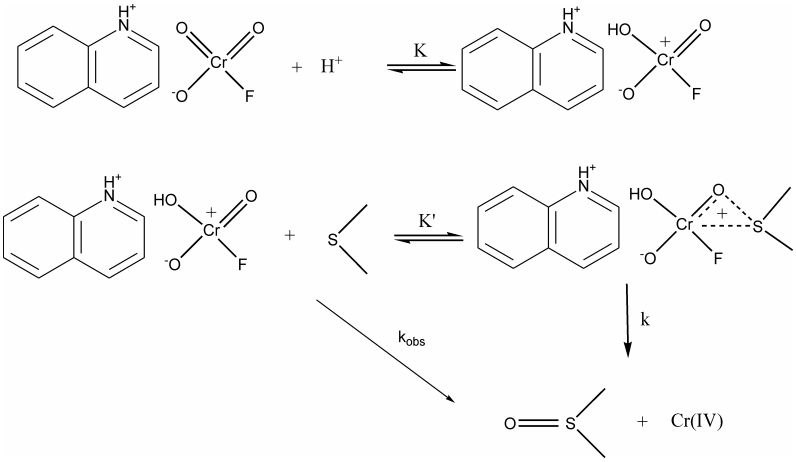

The above mechanism leads to the following rate law:

$$\text{Rate} = kc(\text{Complex})$$
$$c(\text{Complex}) = k'c(\text{Met})c(\text{QFCH}^+)$$
$$c(\text{QFCH}^+) = k''c(\text{QFCH})c(\text{H}^+)$$
$$c(\text{Complex}) = k'k''c(\text{Met})c(\text{QFCH})c(\text{H}^+)$$
$$-\text{d}c(\text{QFCH})/\text{d}t = kk'k''c(\text{Met})c(\text{QFCH})c(\text{H}^+)$$

The rate law in its final form accounts for the observed kinetics. The negative entropy of activation suggests complex formation in the transition state. The linear increase in rate with acidity suggests the involvement of protonated QFC in the rate-determining step.

ИЗВОД

УТИЦАЈ ВИШКА ГИБСОВЕ ЕЕНРГИЈЕ РАСТВАРАЧА НА ОКСИДАЦИЈУ МЕТИОНИНА ХИНОЛИНИУМ-ФЛУОРОХРОМАТОМ. ИСПИТИВАЊЕ КИНЕТИКЕ РЕАКЦИЈЕ

D. S. BHUVANESHWARI и K. P. ELANGO

Department of Chemistry, Gandhigram Rural University, Gandhigram-624302, Tamilnadu, India

Оксидација метионина хинолинијум-флуорохроматом (QFC) испитивана је у присуству хлор-сирћетне киселине, у смеши воде и органских растварача са различитим функцијама вишка моларне Гибсове енергије. Реакција је првог реда у односу на QFC и киселину. Брзина

реакције је одређена на различитим температурама и израчунати су параметри активације. Подаци за брзину реакције корелисани су са различитим параметрима растварача методом линеарне вишеструке регресије. На основу резултата добијене су информације о интеракцијама растварач–реактанти и растварач–прелазно стање.

(Примљено 18. октобра 2007, ревидирано 5. маја 2008)

REFERENCES

1. A. Thirumoorthi, D. S. Bhuvaneshwari, K. P. Elango, *Int. J. Chem. Kinet*. **39** (2007) 362
2. M. Karthikeyan, S. Ghammami, D. S. Bhuvaneshwari, K. P. Elango, *J. Indian Chem. Soc*. **84** (2007) 359
3. D. S. Bhuvaneshwari, K. P. Elango, *Z. Phys. Chem*. **220** (2006) 697
4. D. S. Bhuvaneshwari, K. P. Elango, *J. Indian Chem. Soc*. **83** (2006) 999
5. D. S. Bhuvaneshwari, K. P. Elango, *Z. Naturfosch*. **60b** (2005) 1105
6. G. Fatima Jeyanthi, K. P. Elango, *Int. J. Chem. Kinet*. **35** (2003) 154
7. E. Bosch, F. Rived, M. Roses, *J. Chem. Soc. Perkin Trans. 2* (1966) 2177
8. D. S. Bhuvaneshwari, B. John, M. Pandeeswaran, K. P. Elango, *J. Indian Chem. Soc*. **82** (2005) 616
9. D. Malarvili, M. Pandeeswaran, D. S. Bhuvaneshwari, K. P. Elango, *J. Indian Chem. Soc*. **83** (2006) 895
10. M. Balakrishnan, S. Ghammami, K. P. Elango, *J. Indian Chem. Soc*. **83** (2006) 497
11. V. Sharma, P. K. Sharma, K. K. Banerji, *Indian J. Chem*. **36A** (1997) 418
12. V. Sharma, P. K. Sharma, K. K. Banerji, *J. Indian Chem. Soc*. **74** (1997) 607
13. V. Murugesan, A. Pandurangan, *Indian J. Chem*. **31B** (1992) 377
14. M. J. Blandamer, J. Burgess, *Chem. Soc. Rev*. **4** (1975) 55
15. A. Goyal, S. Kothari, *Indian J. Chem., B* **42** (2003) 2129
16. Y. Marcus, *Ion Solvation*, Wiley, New York, 1985
17. E. S. Amis, J. F. Hinton, *Solvent Effect of Chemical Phenomena*, Vol. 1, Academic Press, New York, 1973
18. C. Reichardt, *Solvents and Solvent Effects in Organic Chemistry*, VCH, Weinheim, 1988
19. M. J. Kamlet, J. M. Abboud, M. H. Abraham, R. W. Taft, *J. Org. Chem*. **48** (1983) 2877
20. Y. Marcus, *J. Chem. Soc*. Perkin Trans. 2 (1994) 1751
21. C. Reichardt, *Angew. Chem. Int. Ed.* **18** (1979) 98.

Journal of the Serbian Chemical Society
JSCS@tmf.bg.ac.yu • www.shd.org.yu/JSCS
J. Serb. Chem. Soc. 73 (7) 745–751 (2008)
JSCS–3757
UDC 666.36–035.26+542.913
Original scientific paper

Synthesis of biomorphic SiC and SiO_2 ceramics

ADELA EGELJA[1#], JELENA GULICOVSKI[1#], ALEKSANDAR DEVEČERSKI[1#], BILJANA BABIĆ[1], MIROSLAV MILJKOVIĆ[2], SNEŽANA BOŠKOVIĆ[1#] and BRANKO MATOVIĆ[1*#]

[1]*Institute of Nuclear Sciences "Vinča", Belgrade and* [2]*Center of Electron Microscopy, University of Niš, Serbia*

(Received 23 October 2007, revised 21 April 2008)

Abstract: Coniferous wood (fir) was transformed by pyrolysis into carbon preforms, which were subsequently converted into biomorphic ceramics by the pressure infiltration technique with colloidal silica. An *in situ* reaction between the silica and the carbon template occurred in the cellular wall at a high sintering temperature. Depending on the employed atmosphere, non-oxide (SiC) or oxide (SiO_2) ceramics were obtained. The morphology of the resulting porous ceramics and their phase composition were investigated by scanning electron microscopy (SEM/EDX) and X-ray diffraction (XRD). The experimental results showed that the biomorphic cellular morphology of the wood maintained in both the SiC and silica ceramics, which consisted of only the β-SiC phase and SiO_2, respectively.

Keywords: biomimetic synthesis; celular SiC; porous ceramics.

INTRODUCTION

The term "ecoceramics" denotes a class of ceramics made of wood-based products. Wood is a natural composite material composed of biopolymeric constituents, such as cellulose, hemicellulose and lignin.[1] Cellulose is the basic structural component of all wood cell walls.[2] Chemically speaking, it is a long chain linear polysaccharide composed of glucose $(C_6H_{10}O_5)_n$. The cellulose superstructure has a matrix of lower molecular weight polysaccharides, named hemicelluloses. Lignin is a three-dimensional polyphenolic molecule with a highly branched structure and high molecular weight. Since it permeates cell walls and the intercellular region, lignin acts as glue, which bonds all wood cells giving the wood its hardness. Wood exhibits a hierarchical architecture with a cellular microstructure of high porosity due to specific functions of living cells, transportation (tracheidal), storage (parenchimal) and mechanical strengthening (libriformal) cells, respectively. The microstructural features of wood are tracheidal cells which are responsible for liquid transportation and they form a pore channel system with a pre-

* Corresponding author. E-mail: mato@vin.bg.ac.yu
# Serbian Chemical Society member.
doi: 10.2298/JSC0807745E

ferential orientation in the axial direction. This feature offers the possibility to use liquid infiltration techniques to transform the hierarchical cellular structure of wood into inorganic materials with the preservation of the original cellular structure.[3–6]

Single phase, porous biomorphic SiC ceramics were manufactured using Si-containing vapors as reactants. The Si-containing vapors were forced to penetrate the pores of the carbon template and react with the biocarbon to form SiC. Different reactive Si vapor sources, such as Si,[7] SiO[8] and CH_3SiCl_3 (methyltrichlorosilane)[9] were applied. Also, Si-melt[10] and TEOS (tetraethyl orthosilicate)[11–13] were used, resulting in biomorphous SiC ceramics. In the other hand, there are only a few investigations about biomorphous oxide-based ceramics. SiO_2-, Al_2O_3-, TiO_2- and ZrO_2- ceramics were prepared from pine wood, as well as from cellulose fiber performs, *via* a sol–gel process with metal-alkoxides.[14–16] However, it seems that no work has been performed to-date on the synthesis of biomorphic ceramics using colloidal silica. Hence, the present work was focused on the synthesis of porous SiC and SiO_2 ceramics by the annealing of premineralized wood with colloidal silica under an argon or ambient atmosphere, respectively.

EXPERIMENTAL

Fir wood was used as the biological template structure. Fir is a coniferous wood which exhibits a monomodal pore distribution with a mean pore diameter of about 20 μm. Colloidal silica was used as the precursor for infiltration. The infiltration/annealing process is described by the schematic diagram in Fig. 1. The fir wood was shaped (10×5×5 mm^3) and dried at 70 °C

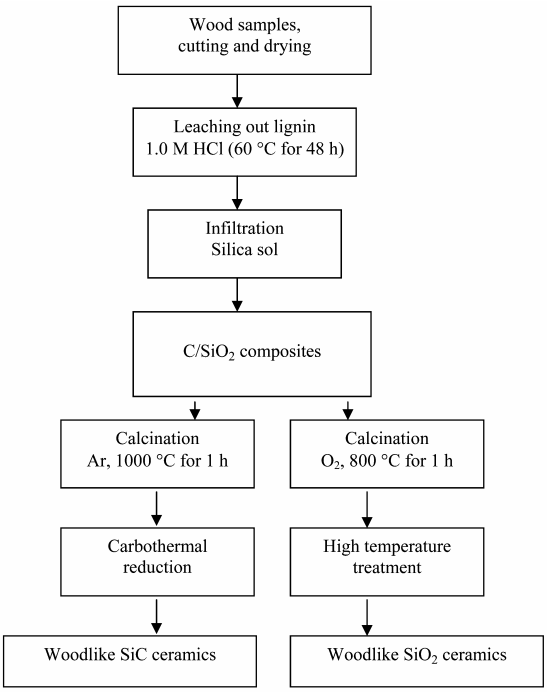

Fig. 1. Flow chart for the manufacture of biomorphic SiC and SiO_2 ceramics.

for 48 h. The dry wood pieces were soaked at 60 °C for 48 h in 1.0 M HCl solution to leach out the lignin and again dried at 60 °C for 48 h. Pieces of treated wood were placed in an infiltration vessel and then backfilled with silica sol, followed by raising the pressure in the vessel up to 5.0 bar. The wood/silica samples were then dried at 110 °C for 8 h.

Two types of experiments were performed. In the first ones, samples were calcinated at 1000 °C under an Ar atmosphere for 1 h. The final thermal treatment was accomplished in a graphite-heated furnace (Astro, USA) under a 0.10 MPa Ar atmosphere at a heating rate of 10 °C min^{-1} to 1450 °C and maintained at this temperature. The samples were cooled down to room temperature under Ar. In the second experiments, the samples were calcinated under ambient atmosphere up to 1300 °C.

Scanning electron microscopy (SEM/EDX) analyses were performed on the "as obtained" surfaces using a JEOL 6300F microscope at 3.0 kV accelerating voltage.

The crystalline phases were identified by X-ray diffraction (XRD) analysis using filtered CuKα radiation (Siemens D5000). For this purpose, the carbon from the samples of experiment one was burnt out at 700 °C in air.

RESULTS AND DISCUSSION

The XRD pattern of the infiltrated wood sample after calcination at 1000 °C for 1 h shows that the obtained C/SiO_2 composite was amorphous (Fig. 2). Two broad peaks centered at around 25 and 44° correspond to the (002) and (004) peaks of carbon.[17]

The phase evolution of the C/SiO_2 composite during heat treatment under an argon atmosphere is depicted in Fig. 3. At 1250 °C there was no evidence of SiC peaks but many weak peaks of SiO_2 (crystobalite) appeared, suggesting that the amorphous silica recrystallized at this temperature. Simultaneously, the baseline line was still high, indicating a rather large amount of amorphous carbon and silica. At 1350 °C, the peaks of the β-SiC phase at $2\theta = 35.68$ and 60.00° were observed, suggesting that carbothermal reduction of silica occurred with the formation of SiC. This was confirmed at 1450 °C, when the high baseline line and the peaks of crystobalite nearly completely disappeared and only the β-SiC peaks existed. Thus, the carbothermal reduction reaction was nearly completed after annealing at 1450 °C for 4 h.

The SEM micrographs of a composite prepared from fir charcoal impregnated with SiO_2 sol and calcinated at 1000 °C as well as the corresponding SiC ceramics obtained at 1450 °C are shown in Fig. 4. In both cases, the porous morphology retains the same structural features as those of fir wood. It was found that the thickness of the SiC-cell wall material, *i.e.*, struts, were less than 1 μm. Cellular SiC ceramic has preferentially oriented pores of diameter up to 5 μm. Energy dispersive spectroscopy (EDS) analysis of the obtained SiC material revealed the peak of Si without O, confirming the results of the measurements. Thus, the porous C/SiO_2 composite was completely converted into SiC ceramic with a similar microstructure.

On the other hand, the C/SiO_2 composite heat treated under an ambient atmosphere at 800 °C was shown by XRD analysis to be still amorphous. How-

ever, weak peaks of SiO_2 (tridimite) appeared, indicating crystallization of the amorphous material. The XRD pattern of the composite treated at higher temperatures exhibited sharp peaks of crystalobalite (SiO_2) and small ones of tridimite (SiO_2). Thus, the XRD analysis showed that after calcination of the infiltrated wood sample under an ambient atmosphere, the carbon was evaporated and the amorphous SiO_2 was transformed into crystalline phases (Fig. 5).

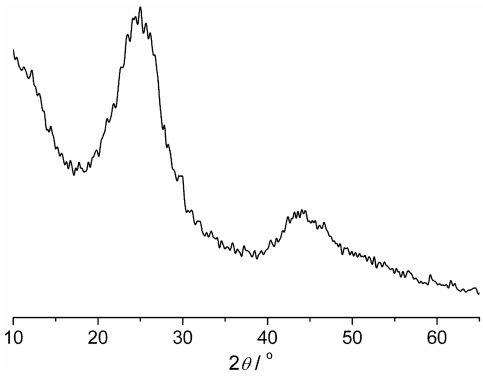

Fig. 2. XRD Pattern of the C/SiO_2 composite.

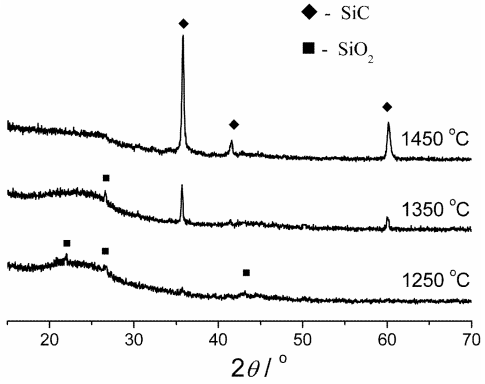

Fig. 3. XRD Patterns of the products obtained from C/SiO2 composites under an argon atmosphere at different temperatures for 4 h.

a)

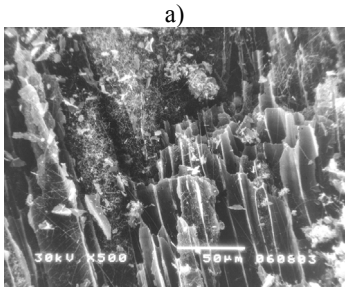

b)

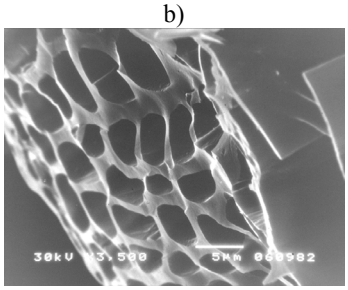

c)

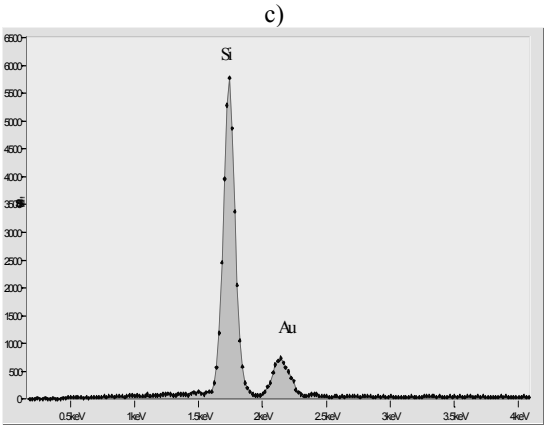

Fig. 4. SEM Microphotographs of the microstructure of an as infiltrated C/SiO_2 composite (a), an SiC ceramic obtained at 1450 °C for 4 h (b) and EDS analysis of the SiC material (c).

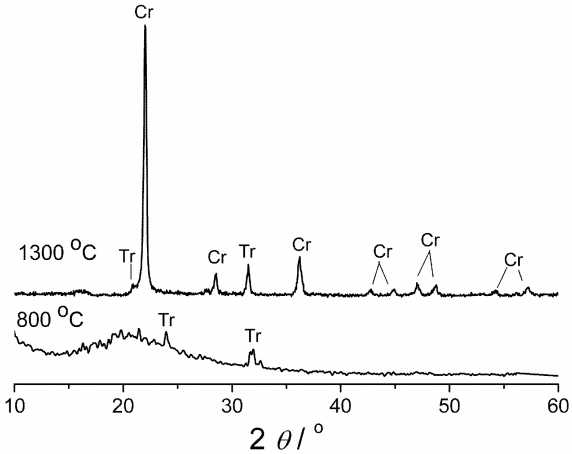

Fig. 5. XRD Patterns of the products obtained from an C/SiO_2 composite under an ambient atmosphere annealed for 4 h (Cr – crystobalite, Tr – tridymite).

The SEM micrographs of the resulting SiO_2 ceramics are shown in Fig. 6. Its morphology in the tangential direction depicts a structure similar to that of the starting wood sample. In comparison with the microstructure of the SiC ceramics, the SiO_2 ceramics possess small pits of 2–3 μm in diameter (Fig. 6b). They were formed during carbon evaporation. The cross sections, perpendicular to the axial direction (Fig. 6c), reveal tracheidal pore channels of diameter up to 10 μm.

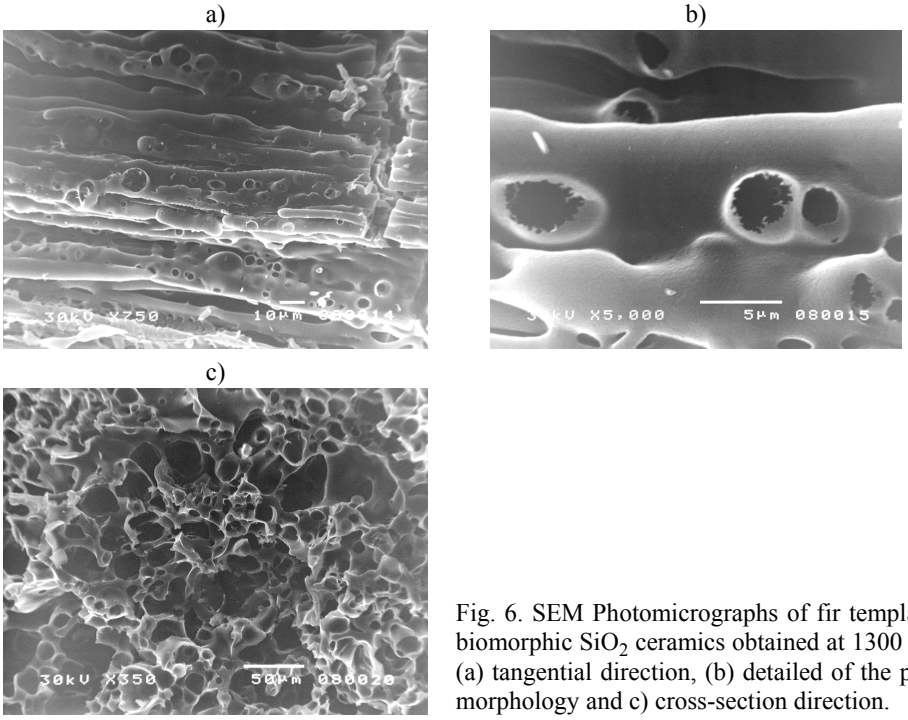

Fig. 6. SEM Photomicrographs of fir template biomorphic SiO_2 ceramics obtained at 1300 °C (a) tangential direction, (b) detailed of the pits morphology and c) cross-section direction.

The mechanism of SiC ceramics formation can be explained by the reaction of SiO vapor, obtained during the reduction of silica, and the carbon wall under an inert protective atmosphere.[18] In contrast, the SiO_2 ceramics with a wood-like structure depend on stable films of infiltrated colloidal silica onto the carbon template,[19,20] which remain after heat treatment and loss of carbon.

CONCLUSIONS

This study demonstrated the conversion of biological cellular tissues structures into a porous ceramic. This porous ceramic with a wood-like microstructure was prepared by sol infiltration and carbothermal reduction techniques using colloidal silica and fir wood as the starting materials. A SiC ceramic was obtained at 1450 °C under an argon atmosphere. XRD Analysis reveals β-SiC as the only phase present in the cellular SiC product. A SiO_2 ceramic was formed at 1300 °C with crystalobalite as the principal phase, after annealing under an ambient atmosphere. This technique provides promising future applications for advanced materials design.

Acknowledgement. This project was financially supported by the Ministry of Science of The Republic of Serbia (Project number: 142016).

И З В О Д

СИНТЕЗА БИОМОРФНЕ SiC И SiO_2 КЕРАМИКЕ

АДЕЛА ЕГЕЉА[1], ЈЕЛЕНА ГУЛИЦОВСКИ[1], АЛЕКСАНДАР ДЕВЕЧЕРСКИ[1], БИЉАНА БАБИЋ[1], МИРОСЛАВ МИЉКОВИЋ[2], СНЕЖАНА БОШКОВИЋ[1] и БРАНКО МАТОВИЋ[1]

[1]Институт за нуклеарне науке Винча, Београд и [2]Центар за електронску микроскопију, Универзитет у Нишу

Карбонизовано дрво јеле је инфилтрирано под притиском са колоидним SiO_2, а затим конвертовано у биоморфну SiC и SiO_2 керамику *in situ* реакцијом између Si и C на високој температури. Морфологија и фазни састав резултујуће оксидне/неоксидне керамике испитивани су скенирајућом електронском микроскопијом (SEM/EDX) и рендгено-структурном анализом (XRD). Резултати су показали да се основна ћелијска морфологија дрвета у SiC и SiO_2 керамици очувала и после третмана на високим температурама.

(Примљено 23. октобра 2007, ревидирано 21. априла 2008)

REFERENCES

1. R. A. Parham, R. L. Gray, in *Advances in Chemistry, Series 207*, R. Rowell, Ed., American Chemical Society, Washington, DC, 1984
2. P. Griel, *J. Eur. Ceram. Soc.* **21** (2001) 105
3. J. Shin, C. Wang, G. J. Eharhus, Adv.Mater. **17** (2005) 73
4. C. R. Rambo, J. Cao, O. Rusina, H. Sieber, *Carbon* **43** (2005) 1147
5. O. Guanjun, M. Rong, C. Ning, Z. Chunguang, J. Zhihao, *J. Mater. Process. Technol.* **120** (2002) 10
6. T. Ota, M. Takahaski, T. Hibi, M. Ozava, S. Suzuki, Y. Hikicki, H. Suzuki, *J. Am. Ceram. Soc.* **78** (1995) 3409
7. E. Vogli, H. Sieber, P. Greial, *J. Eur. Ceram. Soc.* **22** (2002) 2663

8. E. Vogli, J. Mukerji, C. Hoffmann, R. Kladny, H. Sieber, P. Greial, *J. Am. Ceram. Soc.* **84** (2001) 1236
9. H. Sieber, E. Vogli, F. Muler, P. Greial, N. Popovska, H. Gerhard, G. Eming, *Key. Eng. Mater.* **206–213** (2002) 2013
10. M. Sighn, J. A. Salem, *J. Eur. Ceram. Soc.* **22** (2002) 2709
11. T. Ota, M. Takahashi, T. Hibi, M. Ozava, S. Suzuki, Y. Hikichi, *J. Am. Ceram. Soc.* **78** (1995) 3409
12. B. Matović, A. Egelja, B. Babić, J. Gulicovski, E. Volceanov, S. Bošković, *J. Optoelectron. Adv. M.* **10** (2008) 549
13. H. Sieber, A. Kaindl, D. Schwarze, J. P. Werner, P. Greil, *Efi/Ber. DKG* **77** (2000) 21
14. J. Cao, C. R. Rambo, H. Sieber, *J. Porous Mater.* **87** (2004) 163
15. C. R. Rambo, J. Cao, H. Sieber, *Mater. Chem. Phys.* **11** (2004) 345
16. J. Cao, O. Rusina, H. Sieber, *Ceram. Int.* **30** (2004) 1971
17. C. E. Byrne, D. C. Nagle, *Carbon* **35** (1997) 267
18. H. P. Martin, R. Ecke, E. Muller, *J. Eur. Ceram. Soc.* **18** (1998) 1732
19. H. Sieber, *Mater. Sci. Eng. A* **412** (2005) 43
20. Y. Shin, J. Liu, J. Chang, Z. Nie, G. Exarhos, *Adv. Mater.* **13** (2001) 728.

Journal of the Serbian Chemical Society
JSCS@tmf.bg.ac.yu • www.shd.org.yu/JSCS
J. Serb. Chem. Soc. 73 (7) 753–760 (2008)
JSCS–3758
UDC 546.11+546.56:541.135:532.5
Original scientific paper

The ionic equilibrium in the $CuSO_4$–H_2SO_4–H_2O system and the formation of the honeycomb-like structure during copper electrodeposition

NEBOJŠA D. NIKOLIĆ[1]*#, LJUBICA J. PAVLOVIĆ[1#], GORAN BRANKOVIĆ[2], MIOMIR G. PAVLOVIĆ[1#] and KONSTANTIN I. POPOV[1,3#]

[1]ICTM – Department of Electrochemistry, University of Belgrade, Njegoševa 12, P.O. Box 473, 11001 Belgrade, [2]Institute for Multidisciplinary Research, Kneza Višeslava 1a, 11030 Belgrade and [3]Faculty of Technology and Metallurgy, University of Belgrade, Karnegijeva 4, P.O. Box 3503, 11001 Belgrade, Serbia

(Received 26 September 2007, revised 26 March 2008)

Abstract: The ionic equilibrium of the species in the $CuSO_4$–H_2SO_4–H_2O system was employed to systematize the conditions of copper electrodeposition leading to the formation of the honeycomb-like structure. The reason why $CuSO_4$ concentrations higher than 0.15 M are unsuitable for the formation of honeycomb-like structures is shown. The range of H_2SO_4 concentrations enabling the formation of this type of structure was also determined. The conditions leading to the formation of the honeycomb-like structures are: electrodeposition from solutions with lower concentrations of Cu(II) ions (0.15 M $CuSO_4$ and less) in a concentration range from 0.25 to 1.0 M H_2SO_4, at a temperature of 18.0±1.0 °C and at overpotentials outside the plateau of the limiting diffusion current density at which hydrogen evolution is vigorous enough to change the hydrodynamic conditions in the near-electrode layer.

Keywords: electrolysis; hydrodynamics; morphology; hydrogen; copper.

INTRODUCTION

Aqueous solutions of sulfuric acid and cupric sulfate are frequently found in copper hydrometallurgical processes, such as leaching, solvent extraction, electrowinning and electrorefining.[1] Irregular deposits, such as powder deposits[2–5] and open and porous structures with an extremely high surface area,[6] denoted as honeycomb-like ones,[7–9] are most often formed by electrodeposition from these solutions. The main species present in aqueous sulfuric acid solutions containing Cu(II) are: bisulfate ions (HSO_4^-), cupric ions (Cu^{2+}), aqueous cupric sulfate ($CuSO_{4(aq)}$), hydrogen ions (H^+) and sulfate ions (SO_4^{2-}).[1] In an aqueous so-

* Corresponding author. E-mail: nnikolic@tmf.bg.ac.yu
# Serbian Chemical Society member.
doi: 10.2298/JSC0807753N

lution of sulfuric acid and cupric sulfate, two weak electrolytes, HSO_4^- and $CuSO_{4(aq)}$ are formed and the equilibriums between HSO_4^-, H^+ and SO_4^{2-} ions, as well as between $CuSO_{4(aq)}$, Cu^{2+} and SO_4^{2-} species are constituted.[1]

Electrochemical processes dealing with the formation of irregular deposits are very suitable for the analysis of the ionic equilibrium in the $CuSO_4$–H_2SO_4–H_2O system, due to the hydrogen evolution reaction which occurs parallel to copper electrodeposition. The first report which investigated the effect of this ionic equilibrium on the formation of these deposits was reported recently.[10] Considering the high technological significance of honeycomb-like structures as possible electrodes in many electrochemical devices, such as fuel cells, batteries and sensors,[6] a detailed analysis of the ionic equilibrium in the $CuSO_4$–H_2SO_4–H_2O system on the formation of this type of deposit was until this study necessary.

EXPERIMENTAL

Copper was potentiostatically deposited from the following solutions: 0.075 M $CuSO_4$ + + 0.50 M H_2SO_4, 0.30 M $CuSO_4$ + 0.50 M H_2SO_4, 0.60 M $CuSO_4$ + 0.50 M H_2SO_4 and 0.15 M $CuSO_4$ + 0.125 M H_2SO_4.

The electrodepositions were performed in an open cell at a temperature of 18.0±1.0 °C using a Wenking 7103 Girh potentiostat. Doubly distilled water and analytical grade chemicals were used for the preparation of the solutions for the electrodeposition of copper.

The electrodepositions of copper were performed at an overpotential of 1000 mV onto cylindrical copper cathodes previously covered by a thin copper film.

The counter electrode was a copper foil placed close to the walls of the cell; the working electrode was placed in the middle of the cell, while the overpotential was adjusted *vs.* a copper electrode which was positioned at a distance of 0.2 cm from the surface of the working electrode.

For the determination of the average current efficiency of hydrogen evolution, an electrochemical cell with the same arrangement of copper electrodes as that used for the preparation of the copper deposits for SEM analysis was employed. The electrodes were situated under a burette with the surface facing up so that the total amount of hydrogen evolved during the electrodeposition processes went into the burette. During the electrodeposition process, the volume of evolved hydrogen, $V(H_2)$, and the current of the electrodeposition, I, after a time, t, were recorded. Then, after graphical integration I–t, the average current efficiency for hydrogen evolution in a time t, $\eta_{I,av}(H_2)$, was determined according to Eq. (1):

$$\eta_{I,\mathrm{av}}(\mathrm{H_2}) = \frac{nFV(\mathrm{H_2})}{V\int_0^t I\mathrm{d}t} \tag{1}$$

where nF is the number of Faradays per mole of consumed ions and V is the molar volume of a gas under normal conditions (*i.e.*, 22.400 dm^3).

The average current efficiency for hydrogen evolution, $\eta_{av}(H_2)$, is defined as the average value of the $\eta_{I,av}(H_2)$ values over the total electrolysis time.

A detailed procedure for the determination of the average current efficiency of hydrogen evolution has already been given.[7]

SEM Microphotographs corresponding to morphologies of copper deposits, obtained with a quantity of electricity of 10.0 mA h cm^{-2}, were recorded on scanning electron microscope (SEM) JOEL, model T20, and a Tescan Digital Microscope.

RESULTS AND DISCUSSION

The copper deposits obtained at an overpotential of 1000 mV from 0.075, 0.30 and 0.60 M $CuSO_4$ in 0.50 M H_2SO_4 are shown in Fig. 1. For all these solutions, an overpotential of 1000 mV is for 250 mV higher than the plateaus of the limiting diffusion current density.[11] As can be seen from Fig. 1, holes formed due to attached hydrogen bubbles were the main morphological form obtained under these electrodeposition conditions. The shape of the obtained holes changed with increasing $CuSO_4$ concentration, from those forming a honeycomb-like structure to dish-like ones and the mechanism of their formation has been widely studied.[7,8,11]

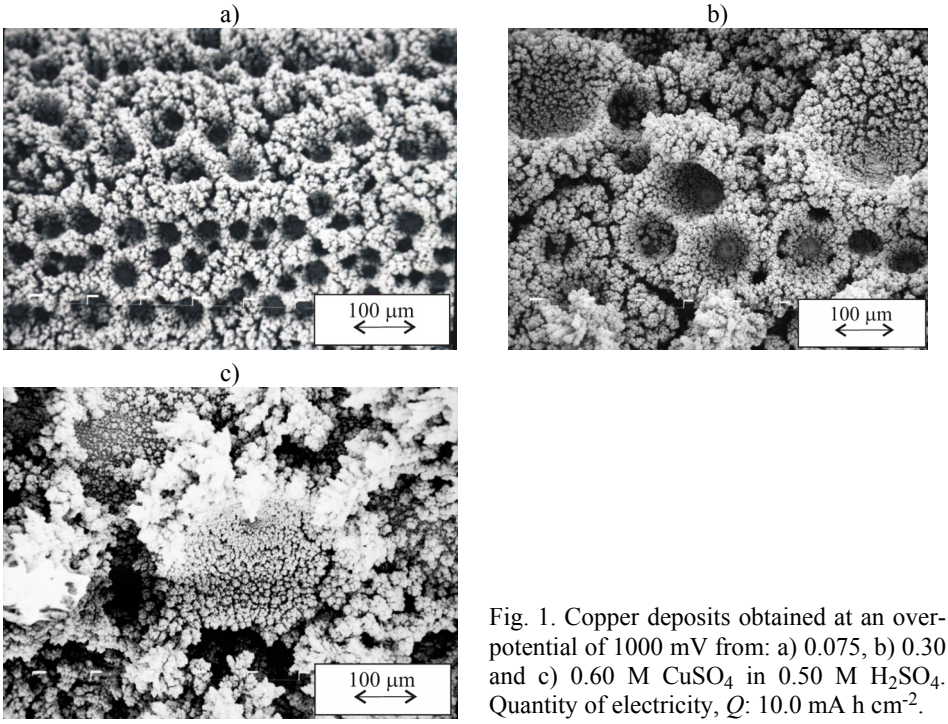

Fig. 1. Copper deposits obtained at an overpotential of 1000 mV from: a) 0.075, b) 0.30 and c) 0.60 M $CuSO_4$ in 0.50 M H_2SO_4. Quantity of electricity, Q: 10.0 mA h cm^{-2}.

The average current efficiencies of hydrogen evolution, $\eta_{av}(H_2)$, obtained under these electrodeposition conditions were 68.7, 16.0 and 4.6 % from 0.075, 0.30 and 0.60 M $CuSO_4$ in 0.50 M H_2SO_4, respectively.[11] These values were derived from the dependences of the current of electrodeposition and the volume of evolved hydrogen on the electrodeposition time, as shown in Fig. 2. It can be seen from Fig. 2 that increasing the concentration of $CuSO_4$ led to a decrease of

the quantity of evolved hydrogen and, hence, the average current efficiencies of hydrogen evolution. At the first sight, this was unexpected because the concentration of H_2SO_4 was the same in all the solutions. The explanation for it can be obtained by analysis of the ionic equilibrium of the species in the $CuSO_4$–H_2SO_4––H_2O system. The dependence of the relative concentration of hydrogen ions (H^+) on the H_2SO_4 concentration for different concentrations of copper ions is shown in Fig. 3. According to this equilibrium, increasing the copper ion concentration produces a sharp decrease in the hydrogen ion concentration, while increasing the concentration of sulfuric acid produces an increase in the hydrogen ion concentration.[1] The reason for this is that the addition of sulfuric acid to the solution decreases the concentration of free sulfate ions due to the formation of bisulfate ions, while the addition of cupric sulfate to the solution increases the concentration of bisulfate ions and decreases the concentration of hydrogen ions.

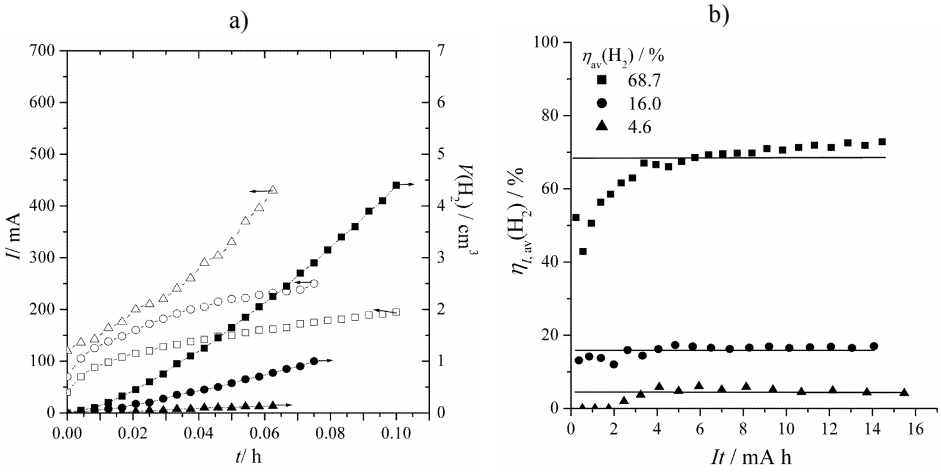

Fig. 2. The dependences of the current of copper electrodeposition and the volume of evolved hydrogen on the electrodeposition time (a) and the average current efficiencies for hydrogen evolution reaction on the quantity of used electricity (b) for copper electrodeposition at 1000 mV from 0.075 (□,■), 0.30 (○,●) and 0.60 M (△,▲) $CuSO_4$ in 0.50 M H_2SO_4.

It is very clear that the decrease of the quantity of evolved hydrogen, and consequently, the average current efficiencies of hydrogen evolution (Fig. 2) is the result of decreasing the hydrogen ion concentration with the increasing copper concentration. Moreover, the acceleration of the electrochemical processes with increasing $CuSO_4$ concentration had an unfavorable effect on the formation of the honeycomb-like structures. It was found[12] that the maximum $CuSO_4$ concentration (in 0.50 M H_2SO_4) which allowed the formation of the honeycomb-like structure was 0.15 M. Hydrogen evolution, which leads to the formation of the honeycomb-like structures, was vigorous enough to change the hydrodynamic conditions in the near-electrode layer. For copper sulfate solutions containing 0.15 M

$CuSO_4$ and less, in 0.50 M H_2SO_4, the critical quantity of evolved hydrogen leading to a change in the hydrodynamic conditions was estimated to correspond to $\eta_{av}(H_2)$ of 10.0 %.[12] This was attained by electrodeposition at an overpotential of 800 mV from 0.15 M $CuSO_4$ in 0.50 M H_2SO_4.[7]

Vigorous hydrogen evolution is only one of the possible ways of changing the hydrodynamic conditions in the near-electrode layer. For example, a change in the hydrodynamic conditions can also be realized under imposed magnetic field (magnetohydrodynamic effects),[13–15] in an ultrasonic field[16] or by rotating the electrode.[17]

The above analysis of the electrodeposition processes with the different $CuSO_4$ concentrations and the same H_2SO_4 concentration corresponds to a vertical analysis of the ionic equilibrium of the species in the $CuSO_4$–H_2SO_4–H_2O system. Horizontal analysis of this ionic equilibrium can be performed by analysis of the electrodeposition processes with a constant $CuSO_4$ concentration and different H_2SO_4 concentrations.

For the horizontal analysis, 0.15 M $CuSO_4$ was selected, while the selected H_2SO_4 concentrations were higher (1.0 M) and lower (0.125 and 0.25 M) than 0.50 M. According to the ionic equilibrium shown in Fig. 3, the H^+ concentration is higher for these solutions (the position of the Cu^{2+} concentration of 0.15 M can easily be calculated) than for copper solutions containing 0.30 and 0.60 M $CuSO_4$ in 0.50 M H_2SO_4. This was confirmed by the higher average current efficiencies of hydrogen evolution obtained at an overpotential of 1000 mV from these solutions than those obtained from 0.30 and 0.60 M $CuSO_4$ in 0.50 M H_2SO_4. The average current efficiencies of hydrogen evolution, $\eta_{av}(H_2)$ were: 20.3 % from 0.15 M $CuSO_4$ in 0.125 M H_2SO_4, 26.4 % from 0.15 M $CuSO_4$ in 0.25 M H_2SO_4 and 45.7 % from 0.15 M $CuSO_4$ in 1.0 M H_2SO_4.[18] Based on the obtained values, it was expected that honeycomb-like structures would be obtained by electrodeposition from these solutions. However, honeycomb-like structures were only formed from 0.15 M $CuSO_4$ in both 1.0 M and 0.25 M H_2SO_4 but not from 0.15 M $CuSO_4$ in 0.125 M H_2SO_4.[18] The copper deposit obtained at an overpotential of 1000 mV from 0.15 M $CuSO_4$ in 0.125 M H_2SO_4 is shown in Fig. 4. Analysis of this copper deposit identified the presence of holes with shoulders of degenerated dendrites, and irregular channels formed by evolved hydrogen around the dendritic and cauliflower-like particles. The appearing of these morphological forms clearly indicates that the hydrodynamic conditions in the near-electrode layer remained unchanged during electrodeposition from this solution. This was very surprising owing to the very high average current efficiency of hydrogen evolution under which this deposit was formed. This indicates that the quantity of evolved hydrogen is not the only parameter responsible for a change in the hydrodynamic conditions in the near-electrode layer. Therefore, the recognition of the properties of the electrodeposition solutions, such as density

and surface tension, is very important.[18] The addition of H_2SO_4 to an electroplating solution increases the density[18,19] and decreases the surface tension of an electroplating solution.[18] An increase of the density and a lowering of the surface tension of the solution decreases the break-off diameter of a hydrogen bubble[18,20] and, consequently, reduces the time required to achieve the critical size for its detachment from the electrode surface. Electrodeposition processes from such solutions will produce an sufficient amount of hydrogen bubbles which can cause an effective stirring of solution in the near-electrode layer and change the hydrodynamic conditions. This can be confirmed by the analysis of number of holes formed per mm^2 of surface area of the copper electrodes and the average diameter of holes obtained from 0.15 M $CuSO_4$ in 0.50 M H_2SO_4 at 800 mV (the formed honeycomb-like structure with a $\eta_{av}(H_2)$ of 10.8 %; changed hydrodynamic conditions in the near-electrode layer) and from 0.15 M $CuSO_4$ in 0.125 M H_2SO_4 at 1000 mV (the honeycomb-like structure was not formed with a $\eta_{av}(H_2)$ of 20.3 %; insufficient change of the hydrodynamic conditions in the near-electrode layer). The number of holes formed due to the attached hydrogen bubbles from 0.15 M $CuSO_4$ in 0.50 M H_2SO_4 at 800 mV was 10 per mm^2 of surface area of the copper electrode,[7] while their average diameter was 98.7 μm. This number was for about 40 % larger than the number of holes formed from 0.15 M $CuSO_4$ in 0.125 M H_2SO_4 at 1000 mV. The average diameter of the holes formed from 0.15 M $CuSO_4$ in 0.125 M H_2SO_4 at 1000 mV was about 20 % larger than the average diameter of those formed from 0.15 M $CuSO_4$ in 0.50 M H_2SO_4 at 800 mV.

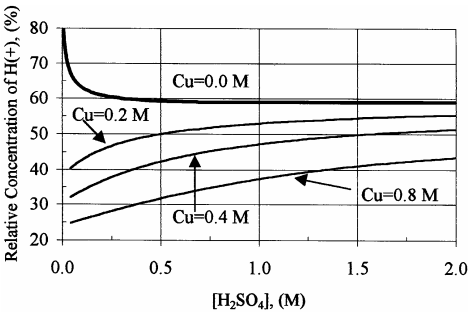

Fig. 3. Relative concentration of hydrogen ions as function of sulfuric acid and total copper concentrations, at 25 °C ($c_{RH^+} = [H^+]/[HT]$) (Reprinted with permission of Elsevier).[1]

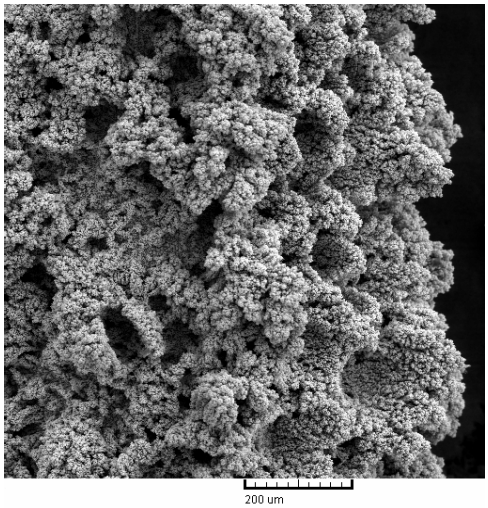

Fig. 4. The copper deposit obtained at an overpotential of 1000 mV from 0.15 M $CuSO_4$ in 0.125 M H_2SO_4. Quantity of electricity: 10.0 mA h cm^{-2}.

The acceleration of electrochemical processes through increasing the temperature of electrolysis had an unfavorable effect on the formation of honeycomb-like structures.[21] Increasing the temperature led to a decrease in the number of holes because of the effect of temperature on some properties of the solutions, such as viscosity and surface tension.[20–22]

Horizontal and vertical analysis of the ionic equilibrium in the $CuSO_4$–$–H_2SO_4–H_2O$ system enabled the electrodeposition conditions leading to the formation of honeycomb-like structures to be systematized. It explained why $CuSO_4$ concentrations higher than 0.15 M are unsuitable for the formation of this type of structures. The minimal H_2SO_4 concentration of 0.25 M H_2SO_4 (for 0.15 M $CuSO_4$) allowing the formation of honeycomb-like structures was also determined.

CONCLUSIONS

Systematization of the electrodeposition conditions allowing the formation of honeycomb-like copper structures from acid sulfate solutions was made by analyzing the ionic equilibrium in the $CuSO_4–H_2SO_4–H_2O$ system. The honeycomb-like structures can be formed by electrodeposition from solutions with low concentrations of Cu(II) ions (0.15 M $CuSO_4$ and less) in an H_2SO_4 concentration in the range from 0.25 to 1.0 M, at a temperature of 18.0±1.0 °C, and at overpotentials positive with respect to the plateau of the limiting diffusion current density at which hydrogen evolution is vigorous enough to change the hydrodynamic conditions in the near-electrode layer.

Acknowledgement. The work was supported by the Ministry of Science of the Republic of Serbia under the research project: “Deposition of ultrafine powders of metals and alloys and nanostructured surfaces by electrochemical techniques” (No. 142032G).

ИЗВОД

ЈОНСКА РАВНОТЕЖА У СИСТЕМУ $CuSO_4–H_2SO_4–H_2O$ И ФОРМИРАЊЕ СТРУКТУРЕ ПЧЕЛИЊЕГ САЋА ЕЛЕКТРОХЕМИЈСКИМ ТАЛОЖЕЊЕМ БАКРА

НЕБОЈША Д. НИКОЛИЋ[1], ЉУБИЦА Ј. ПАВЛОВИЋ[1], ГОРАН БРАНКОВИЋ[2], МИОМИР Г. ПАВЛОВИЋ[1] и КОНСТАНТИН И. ПОПОВ[1,3]

[1]ИХТМ – Центар за електрохемију, Универзитет у Београду, Његошева 12, Београд, [2]Институт за мултидисциплинарна истраживања, Кнеза Вишеслава 1а, Београд и [3]Технолошко–металуршки факултет, Универзитет у Београду, Карнегијева 4, Београд

Анализирана је јонска равнотежа у систему $CuSO_4–H_2SO_4–H_2O$ да би се систематизовали услови електрохемијског таложења бакра који доводе до формирања структуре пчелињег саћа. Показано је да су концентрације $CuSO_4$ веће од 0,15 М непогодне за формирање структуре пчелињег саћа. Одређен је и опсег концентрација H_2SO_4 у којем се формира оваква структура. Услови који доводе до формирања структуре пчелињег саћа су: електрохемијско таложење из раствора са концентрацијом Cu(II) од највише 0,15 М и опсегом концентрација H_2SO_4 од 0,25 до 1,0 М, температуре од 18,0±1,0 °C, и на пренапетостима позитивнијим од оних који одговарају платоу граничне дифузионе густине струје, на којима

је издвајање водоника довољно интензивно да промени хидродинамичке услове у прикатодном слоју.

(Примљено 26. септембра 2007, ревидирано 26. марта 2008)

REFERENCES

1. J. M. Casas, F. Alvarez, L. Cifuentes, *Chem. Eng. Sci.* **55** (2000) 6223
2. A. Calusaru, *Electrodeposition of Metal Powders*, Elsevier, Amsterdam, 1979
3. K. I. Popov, M. G. Pavlović, in *Modern Aspects of Electrochemistry*, Vol. 24, R. W. White, J. O'M. Bockris, B. E. Conway, Eds., Plenum Press, NY, 1993, pp. 299–391
4. K. I. Popov, S. S. Djokić, B. N. Grgur, *Fundamental Aspects of Electrometallurgy*, Kluwer Academic/Plenum Publishers, New York, 2002
5. N. D. Nikolić, Lj. J. Pavlović, M. G. Pavlović, K. I. Popov, *Powder Technol.* **185** (2008) 195
6. H.-C. Shin, J. Dong, M. Liu, *Adv. Mat.* **15** (2003) 1610
7. N. D. Nikolić, K. I. Popov, Lj. J. Pavlović, M. G. Pavlović, *J. Electroanal. Chem.* **588** (2006) 88
8. N. D. Nikolić, K. I. Popov, Lj. J. Pavlović, M. G. Pavlović, *Surf. Coat. Technol.* **201** (2006) 560
9. N. D. Nikolić, K. I. Popov, Lj. J. Pavlović, M. G. Pavlović, *J. Solid State Electrochem.* **11** (2007) 667
10. N. D. Nikolić, Lj. J. Pavlović, S. B. Krstić, M. G. Pavlović, K. I. Popov, *Chem. Eng. Sci.* **63** (2008) 2824
11. N. D. Nikolić, Lj. J. Pavlović, M. G. Pavlović, K. I. Popov, *Electrochim. Acta* **52** (2007) 8096
12. N. D. Nikolić, K. I. Popov, Lj. J. Pavlović, M. G. Pavlović, *Sensors* **7** (2007) 1
13. H. Matsushima, A. Bund, W. Plieth, S. Kikuchi, Y. Fukunaka, *Electrochim. Acta* **53** (2007) 161
14. N. D. Nikolić, *J. Serb. Chem. Soc.* **71** (2006) 1083
15. N. D. Nikolić, *J. Serb. Chem. Soc.* **72** (2007) 787
16. M. E. Hyde, O. V. Klymenko, R. G. Compton, *J. Electroanal. Chem.* **534** (2002) 13
17. G. Hinds, F. E. Spada, J. M. D. Coey, T. R. Ni Mhiochain, M. E. G. Lyons, *J. Phys. Chem. B* **105** (2001) 9487
18. N. D. Nikolić, G. Branković, M. G. Pavlović, K. I. Popov, *J. Electroanal. Chem.* (2008), doi: 10.1016/j.jelechem.2008.04.006
19. D. C. Price, W. G. Davenport, *Metall. Trans. B* **11B** (1980) 159
20. H. Vogt, R. J. Balzer, *Electrochim. Acta* **50** (2005) 2073
21. N. D. Nikolić, Lj. J. Pavlović, M. G. Pavlović, K. I. Popov, *J. Serb. Chem. Soc*. **72** (2007) 1369
22. A. Amadi, D. R. Gabe, M. Goodenough, *J. Appl. Electrochem.* **21** (1991) 1114.

Journal of the Serbian Chemical Society
JSCS@tmf.bg.ac.yu • www.shd.org.yu/JSCS
J. Serb. Chem. Soc. 73 (7) 761–770 (2008)
JSCS–3759
UDC 546.733:532.74:544.6.004.12:543.422.25
Original scientific paper

Molecular structure in correlation with electrochemical properties of mixed-ligand cobalt(III) complexes

K. BABIĆ-SAMARDŽIJA[1§], V. M. JOVANOVIĆ[2*#] and S. P. SOVILJ[3]

[1]*Rice University, Chemistry Department, 6100 Main St., Houston, TX 77005, USA,* [2]*University of Belgrade, ICTM – Department of Electrochemistry, P.O. Box 473, Belgrade, and* [3]*University of Belgrade, Faculty of Chemistry, P.O. Box 158, 11001 Belgrade, Serbia*

(Received 9 October 2007, revised 3 March 2008)

Abstract: Four mixed-ligand cobalt(III) complexes (**1**–**4**) of the general formula [Co(Rdtc)cyclam]$(ClO_4)_2$ and [Co(Rac)cyclam]$(ClO_4)_2$ (cyclam = 1,4,8,11-tetraazacyclotetradecane; Rdtc = thiomorpholine-(Timdtc) or 2-methylpiperidine--(2-Mepipdtc) dithiocarbamates; Rac = 1,1,1,5,5,5-hexafluoro-2,4-pentanedionato (Hfac) or 2,2,6,6-tetramethyl-3,5-heptanedionato (Tmhd), respectively) were electrochemically examined on a glassy carbon and an iron electrode in perchloric acid solution. The obtained results showed the influence of these complexes on hydrogen evolution, the oxygen reduction reaction and iron dissolution. The exhibited effects of the complexes on these reactions depend on structure related to the bidentate dithiocarbamato or β-diketonato ligand. The electrochemical properties of the complexes were correlated with molecular structure and parameters derived from spectral analysis and molecular modeling.

Keywords: cobalt(III) complexes; cyclam; dithiocarbamato ligands; β-diketonato ligands; MOT.

INTRODUCTION

In many respects, tetraazamacrocycles have attracted considerable attention as biomimetic and catalytic systems.[1] They can sequestrate many transition metal ions to form complexes which exhibit various chemical and physical properties, such as molecular recognition of DNA and RNA,[2,3] electro- or photo-activation of CO_2,[4,5] and can act as metalloenzyme models,[6,7] depending on the coordination properties of the pendant donor group. Furthermore, among these series, some complexes have found application in medical and pharmaceutical fields as contrast-enhancing agents.[9–11]

The macrocyclic [14]ane-N_4 ligand cyclam is prone to coordinate the metal in a pseudo planar geometry due to its flexibility, which induces favored con-

* Corresponding author. E-mail: vlad@tmf.bg.ac.yu
§ Present address: Baker Petrolite Corp., 12645 W. Airport Blvd., Sugar Land, TX 77478, USA.
# Serbian Chemical Society member.
doi: 10.2298/JSC0807761B

figurations.[12–15] However, the topology of the bidentate extracyclic ligand directly influences the size of the cavity and the coordination parameters. This paper is focused on a model study of previously synthesized cobalt(III)–cyclam complexes containing dithiocarbamato[14] or β-diketonato ligands.[15] There is, indeed, an interest in elucidating the role played by dithiocarbamato as well as β-diketonato ligands, since similar complexes exhibit certain electrochemical properties.[12,16,19] It is interesting to point out the relation between structural parameters and the results obtained from electrochemical measurements, *i.e.*, electrocatalysis and inhibition studies. In this respect, the ability to predict and hence to interpret principal modes of interactions of structurally diverse compounds will help to develop a parallel route to analogues.

EXPERIMENTAL

All the employed chemicals were commercial products of analytical reagent grade. The corresponding cobalt(III)–cyclam complexes were obtained according to the procedures described in the literature.[14,15]

The complexes were examined on a glassy carbon (GC) and an iron electrode in 0.10 M $HClO_4$ and 0.10 M $NaClO_4$ solution. A GC disc (Sigardur-Sigri Electrographite, GmbH, Germany) was used as the working electrode for the characterization of the complexes. The electrode surface was mechanically treated with emery paper of decreasing grain size, polished with alumina (0.5 μm particle size) and cleaned in double-distilled deionized water in an ultrasonic bath. The GC electrode was tested in blank electrolyte by cyclic voltammetry (CV) before the substance was added to the solution. The reduction of oxygen in the presence of the $[Co(Rdtc)cyclam](ClO_4)_2$ complexes was examined in 0.10 M $HClO_4$ saturated with O_2 at a rotating GC electrode at a sweep rate of 5.0 mV s^{-1} and a rotation rate 900 rpm.

The iron rod electrode (Puratronic 99.99 %, Johnson Matthey Company) used for the corrosion tests was mechanically finished with emery paper. The electrode was immersed in electrolyte solution for 1 h before commencing the measurements. The inhibiting effect of the complexes was studied by potentiodynamic measurements in an oxygenated atmosphere. The measurements were performed using a Potentiostat/Galvanostat/ZRA, Gamry Instruments, and data were processed using Elchem Analyst software. The current–potential curves were obtained by changing the electrode potential automatically from –250 to 250 mV_{SCE} at a scan rate of 1.0 mV s^{-1}.

The solutions were prepared from analytical grade reagents using double-distilled deionized water. All of the experiments were performed at room temperature in a three-electrode compartment electrochemical cell. The counter electrode was a Pt wire and saturated calomel electrode (SCE) was used as the reference. All potentials are given *vs.* SCE.

For molecular modeling, a quantum-mechanical Hyperchem program was used (Hypercube Inc., Version 7). The molecular orbital (MO) calculations were based on the semi-empirical self-consistent field (SCF) method. A full optimization of all geometrical variables without any symmetry constraint was performed using the Zindo/1 method.

RESULTS AND DISCUSSION

The analytical results confirmed the proposed compositions of the complexes.

*[Co(Timdtc)cyclam](ClO4)2 (**1**)*. Anal. Calcd. (%) for $C_{15}H_{32}Cl_2CoN_5O_8S_3$ (636.47): C, 28.66; H, 5.27; N, 10.62. Found: C, 28.31; H, 5.07; N, 11.00.

[Co(2-Mepipdtc)cyclam](ClO4)2 ***(2)***. Anal. Calcd. (%) for $C_{17}H_{36}Cl_2CoN_5O_8S_2$ (632.46): C, 32.17; H, 5.80; N, 11.22. Found: C, 32.28; H, 5.74; N, 11.07.

[Co(Hfac)cyclam](ClO4)2 ***(3)***. Anal. Calcd. (%) for $C_{15}H_{25}Cl_2CoN_4O_{10}F_6$ (665.20): C, 27.08; H, 3.79; N, 8.42. Found: C, 27.33; H, 3.93; N, 8.82.

[Co(Tmhd)cyclam](ClO4)2 ***(4)***. Anal. Calcd. (%) for $C_{21}H_{43}Cl_2CoN_4O_{10}$ (641.51): C, 39.32; H, 6.76; N, 8.73. Found: C, 39.36; H, 6.89; N, 8.95.

Dithiocarbamato-Co(III)cyclam complexes

The [Co(Rdtc)cyclam]$(ClO_4)_2$ complexes were electrochemically characterized on a GC electrode in 0.10 M $NaClO_4$. A 0.10 M perchloric acid solution was used to study their possible effects on oxygen reduction and corrosion inhibition. The cyclic voltammograms recorded for the complexes in 0.10 M $HClO_4$ are presented in Fig. 1. The recorded voltammograms are similar for both complexes with a redox peak pair in the negative potential region and a less pronounced peak pair in the positive potential region. The redox pair in the positive region is a characteristic of the electrode material itself in acidic solutions, *i.e.*, it corresponds to glassy carbon.[20] The potential values of the redox pair in the negative region do not depend on pH, being the same in $NaClO_4$ and $HClO_4$ solution. This pair of peaks was recorded only on the CVs of the complexes and was not present on the voltammograms of either of the ligands.[16] Thus, this pair of redox peaks marks the redox reaction of the central metal ion in the complex, *i.e.*, it belongs to the Co(III)/Co(II) couple. As can be seen from Fig. 1, the potential values depend on the structural nature of the chelate-*S*,*S'* ligands, being more negative in the presence of [Co(2-Mepip)cyclam]$(ClO_4)_2$. The CV data also indicate the influence of the complexes on hydrogen evolution in perchloric acid, by shifting its potential cathodically (Fig. 1). The higher potential shift in case of the [Co(2-Mepipdtc)cyclam]$(ClO_4)_2$ complex shows its larger influence on the cathodic reaction.

Preliminary examinations of oxygen reduction in the presence of the dithiocarbamato Co(III)–cyclam complexes showed a possible catalytic effect on the reaction in acidic media (Fig. 2). The obtained results illustrate that the complexes influence oxygen reduction by shifting the potential in the anodic direction. In this case, a larger effect was observed with the [Co(Timdtc)cyclam]$(ClO_4)_2$ complex.

Corrosion tests on an iron electrode in the presence of either of the dithiocarbamato complexes showed their inhibiting effect in acidic solution, influencing both the anodic and cathodic reaction. Both complexes demonstrate a strong effect on the hydrogen evolution reaction. The polarization curves (Fig. 3) indicate the influence of the [Co(Timdtc)cyclam]$(ClO_4)_2$ complex on the anodic reaction in comparison with the free acid, although, the [Co(2-Mepipdtc)cyclam]$(ClO_4)_2$ complex showed a greater cathodic protection and a higher inhibitor efficiency. Thus, the complex that suppresses hydrogen evolution more was found to be a better corrosion inhibitor.

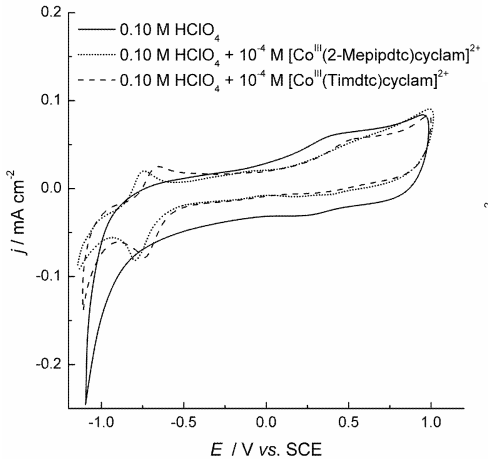

Fig. 1. Cyclic voltammograms at a GC electrode in 0.10 M $HClO_4$ without and with 10^{-4} M [CoIII(Rdtc)cyclam]$(ClO_4)_2$ complexes (sweep rate: 50 mV s^{-1}).

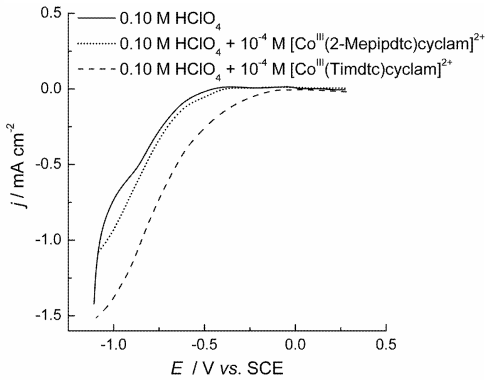

Fig. 2. Oxygen reduction curves at a GC electrode in 0.10 M $HClO_4$ without and with 10^{-4} M [CoIII(Rdtc)cyclam]$(ClO_4)_2$ complexes (sweep rate: 5.0 mV s^{-1}, ω = 900 rpm).

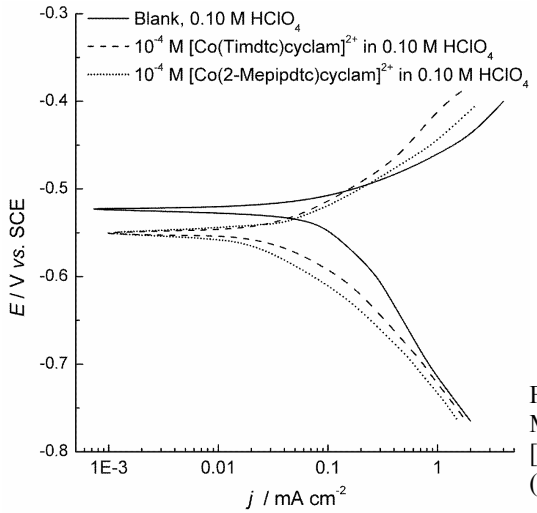

Fig. 3. Polarization curves for iron in 0.10 M $HClO_4$ and in the presence of 10^{-4} M [Co(III)(Rdtc)cyclam]$(ClO_4)_2$ complexes (sweep rate: 1.0 mV s^{-1}).

The position of the methyl group on the piperidine ring and/or the presence of a heteroatom in the ring is reflected in a shift of the CN bond frequencies in the part of the $Rdtc^-$ ligand in the IR spectra.[13,14] Selected IR spectral data of the examined complexes are given in Table I. The data show that the ν(C=N) in the [Co(2-Mepipdtc)cyclam]$(ClO_4)_2$ complex was shifted to lower energies due to the positive inductive effect of the methyl group in the complex. On the other hand, the heteroatom in the [Co(Timdtc)cyclam]$(ClO_4)_2$ complex influenced the C=N bond frequency, ν(C=N), by shifting it to higher energies. Electronic effects, as noticed, consequently affect the potential shift of the cobalt re-

dox reaction and electrochemical reactions. Accordingly, with a stronger CN bond, the potentials will be shifted to more negative values.

TABLE I. Selected IR spectral data (cm^{-1}) of the [Co(Rdtc)cyclam]$(ClO_4)_2$ complexes

Complex	ν(C=N)	ν(C=S)
[Co(Timdtc)cyclam]$(ClO_4)_2$ (**1**)	1528_{vs}[a]	1013_s
[Co(2-Mepipdtc)cyclam]$(ClO_4)_2$ (**2**)	1438_{vs}	954_s

[a]*vs*: Very strong; *s*: strong

The chemical shifts in ^{13}C-NMR spectra of the $>NCS_2$ group on the $Rdtc^-$ ligands showed slight differences between the complexes in the same order as was established from the electrochemical data. The deshielding effect on these resonances is an indication of the stronger metal–ligand bond[21] and greater electron density of the ligating group. As the effect was greater for the $[Co(2\text{-Mepipdtc})cyclam]^{2+}$ than for the $[Co(Timdtc)cyclam]^{2+}$ complex, its inhibiting effect on iron corrosion was also bigger. In general, the adsorption of the complexes on the metal surface is most likely realized through a coordinate type of bond formed due to electron transfer from the inhibitor molecule to the metal. The coordinated $Rdtc^-$ ligand with a higher density towards the $>NCS_2$ group results in a stronger Co–ligand bond. The stronger metal–ligand bond in the complex leads to a higher electron density on the adsorption part of the molecule and, thus, greater inhibittion. Therefore, a greater adsorption and larger inhibition efficiency should be expected for those compounds with a greater electron density at the adsorption centre.

Molecular modeling calculations were used to correlate the structural properties of the complex species and their inhibition efficiency.[17,18] According to the known crystal data,[12,22] the complex molecules are in a distorted octahedron geometry with the typical conformational flexibility of a large cyclic ring with a minimum steric constrains and with significant delocalization along the $>NCS_2$ group of the $Rdtc^-$ ligand. The Zindo/1 optimized structure for the [Co(Timdtc)cyclam]$(ClO_4)_2$ complex is shown in Fig. 4.

The Homo (highest occupied MO) energy is often associated with the electron donating ability of a molecule. The presence of a methyl group on the heterocyclic ring decreases the ionization potential ($I = -E_{HOMO}$) and the energy gap ($\Delta E = E_{LUMO} - E_{HOMO}$; E_{LUMO} is the lowest unoccupied MO), which is reflected in a stronger chemisorption bond and perhaps a greater inhibitor efficiency. In addition, the presence of a methyl group on the $Rdtc^-$ ligand intensifies the ligand field strengths and amine basicities, and thus affects the inhibitor efficiency. These facts can be used to show that small differences in the inhibiting behavior of the complexes are a consequence of their electronic and structural effects, together with conjugation of the double bonds through the $>NCS_2$ group of the dithiocarbamato ligand.

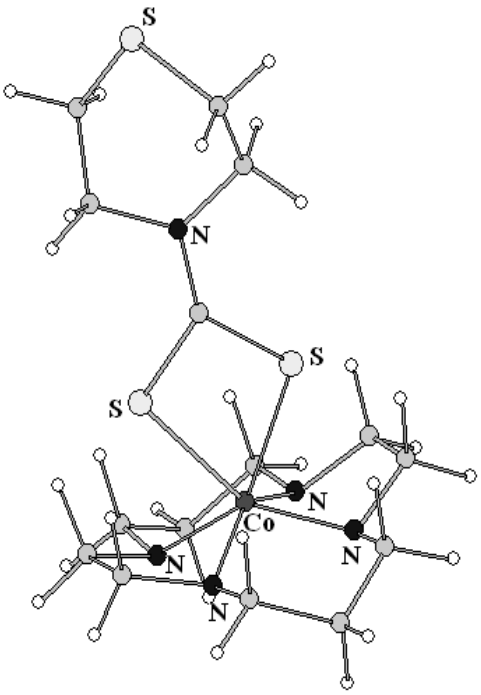

Fig. 4. Zindo/1 optimized structure for the complex $[Co(Timdtc)cyclam]^{2+}$.

β-*Diketonato-Co(III)cyclam complexes*

The CVs of the $[Co(Rac)cyclam](ClO_4)_2$ complexes examined at a GC electrode in aqueous $NaClO_4$ solution are presented in Fig. 5. A single quasi-reversible redox wave in the range –250 to –400 mV, depending on the diketonato Rac^- ligand, with a peak-to-peak separation of about 100 mV, was recorded on both voltammograms. This pair of peaks should present the Co(III)/Co(II) redox reaction. Such a redox pair, as previously found, characterizes $[Co(Rdtc)cyclam]^{2+}$ complexes (at about –700 mV) as well as the $[Co(ox)cyclam]^+$ complex (at about –400 mV).[12] Therefore, the anodic shift of the redox potential, in the order of the bidentates $Rac^- > ox^{2-} > Rdtc^-$, is most likely related to the σ- and π-ligand donor properties.

The CVs in aqueous $NaClO_4$ solutions (Fig. 5) show that, in the presence of the complexes, the cathodic hydrogen evolution reaction was influenced as evidenced by the shift of the potential to more negative values. The effect depends on the structural nature of the *β*-diketonato ligands, being more pronounced in presence of the $[Co(Tmhd)cyclam](ClO_4)_2$ complex.

The inhibiting effect of the $[Co(Rac)cyclam](ClO_4)_2$ complexes was studied on the corrosion of iron in perchloric acid solution. The results of the polarization measurements are presented in Fig. 6. According to the electrochemical results,

the cobalt(III) complexes exhibit anticorrosion properties. Compared with an inhibitor-free solution, these inhibitors decrease the corrosion current. A similar range of inhibitor efficiency was found for the complex with Tmhd > Hfac ligand.

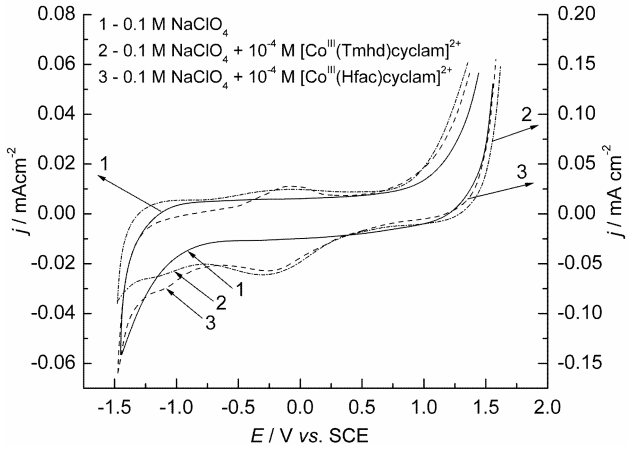

Fig. 5. Cyclic voltammograms at a GC electrode in 0.10 M $NaClO_4$ without and with 10^{-4} M $[CoIII(Rac)cyclam](ClO_4)_2$ complexes (sweep rate: 50 mV s^{-1}).

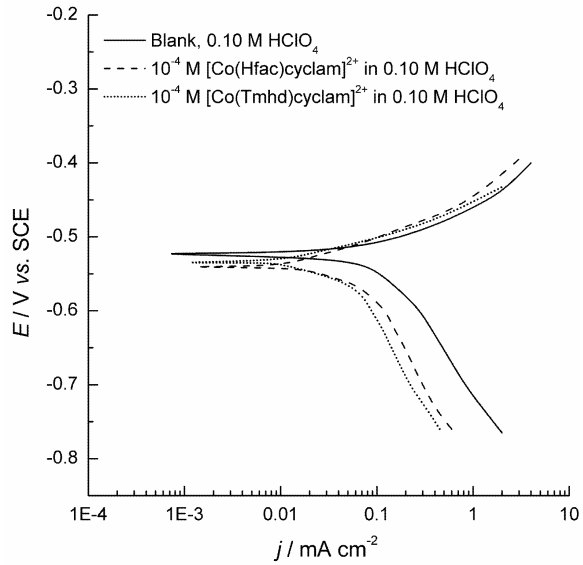

Fig. 6. Polarization curves for iron in 0.10 M $HClO_4$ and in the presence of 10^{-4} M $[CoIII(Rac)cyclam](ClO_4)_2$ complexes (sweep rate: 1.0 mV s^{-1}).

IR Spectroscopy data of the $[Co(Rac)cyclam](ClO_4)_2$ complexes are summarized in Table II. Based on the spectral data, it was observed that R groups on the β-diketone influence the ν(C=====C) and ν(C=====O) band frequencies, due to different resonance and inductive effects along the conjugated double bonds through the Rac^- anion, in the order Hfac > Tmhd ligand. The presence of the trifluoromethyl group, due to the electron-withdrawing effect, decreases the electronic density and consequently shifts CC and CO bands toward higher frequen-

cies. On the contrary, due to the positive inductive effect of the methyl group, the other complex showed strong but opposite effects in its IR spectrum. β-Diketonato protons have an "aromatic" character and the chemical shifts in the NMR spectra are under the direct influence of the R groups. The powerful efficacy of the six fluor atoms of the Hfac ligand moves the chemical shifts strongly downfield.

TABLE II. Selected IR spectral data (cm^{-1}) of the [Co(Rac)cyclam]$(ClO_4)_2$ complexes

Complex	ν(C=C)	ν(C=O)
[Co(Tmhd)cyclam]$(ClO_4)_2$ (**3**)	1560_s[a]	1507_m
	1549_s	
[Co(Hfac)cyclam]$(ClO_4)_2$ (**4**)	1627_m	1530_w
	1576_s	

[a] *s*: Strong; *m*: medium; *w*: weak

Some molecular parameters were calculated within the framework of SCF-MO using the Zindo/1 method. The optimized structure for the complex that exhibits the better inhibiting effect on iron corrosion is presented in Fig. 7. The total charge density of the molecules is displayed typically on and around the central metal ion and the delocalized part of the molecule, typically the oxygen atom. Orientation of such a large complex molecules towards the metal surface is important and, therefore, it is an electronic effect.

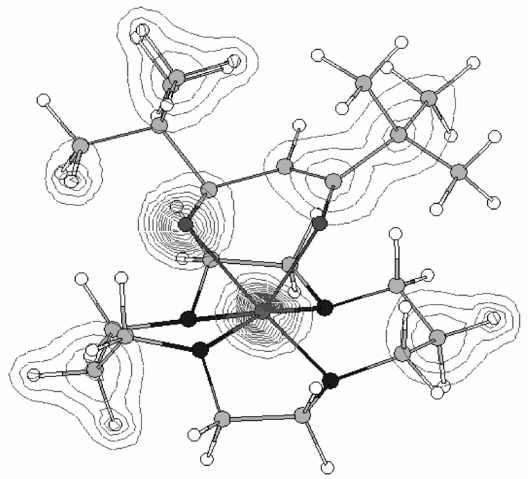

Fig. 7: Zindo/1 optimized structure for the complex $[Co(Tmhd)cyclam]^{2+}$; total charge density.

Based on MO calculations, some global reactivity parameters can be established. For the compound with a large dipole moment, a chemical bond with a metal surface may be stronger than that for adsorbed water. If this is the case then the inhibitor might displace the water molecules and adsorb *via* electrostatic bonding. As calculated by the Zindo/1 method, the [Co(Tmhd)cyclam]$(ClO_4)_2$ complex has a dipole moment of 12.76 D, as well as high global softness and electrophilicity. This complex exhibits a high inhibition effect. This criterion aids in

the understanding of the mechanism of inhibitor function, although it cannot be used as a general principle for such a complex entity because the reactivity of the molecule is defined not only by global indexes but also by the local selectivity of every atom of the molecule when it participates in the corrosion process.[23]

CONCLUSIONS

Based on the obtained results, some conclusions and correlations between the structure and electrochemical properties of the examined complexes can be made.

The electrochemical behavior depends on the bidentate dithiocarbamato or β-diketonato ligand. The effects of the complexes manifested themselves on the evolution of hydrogen and the dissolution of iron, with the $Rdtc^-$ ligand as 2-Mepipdtc > Timdtc and with the Rac^- ligand as Tmhd > Hfac.

The [Co(2-Mepipdtc)cyclam]$(ClO_4)_2$ complex is a weaker catalyst for oxygen reduction than the [Co(Timdtc)cyclam]$(ClO_4)_2$ complex but is more efficient as a corrosion inhibitor. The presence of the methyl group results in the ν(CN) bond frequencies being shifted to lower energies. The deshielding effect on the $>NCS_2$ resonances indicates a stronger metal–ligand bond due to the inductive effect of the methyl group. The stronger metal–ligand bond in the complex leads to a higher electron density on the adsorption part of the molecule and, thus, to higher inhibition. Regarding the molecular parameters, a lower ionization potential and energy gap reflects in a stronger chemisorption and perhaps a greater inhibitor efficiency.

In case of the diketonato ligands, the [Co(Tmhd)cyclam]$(ClO_4)_2$ complex influence the hydrogen evolution reaction more, thus exhibiting a higher inhibition effect on the corrosion of iron. As calculated by the Zindo/1 method, its higher dipole moment, as well as high global softness and electrophilicity are in correlation with its inhibitor properties.

Acknowledgements. The authors are pleased to acknowledge the financial support provided by Ministry of Science of the Republic of Serbia (project No. 142056) and the Robert A. Welch Foundation, Houston, TX.

И З В О Д

КОРЕЛАЦИЈА МОЛЕКУЛСКЕ СТРУКТУРЕ И ЕЛЕКТРОХЕМИЈСКИХ СВОЈСТАВА КОБАЛТ(III) КОМПЛЕКСА СА МЕШОВИТИМ ЛИГАНДИМА

К. БАБИЋ-САМАРЏИЈА[1], В. М. ЈОВАНОВИЋ[2] и С. П. СОВИЉ[3]

[1]Rice University, Chemistry Department, 6100 Main St., Houston, TX 77005, USA [2]Универзитет у Београду, ИХТМ – Центар за електрохемију, п. пр. 473, 11 001 Београд и [3]Универзитет у Београду, Хемијски факултет, п. пр. 158, 11001 Београд

Четири мешовито-лигандна кобалт(III) комплекса опште формуле [Co(Rdtc)cyclam]$(ClO_4)_2$ и [Co(Rac)cyclam]$(ClO_4)_2$ (cyclam = 1,4,8,11-тетраазациклотетрадекан; Rdtc = тиоморфолин--(timdtc) или 2-метилпиперидин-(2-mepipdtc) дитиокарбамат; Rac = 1,1,1,5,5,5-хексафлуоро--2,4-пентанедионато (hfac) или 2,2,6,6-тетраметил-3,5-хептанедионато (tmhd)) испитана су

електрохемијски на електродама од стакластог угљеника и гвожђа у раствору перхлората. Добијени резултати указују на то да ови комплекси утичу на издвајање водоника, редукцију кисеоника као и на растварање гвожђа. Електрохемијско понашање зависи од структуре координованог бидентатног дитиокарбамато или β-дикетонато лиганда. Молекулска структура комплексних једињења одређена је на основу спектроскопских анализа и молекулског моделовања. Електрокаталитички и инхибиторски ефекат повезан је са молекулском структуром комплекса.

(Примљено 9. октобра 2007, ревидирано 3. марта 2008)

REFERENCES

1. J. Costamagna, G. Ferraudi, B. Matsuhiro, M. Campos-Vallette, J. Canales, M. Villagran, J. Vargas, M. J. Aguirre, *Coord. Chem.* **196** (2000) 125 (and references cited therein)
2. T. Koike, T. Watanabe, S. Aoki, E. Kimura, M. Shiro, *J. Am. Chem. Soc.* **118** (1996) 12696
3. M. Shionoya, T. Ikeda, E. Kimura, M. Shiro, *J. Am. Chem. Soc.* **116** (1994) 3848
4. J. Costamagna, G. Ferraudi, J. Canales, J. Vargas, *Coord. Chem. Rev.* **221** (1996) 148
5. G. L. Estiu, A. H. Jubert, J. Molina, J. Costamagna, J. Canales, J. Vargas, *Inorg. Chem.* **34** (1995) 1212
6. E. Kimura, I. Nakamura, T. Koike, M. Shionoya, Y. Kodama, T. Ikeda, M. Shiro, *J. Am. Chem. Soc.* **116** (1994) 4764
7. L. Fabrrizzi, M. Liccelli, P. Pallavicini, L. Parodi, *Angew. Chem. Int. Ed.* **37** (1998) 800
8. W. H. Chapman, R. Breslow, *J. Am. Chem. Soc.* **117** (1995) 5462
9. W. Alexander, *Chem. Rev.* **95** (1995) 273
10. S. Aime, N. Botta, S. G. Crich, G. B. Giovenzana, G. Jommi, R. Pagliarin, M. Sisti, *J. Chem. Soc. Chem. Commun.* (1995) 1885
11. W. D. Kim, G. E. Kiefer, F. Maton, K. McMillan, R. N. Muller, A. D. Sherry, *Inorg. Chem.* **34** (1995) 2233
12. S. P. Sovilj, G. Vučković, K. Babić, N. Matsumoto, M. Avramov-Ivić, V. M. Jovanović, *J. Coord. Chem.* **31** (1994) 167
13. S. P. Sovilj, G. Vučković, K. Babić, S. Macura, N. Juranić, *J. Coord. Chem.* **41** (1997) 19
14. S. P. Sovilj, K. Babić-Samardžija, *Synth. React. Inorg. Met.-Org. Chem.* **29** (1999) 1655
15. S. P. Sovilj, K. Babić-Samardžija, D. Stojšić, *Spectrosc. Lett.* **36** (2003) 183
16. V. M. Jovanović, K. Babić-Samardžija, S. P. Sovilj, *Electroanal*. **13** (2001) 1129
17. K. Babić-Samardžija, K. F. Khaled, N. Hackerman, *Appl. Surf. Sci.* **240** (2005) 327
18. K. F. Khaled, K. Babić-Samardžija, N. Hackerman, *Corros. Sci.* **48** (2006) 3014
19. K. Babić-Samardžija, N. Hackerman, S. P. Sovilj, V. M. Jovanović, *J. Solid State Electrochem.* **12** (2008) 155
20. A. Dekanski, J. Stevanović, R. Stevanović, B. Ž. Nikolić, V. M. Jovanović, *Carbon* **39** (2001) 1195
21. N. Juranić, R. L. Lichter, *J. Am. Chem. Soc.* **105** (1983) 406
22. S. P. Sovilj, K. Babić-Samardžija, *Hem. Ind.* **54** (2000) 534 (in Serbian)
23. K. F. Khaled, K. Babić-Samardžija, N. Hackerman, *Electrochim. Acta* **50** (2005) 2515.